$\mathcal{PT}$-symmetric dipolar Bose-Einstein condensates: Embedding in a Hermitian system and higher-order exceptional points

Von der Fakultät Mathematik und Physik der Universität Stuttgart
zur Erlangung der Würde eines Doktors der Naturwissenschaften
(Dr. rer. nat.) genehmigte Abhandlung

Vorgelegt von

Robin Gutöhrlein

aus Stuttgart

Hauptberichter:	Prof. Dr. Jörg Main
Mitberichter:	Prof. Dr. Christian Holm

Tag der mündlichen Prüfung: 21. Juli 2017

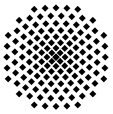

1. Institut für Theoretische Physik der Universität Stuttgart

2017

Inhaltsangabe

Offene Systeme mit Doppelmulden Bose-Einstein-Kondensaten verwenden komplexe Potentiale um den Ein- und Ausfluss von Atomen zu beschreiben. Der Imaginärteil des Potentials erlaubt eine effektive Beschreibung der Ein- und Auskopplung von Teilchen. Wenn solche System einen ausgeglichenen Gewinn und Verlust zeigen, lassen sie sich durch einen nichthermitschen $\mathcal{PT}$-symmetrischen Hamiltonoperator beschreiben. Es wurde gezeigt, dass $\mathcal{PT}$-symmetrische Zustände existieren, welche sowohl die Paritäts- als auch Zeitsumkehrsymmetrie berücksichtigen.

Im ersten Teil dieser Arbeit wird die Frage beantwortet, wie sich der Ein- sowie Ausfluss realisieren lässt, indem ein Hermitisches System eingeführt wird, in welches zwei $\mathcal{PT}$-symmetrische Untersystem integriert werden. Dieses System benötigt dann nicht länger ein Ein- und Auskoppeln nach und von der Umgebung. Wir zeigen, dass die Untersysteme immer noch $\mathcal{PT}$-symmetrische Zustände haben. Zusätzlich untersuchen wir, welcher Detailgrad in der Beschreibung notwendig ist, um die $\mathcal{PT}$-symmetrischen Eigenschaften und Bifurkationen des Systems korrekt zu modellieren. Wir untersuchen hierfür ein vierdimensionales Matrixmodell und ein System, das durch die eindimensionale Gross-Pitaevskii-Gleichung beschrieben wird. Der Vergleich der Systeme zeigt, dass das einfache Matrixmodell das qualitative Verhalten des Systems korrekt beschreibt. Es kann, für hinreichend isolierte Potentialmulden, auch eine gute quantitative Übereinstimmung mit den räumlich aufgelösten Modellen erreicht werden. Wir untersuchen auch, welche Eigenschaften die Wellenfunktion erfüllen muss, damit $\mathcal{PT}$-symmetrische Zustände überhaupt zustande kommen können. Insbesondere gehen wir auf die Phasenbeziehung zwischen den Wellenfunktionen in den beiden Untersystemen ein. Zusätzlich zeigen wir, welche Art von Wahrscheinlichkeitsströmen in dem geschlossenen Hermitischen System auftreten.

Im zweiten Teil der Arbeit wird die Bifurkationsstruktur von stationären Zuständen in einem dipolaren Bose-Einstein Kondensat untersucht, welches sich in einem von außen angelegten $\mathcal{PT}$-symmetrischen Potential befindet. Um die vollständige

Bifurkationsstruktur aufzudecken und um die Eigenschaften der auftretenden Ausnahmepunkte untersuchen zu können, wird eine analytische Fortsetzung der Gross-Pitaevskii-Gleichung, die das System beschreibt, unter Verwendung bikomplexer Zahlen durchgeführt. Das Bose-Einstein-Kondensat mit dipolaren Wechselwirkungen zeigt im Vergleich zu einem Kondensat ohne langreichweitige Wechselwirkungen ein reichhaltigeres Bifurkationszenario. Unter Einbeziehung von Zuständen der analytisch fortgesetzten Gleichung können Eigenschaftsänderungen an Bifurkationspunkten, die zuvor unsichtbar waren, erklärt werden. Außerdem erlauben sie die Untersuchung von Ausnahmepunkten, die mit den Verzweigungspunkten verbunden sind. Mithilfe der Zustände aus der analytischen Fortsetzung kann zudem die Existenz von Ausnahmepunkten fünfter Ordnung nachgewiesen werden.

Abstract

Open double-well Bose-Einstein condensate systems use complex potentials to describe the in- and and outfluxes of atoms. The imaginary part of the potentials allows for the effective description of in- and out-coupling of particles. If such systems exhibit balanced gain and loss, they are effectively described by a non-Hermitian $\mathcal{PT}$-symmetric Hamiltonian. $\mathcal{PT}$-symmetric states obeying parity and time reversal symmetry have been shown to exist.

In the first part of this work, the question is tackled of how the in- and outfluxes can be realized by introducing a Hermitian system in which two $\mathcal{PT}$-symmetric subsystems are embedded. This system no longer requires an in- and outcoupling into and from the environment. We show that the subsystems still have $\mathcal{PT}$-symmetric states. In addition we examine what degree of detail is necessary to correctly model the $\mathcal{PT}$-symmetric properties and the bifurcation structure of such a system. We examine a four-mode matrix model and a system described by the Gross-Pitaevskii equation in one dimension. The comparison shows that a simple matrix model correctly describes the qualitative properties of the system. For sufficiently isolated potential wells there is also quantitative agreement with the spatial extended system descriptions. We also investigate which properties must be fulfilled by the wave functions of a system to allow for $\mathcal{PT}$-symmetric states. In particular, the requirements for the phase difference between different parts of the system are examined. In addition we show which probability currents occur in the closed Hermitian system.

In the second part of this work, the bifurcation structure of stationary states in a dipolar Bose-Einstein condensate located in an external $\mathcal{PT}$-symmetric potential is investigated. To unveil the complete bifurcation structure and the properties of the exceptional points we perform an analytical continuation of the Gross-Pitaevskii equation. We use an elegant and numerically efficient method for the analytical continuation of the Gross-Pitaevskii equation with dipolar interactions by making use of bicomplex numbers. The Bose-Einstein condensate with dipolar interaction shows

a much richer bifurcation scenario than a condensate without long-range interactions. The inclusion of analytically continued states can also explain changes in the behaviour at the bifurcation points which were hidden before. Furthermore, this allows for the examination of the properties of the exceptional points associated with the branch points. With the help of the analytically continued states we are able to prove the existence of an exceptional point of fifth order.

Contents

1 Introduction

While the idea of Bose-Einstein condensates dates back to 1924 and 1925 when Albert Einstein [1, 2] and Satyendranath Bose [3] laid the theoretical cornerstone, the experimentally realisation took nearly seventy years [4–6]. The possibility of this realisation was enabled by the discovery of laser cooling, for which Wolfgang Ketterle, Eric A. Cornell and Carl E. Wieman received the Nobel prize in 2001. Bose-Einstein condensation allows for the observation of quantum mechanical phenomena on a macroscopic length and time scale.

The first realisations of Bose-Einstein condensates were performed using alkali atoms. Soon a larger diversity of basic building blocks were used. In particular, Bose-Einstein condensates condensed from chromium atoms, which have a non-vanishing magnetic dipole moment [7–10], were used. Since such condensates posses a long range $1/r^3$ interaction completely new phenomena were discovered.

While the examination and observed effects of Bose-Einstein condensates have become much more diverse in recent years, in this work we will concentrate in two parts on a specific topic. Since Bender described the special properties of $\mathcal{PT}$-symmetric systems in [11], systems fulfilling this symmetry have gained much attention. These systems feature a special class of non-Hermitian Hamiltonians which exhibit special properties, among them real eigenvalue spectra.

An operator is considered $\mathcal{PT}$-symmetric if it is invariant with respect to the combined action of the parity and time-reversal operator. Systems fulfilling this property have been studied in [11–14]. However, the concept of $\mathcal{PT}$-symmetry is not restricted to quantum mechanics. The first experimental realization of $\mathcal{PT}$-symmetric systems was actually achieved in optical wave guides where the effects of $\mathcal{PT}$-symmetry and $\mathcal{PT}$-symmetry breaking were observed [15]. These first breakthroughs have increased the research effort put into this field [16–19]. $\mathcal{PT}$-symmetric systems have also been studied in microwave cavities [20], electronic devices [21, 22], and in futher optical systems [23–31]. Also in quantum mechanics the stationary Schrödinger equa-

tion was solved for scattering solutions [13] and bound states [14]. The characteristic $\mathcal{PT}$-symmetric properties are still found when a many-particle description is used [32]. In [33] a $\mathcal{PT}$-symmetric system was embedded as a subsystem into a Hermitian system, showing that the subsystem retained its $\mathcal{PT}$-symmetric properties.

A $\mathcal{PT}$-symmetric system must have a potential which fulfils the relation

$$V(x) = V^*(-x), \tag{1.1}$$

i.e., the potential must have an even function as the real part and an odd function as the imaginary part. In quantum mechanic the imaginary part of a potential describes the in- and outcoupling to an external reservoir. This allows for an elegant description without the need to describe the reservoir itself. In the first part of this work, we will search for a Hermitian Hamiltonian describing the reservoir and the system itself. Therefore the $\mathcal{PT}$-symmetric system is embedded as a subsystem in the Hamiltonian. To do so, two double-well systems will be coupled appropriately. We also check how different descriptions of the double well influence the system. Starting with a simple matrix model, where each well is only described by a single complex entry in the state vector, the model is extended to include a continuous spatial description in one dimension. The results of the matrix model will be compared with a model where the wells are represented by delta-functions, that is the interaction between the subsystems is restricted to one point, and to a model where the potential wells themselves are described by a spatially extended function.

In the meanfield limit the Bose-Einstein condensates are described by the Gross-Pitaevskii equation. This equation is nonlinear. Therefore, stationary states found for this equation can undergo bifurcations if system parameters are varied. These bifurcation points are exceptional points. Exceptional points are points in the parameter space where not only two or more eigenvalues, but also their eigenfunctions coalesce. Exceptional points in Bose-Einstein condensates were examined before [34–40]. While Bose-Einstein condensates described by the Gross-Pitaevskii equation can be placed in a $\mathcal{PT}$-symmetric potential and many results have been obtained for such systems, e.g. for Bose-Einstein condensates in a double-well potential [32], in most of these papers only short-range interactions between the atoms were considered. Since the $\mathcal{PT}$-symmetry of the Gross-Pitaevskii equation depends on the $\mathcal{PT}$-symmetry of the wave function, effects which change the geometry of the wave function can lead to additional phenomena. Dipolar Bose-Einstein condensates exhibit such effects, e.g., structured ground states have been found [41]. Therefore, one would expect that the combination of dipolar Bose-Einstein condensates with a $\mathcal{PT}$-symmetric trap will lead to a new behaviour. In [42] a Bose-Einstein condensate with long-range dipole-dipole interaction in a $\mathcal{PT}$-symmetric double-well potential was examined. This condensate shows a richer, much more elaborate bifurcation scenario with more states involved than in the case of a condensate with only short-range interactions. Some of these bifurcations include up to five states, and therefore allow for the possibility that exceptional points of high order exist in this system.

In the second part of this work, an analytical continuation of the Gross-Pitaevskii equation provides the mathematical tool to examine bifurcations and exceptional points in detail. An encircling of exceptional points in complex parameter space can reveal, through the exchange behaviour of the participating states, the order of the exceptional point [43]. Also additional states and bifurcations which only exist in the analytically continued space are revealed. We apply this method to the system investigated in [42] where bifurcations with up to five states have been observed.

2 Theory

In this chapter important basic theoretical concepts for this work are summarized. The first section 2.1 gives a short derivation of the Gross-Pitaevskii equation starting from the many-body Schrödinger equation. An introduction of the time-dependent variational principle is given. In section 2.2 some basic properties of bifurcation theory are presented. In order to examine the Gross-Pitaevskii equation for exceptional points it is important to understand how an equation can be analytically continued into the complex number space. In the last section 2.3 of this chapter the notion of $\mathcal{PT}$-symmetry is introduced. Also the handling of the $\mathcal{PT}$-symmetry in nonlinear systems is discussed.

2.1 Meanfield theory of Bose-Einstein condensates

Bose-Einstein condensates are ultra-cold atomic gases consisting of bosons. They form a phase, in which a macroscopic number of particles occupies the ground state. In this chapter an overview of the theoretical description of Bose-Einstein condensates will be given. A meanfield description will be derived, resulting in the Gross-Pitaevskii equation. A method will be presented, with which approximate solutions of the Gross-Pitaevskii equation can be obtained.

2.1.1 Many-body quantum dynamics

In many-body quantum theory it is postulated that, if particles are identical, they can not be distinguished [44]. In classical mechanics, if two identical particle positions are measured at time t_0, it is in principle possible to identify them for all times t

since their trajectories can be determined. This is no longer possible in quantum systems. In such systems only statistical probability predictions can be made. This has consequences for possible operators. A measurement in many-body quantum mechanics of identical particles can tell if a particle with certain properties (e.g. an electron) is at a certain position. However, it is not possible to identify exactly which particle was measured (since they are identical). Therefore only operators which fulfil the necessary symmetry conditions are applicable. Such operators can only measure if, e.g. an electron was detected, but not which one.

Using the transposition operator $\mathcal{P}_{ij}$, which exchanges the particle i with particle j, one can identify two subspaces of the Hilbert space $\mathcal{H}_N$ for N particles [44]:

- The symmetric subspace $\mathcal{H}_N^+$ of the particles which posses an integer spin. They are called bosons.
- The antisymmetric subspace $\mathcal{H}_N^-$ of particles which posses an half-integer spin (called fermions).

Fermions obey Pauli's exclusion principle, that is the occupation number of a single particle state can not be larger than one or, in other words, two identical fermions may not coincide in all their quantum numbers. On the other hand there is no such restriction for bosons which is one of the reasons that Bose-Einstein condensates can exist.

2.1.2 Bose-Einstein condensation

In contrast to Fermi gases a macroscopic occupation of the ground state for finite temperatures is possible in Bose gases. Let us consider a non-interacting Bose gas in a box potential. The energy states of such a potential are given by

$$\epsilon_{\mathbf{k}} = \frac{\hbar^2 k^2}{2m}. \tag{2.1}$$

It is now possible to show that in the limit $N \to \infty$, $V \to \infty$ and $\frac{N}{V} = n = \text{const.}$ there exists a critical temperature $T_c > 0$ at which a macroscopic occupancy of the ground state can be observed [45–47].

In a grand canonical ensemble the particle number of state $\mathbf{k}$ is given by

$$n_{\mathbf{k}} = \frac{1}{\exp\left(\beta(\epsilon_{\mathbf{k}} - \mu)\right) - 1}. \tag{2.2}$$

It becomes obvious that the relation $\mu < \epsilon_0 \leq \epsilon_{\mathbf{k}}$ must be fulfilled, otherwise there would be negative occupation numbers. With the particle number n_k in each mode, the total number of particles N, and the total energy E can be written as

$$N = \sum_{\mathbf{n}} n_{\mathbf{k}} = N_0 + N_T, \tag{2.3}$$

and

$$E = \sum_{\mathbf{n}} \epsilon_{\mathbf{k}} n_{\mathbf{k}}. \tag{2.4}$$

If the total particle number is kept constant, for decreasing temperature the chemical potential has to increase. We can separate the particles into particles N_0 which are in the condensate, that is the ground state, and particles N_T which are in an excited state and therefore do not belong to the condensate. For the particle number in the ground state, we immediately obtain

$$N_0 = \frac{1}{\exp\left(\beta(\epsilon_0 - \mu)\right) - 1}. \tag{2.5}$$

For the particles outside of the ground state

$$N_T = \sum_{\mathbf{k}\neq 0} \frac{1}{\exp\left(\beta\left(\epsilon_{\mathbf{k}} - \mu\right)\right) - 1} \tag{2.6}$$

the sum can be replaced with an integral over the wave number

$$\sum \to \frac{V}{(2\pi)^3} \int \mathrm{d}^3 k, \tag{2.7}$$

and one obtains

$$\begin{aligned} N_T &= \frac{V}{(2\pi)^3} \int \mathrm{d}^3 k \frac{1}{\exp\left(\beta\left(\frac{\hbar^2 k^2}{2m} - \mu\right)\right) - 1} \\ &= \frac{V}{(2\pi)^3} (4\pi) \int \mathrm{d}k k^2 \frac{1}{\exp\left(\beta\left(\frac{\hbar^2 k^2}{2m} - \mu\right)\right) - 1}. \end{aligned} \tag{2.8}$$

Note that this can only be done if the system is large enough, such that the energy level spacing is small compared to $k_\mathrm{B}T$. This is true if we consider the system in the thermodynamic limit. By substituting $x = \beta\hbar^2 k^2/(2m)$ one can rewrite the integral as

$$N_T = V \underbrace{\left(\sqrt{\frac{2\hbar^2\pi}{m k_\mathrm{B} T}}\right)^{-3}}_{=\lambda_T^{-3}} \underbrace{\frac{2}{\sqrt{\pi}} \int_0^\infty \frac{\sqrt{x}}{\mathrm{e}^{-\beta\mu}\mathrm{e}^x - 1}}_{=g_{\frac{3}{2}}(\mathrm{e}^{\beta\mu})} \tag{2.9}$$

with the thermal De-Broglie wave length λ_T. For the Bose integral one obtains [45]

$$g_{\frac{3}{2}}(z) = \sum_{l=1}^{\infty} \frac{z^l}{l^{\frac{3}{2}}}. \tag{2.10}$$

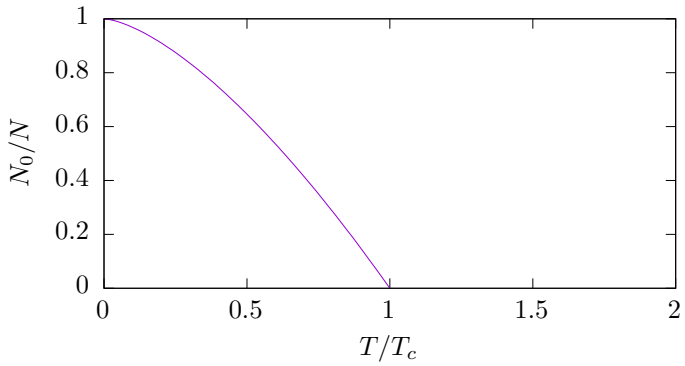

Figure 2.1.: Fraction of particles in the ground state, as function of the temperature.

If we compare the occupation in the ground state and excited states we note in equation (2.9) that the particle number N_T depends on the state density. Furthermore the maximum $\hat{N}_T$ of N_T for a given temperature is at $\mu = \epsilon_0$. We define a critical temperature T_c for which the gas is dominated by the particles in excited states, that is $N_T \to N$. From equation (2.9) it follows that

$$N = N_T(T_c, \mu = \epsilon_0 = 0) = \frac{V}{\lambda_T^3} g_{\frac{3}{2}}(1) \tag{2.11}$$

and therefore one obtains for the critical temperature

$$T_c = \frac{2\pi\hbar^2}{k_B m} \left(g_{\frac{3}{2}}(1)\right)^{-\frac{2}{3}} n^{\frac{2}{3}}. \tag{2.12}$$

For temperatures T which are smaller than the critical temperature T_c, the chemical potential cannot increase further and must remain at $\mu = \epsilon_0$, therefore with equations (2.9) and (2.12) for $\mu = \epsilon_0$ the relation

$$N_T = \left(\frac{T}{T_c}\right)^{\frac{3}{2}} N \tag{2.13}$$

follows and with equation (2.3) the particle number in the condensate must be

$$N_0 = N\left(1 - \left(\frac{T}{T_c}\right)^{\frac{3}{2}}\right) \tag{2.14}$$

for $T < T_c$. The fraction of particles in the ground state depends on the temperature and is shown in figure 2.1.

One can now obtain relevant thermodynamic values. For the energy the relation

$$E = \begin{cases} \frac{3}{2} k_B T \frac{V}{\lambda_T^3} g_{\frac{5}{2}}(1) & \text{for } T < T_c \\ \frac{3}{2} k_B T \frac{V}{\lambda_T^3} g_{\frac{5}{2}}(z) & \text{for } T > T_c \end{cases} \tag{2.15}$$

is obtained [45]. Furthermore it is now possible to obtain equations for the specific heat c_V

$$\frac{c_V}{k_B N} = \begin{cases} \frac{15}{4} \frac{v}{\lambda_T^3} g_{\frac{5}{2}}(1) & \text{for } T < T_c \\ \frac{15}{4} \frac{v}{\lambda_T^3} g_{\frac{5}{2}}(z) - \frac{9}{4} \frac{g_{\frac{3}{2}}(z)}{g_{\frac{5}{2}}(z)} & \text{for } T > T_c \end{cases}. \tag{2.16}$$

The specific heat exhibits a cusp at $T = T_c$ which indicates a phase transition.

2.1.3 Gross-Pitaevskii equation

In the preceding section, the general phenomenon of Bose-Einstein condensation was introduced. It was also shown that for very small temperatures, that is for temperatures $T \to 0\,\mathrm{K}$, almost all particles occupy the ground state. In this section we will use this property to further simplify the description by applying a meanfield ansatz to the many-particle Hamiltonian. It is clear that this ansatz cannot capture all properties of the systems. Especially effects which are driven by fluctuations and which become import for low particle numbers cannot be described by such an ansatz. However, for condensates with a sufficiently high particle number this ansatz provides a mathematical description simple enough to examine the relevant properties.

The Hamiltonian of the system is given by

$$H = \sum_{k=1}^{N} -\frac{\hbar^2}{2m} \Delta_k + V_{\text{ext}}(\mathbf{r}_k) + \frac{1}{2} \sum_{\substack{l,k=1 \\ l \neq k}}^{N} W(\mathbf{r}_k, \mathbf{r}_l), \tag{2.17}$$

with an external potential V_{ext} and a two-particle interaction $W(\mathbf{r}_k, \mathbf{r}_l)$.

It is assumed that close to $T = 0\,\mathrm{K}$, all particles are in the single particle ground state, and therefore the wave function ψ can be written with the single particle wave function ξ

$$\psi(\mathbf{r}_1, \ldots \mathbf{r}_N) = \prod_{k=1}^{N} \xi(\mathbf{r}_k). \tag{2.18}$$

The meanfield energy of the system can then be calculated by

$$E_{\text{mf}} = \langle \psi | H | \psi \rangle \tag{2.19}$$

and the norm of the single particle wave function is given by

$$1 = \int_{\mathbb{R}^3} \mathrm{d}\mathbf{r} \, |\xi(\mathbf{r})|^2. \tag{2.20}$$

Therefore the wave function of all particles is normalized to the particle number N for stationary states.

Stationary states must minimize the meanfield energy in equation (2.19) for a given ξ. The constraint (2.20) must also be fulfilled. For such a mathematical optimization problem the method of Lagrange multipliers provides a good strategy to find a solution. A minimum can be found by using μN as Lagrange multiplier and calculating the derivative of

$$E_{\mathrm{mf}} - \mu N \left(\int_{\mathbb{R}^3} \mathrm{d}\mathbf{r}\, |\xi(\mathbf{r})|^2 - 1 \right) = 0. \tag{2.21}$$

The derivative

$$-N\frac{\hbar^2}{2m}\Delta\xi(\mathbf{r}) + NV_{\mathrm{ext}}(\mathbf{r})\xi(\mathbf{r}) + N(N-1)\int_{\mathbb{R}^3} d\mathbf{r}' W(\mathbf{r},\mathbf{r}')|\xi(\mathbf{r}')|^2\xi(\mathbf{r}) = \mu\xi(\mathbf{r}) \tag{2.22}$$

can be further simplified. Since we assume that we are in the thermodynamic limit or at least have sufficiently large particles numbers, we assume

$$N - 1 \approx N \tag{2.23}$$

and therefore

$$\left[-\frac{\hbar^2}{2m}\Delta + V_{\mathrm{ext}}(\mathbf{r}) + N\int_{\mathbb{R}^3} \mathrm{d}\mathbf{r}'\, W(\mathbf{r},\mathbf{r}')|\xi(\mathbf{r}')|^2 \right] \xi(\mathbf{r}) = \mu\xi(\mathbf{r}). \tag{2.24}$$

We obtain the time-dependent Gross-Pitaevskii equation by replacing the chemical potential μ with $\mathrm{i}\hbar\frac{\partial}{\partial t}$. Then the time-dependent GPE reads

$$\left[-\frac{\hbar^2}{2m}\Delta + V_{\mathrm{ext}}(\mathbf{r}) + N\int_{\mathbb{R}^3} \mathrm{d}\mathbf{r}'\, W(\mathbf{r},\mathbf{r}')|\xi(\mathbf{r}')|^2 \right] \xi(\mathbf{r}) = \mathrm{i}\hbar\frac{\partial}{\partial t}\xi(\mathbf{r}). \tag{2.25}$$

2.1.4 Potential and interaction terms

Furthermore we must determine which interactions have to be considered in the potential term $W(\mathbf{r},\mathbf{r}')$. This part of the potential describes the interaction between two particles. In general we can split this interaction term into two interaction terms:

- The interaction between two particles (without dipolar interaction) is developed into a series using scattering theory. We consider only s-wave scattering [44] for this first term, and therefore the scattering part of the potential can be written as

  $$W_{\mathrm{sc}}(\mathbf{r},\mathbf{r}') = \frac{4\pi\hbar^2 a_{\mathrm{sc}}}{m}\delta(\mathbf{r}-\mathbf{r}') \tag{2.26}$$

  with the scattering length a_{sc}. This parameter is experimentally tuneable using Feshbach resonances [48, 49].

- If the constituents of the Bose-Einstein condensate have a dipole moment an additional dipole-dipole interaction term has to be taken into account [50],

$$W_{\mathrm{d}}(\mathbf{r},\mathbf{r}') = \frac{\mu_0\mu^2}{4\pi}\frac{1-3\cos^2\theta}{|\mathbf{r}-\mathbf{r}'|^3}, \tag{2.27}$$

  with θ being the angle between the vector $\mathbf{r}-\mathbf{r}'$ and the alignment of the dipole moments.

In order to realize a Bose-Einstein condensate in an experiment, the condensate must be localized. Therefore different traps are used. The explicit layout of the external trap potential V_{ext} depends on the trap and will be introduced later on as required.

2.1.5 Time-dependent variational principle

It is not always feasible to solve an equation like the Gross-Pitaevskii equation exactly. One way to solve an equation which can not be solved analytically, is the finite difference method. Such a method requires that the domain of the equation is discretised. The accuracy of the solution is largely determined by the points used in the grid. Such a method while feasible [50] often requires a major computational effort. Another approach is the time-dependent variational principle (TDVP) introduced by McLachlan [51]. This numerical method requires an ansatz for the wave function, which depends on various parameters. It has been found that for Bose-Einstein condensates which are trapped an ansatz of coupled Gaussians approximates the solution with very good accuracy while keeping the computational costs relatively low [52, 53]. This approach has not only been used for Bose-Einstein condensates with short-range interaction [54], but also for condensates with long-range interactions [55, 56]. In this section a general overview over the time-dependent variational principle (TDVP) will be given.

It is assumed that the wave function is parametrized by the time-dependent parameters $\mathbf{z}(t)$. We will not assume any special parametrization yet. The goal is to transform the GPE into equations of motion for these parameters. Therefore we examine the quantity

$$I = ||\mathrm{i}\frac{\mathrm{d}}{\mathrm{d}t}\psi(t) - H\psi(t)||, \tag{2.28}$$

which represents the difference between the left- and the right-hand side of the GPE. By minimizing this difference we search for solutions which best fulfil the GPE. This minimization is done by replacing $\dot{\psi}(t)$ which χ. Now for a given point in time the rate of change χ is varied. If this is a minimum the relation

$$\delta I = \langle\delta\chi|\chi\rangle + \langle\chi|\delta\chi\rangle + \mathrm{i}\langle\delta\chi|H\chi\rangle - \mathrm{i}\langle H\chi|\delta\chi\rangle \tag{2.29}$$

must vanish. Since the variation is driven by the time-derivative of the wave function χ and the wave function itself is kept constant, only the time-derivatives of the variational parameters may vary. Therefore variation of the time-derivative of the wave function reads

$$|\delta\chi\rangle = \delta|\dot{\psi}(\mathbf{z},\dot{\mathbf{z}})\rangle = \underbrace{\left|\frac{\partial\dot{\psi}}{\partial\mathbf{z}}\delta\mathbf{z}\right\rangle}_{=0,\text{ since }\delta\mathbf{z}=0} + \left|\frac{\partial\dot{\psi}}{\partial\dot{\mathbf{z}}}\delta\dot{\mathbf{z}}\right\rangle = \left|\frac{\partial}{\partial\dot{\mathbf{z}}}\left(\frac{\partial\psi}{\partial\mathbf{z}}\dot{\mathbf{z}}\right)\delta\dot{\mathbf{z}}\right\rangle. \tag{2.30}$$

By applying this relation to δI, one obtains

$$0 = \langle\delta\chi|\chi + \mathrm{i}H\psi\rangle + \langle\chi + \mathrm{i}H\psi|\delta\psi\rangle = \left\langle\frac{\partial\psi}{\partial\mathbf{z}}\delta\dot{\mathbf{z}}\middle|\dot{\psi} + \mathrm{i}H\psi\right\rangle + \left\langle\dot{\psi} + \mathrm{i}H\psi\middle|\frac{\partial\psi}{\partial\mathbf{z}}\delta\dot{\mathbf{z}}\right\rangle. \tag{2.31}$$

This relation must hold for all variations of $\delta\dot{\mathbf{z}} \in \mathbb{C}^m$, that is for real and complex variations. Therefore the equation

$$\left\langle\frac{\partial\psi}{\partial\mathbf{z}}\middle|\dot{\psi} + \mathrm{i}H\psi\right\rangle = 0 \tag{2.32}$$

remains, which can be transformed into

$$\left\langle\frac{\partial\psi}{\partial\mathbf{z}}\middle|\frac{\partial\psi}{\partial\mathbf{z}}\dot{\mathbf{z}}\right\rangle = -\mathrm{i}\left\langle\frac{\partial\psi}{\partial\mathbf{z}}\middle|H\psi\right\rangle, \tag{2.33}$$

representing the equations of motions for the variational parameters. This equation can be written in matrix form as

$$\mathbf{K}\dot{\mathbf{z}} = -\mathrm{i}\mathbf{h}. \tag{2.34}$$

For the further calculation we choose a specific parametrization of the wave function. As mentioned above an ansatz with coupled Gaussian functions provides a good approximation [52, 53]. Such an ansatz can be parametrized by

$$\psi(\mathbf{x},t) = \sum_{i=1}^{N}\exp\left(\mathbf{x}^T\mathbf{A}_k\mathbf{x} + (\mathbf{p}_k)^T\mathbf{x} + \gamma_k\right), \tag{2.35}$$

with the complex symmetric 3×3 matrices $\mathbf{A}_k$, the complex three-dimensional vectors p_k and the complex phases and amplitudes γ_k. Alternatively the parametrization [55]

$$\tilde{\mathbf{q}}_k = -\frac{1}{2}(\operatorname{Re}\mathbf{A}_k)^{-1}\operatorname{Re}p_k, \tag{2.36a}$$

$$\tilde{\mathbf{p}}_k = -\operatorname{Im}p_k - 2\operatorname{Im}\mathbf{A}_k\mathbf{q}_k \tag{2.36b}$$

with the real vectors $\tilde{\mathbf{q}}_k$ representing the position of the Gaussian and the real momentum vector $\tilde{\mathbf{p}}_k$ can be used. The first representation simplifies the following calculation and will therefore be used. So the variational parameters are $\mathbf{z} = \{\mathbf{A}_k, \mathbf{p}_k, \gamma_k\}$ with $k = 1 \dots N$.

The use of this parametrization yields for the different derivatives of the wave function

$$\frac{\partial \psi}{\partial A_k^{ij}} = -x^i x^j g_k, \qquad \frac{\partial \psi}{\partial p_k^i} = -x^i g_k, \qquad \frac{\partial \psi}{\partial \gamma_k} = -g_k, \tag{2.37}$$

and

$$\Delta g_k = -\left[2\,\mathrm{Tr}\mathbf{A}_k + 4\,\mathbf{p}_k^T \mathbf{A}_k \mathbf{x} + 4\,\mathbf{x}^T (\mathbf{A}_k)^2 \mathbf{x} + \mathbf{p}_k^T \mathbf{p}_k\right] g_k. \tag{2.38}$$

Inserted into equation (2.34) and with the Hamiltonian $H = c_{\mathrm{kin}}\Delta + V$ this results in

$$\sum_{k=1}^{N} \left[\mathrm{i}\left\langle g_l \middle| \sigma^{l,s} \middle| \dot{g}_k \right\rangle - c_{\mathrm{kin}} \langle g_l | \Delta | g_k \rangle\right] = \sum_{k=1}^{N} \langle g_l | V | g_k \rangle. \tag{2.39}$$

The different powers of x, y and z are summarized in $\sigma^{l,s}$. For each derivative of the variational parameters one equation is obtained, and indexed using l and s. The index of the Gaussian function is l, while s denotes which variational parameter of this Gaussian is used (e.g. the derivatives for the matrix element A_{xy}). As an example if we use $l = 1$ and $s = A_{xy}$ we obtain the powers $\sigma^{l,s} = x^1 y^1$ from equation (2.37). We introduce a new factor c_{kin} before the kinetic term. Later on we introduce additional factors c_i before the relevant potential terms. All nonfunctional parts are summarized in these factors, allowing for a shorter notation and easier implementation. If the terms are expanded one obtains

$$\begin{aligned} \mathrm{i}\sum_{k=1}^{N} \left\langle g_l \middle| \sigma^{l,s} \left(\sum_{m=1}^{3}\sum_{n=1}^{3} -x_m x_n \dot{A}_{k,m,n} + \sum_{m=1}^{3} -x_m \dot{p}_{k,m} + \dot{\gamma}_k \right) \middle| g_k \right\rangle \\ + c_{\mathrm{kin}} \left\langle g_l \middle| \sigma^{l,s} \left(2\mathrm{Tr}\mathbf{A}_k + 4\mathbf{p}_k^T \mathbf{A}_k \mathbf{x} + 4\mathbf{x}^T \mathbf{A}_k^2 \mathbf{x} + \mathbf{p}_k^T \mathbf{p}_k \right) \middle| g_k \right\rangle \\ = \sum_{k=1}^{N} \left\langle g_l \middle| \sigma^{l,s} V \middle| g_k \right\rangle. \end{aligned} \tag{2.40}$$

If sorted by the powers of the spacial coordinates, the equation reads

$$\begin{aligned} \sum_{k=1}^{N} \left[\sum_{m=1,n=1}^{3} \left\langle g_l \middle| \sigma^{l,s} x_m x_n \middle| g_k \right\rangle v_{2,k,m,n} + \sum_{m=1}^{3} \left\langle g_l \middle| \sigma^{l,s} x_m \middle| g_k \right\rangle v_{1,k,m} + \left\langle g_l \middle| \sigma^{l,s} \middle| g_k \right\rangle v_{0,k} \right] \\ = \sum_{k=1}^{N} \left\langle g_l \middle| \sigma^{l,s} V \middle| g_k \right\rangle, \end{aligned} \tag{2.41}$$

with

$$v_{2,k,m,n} = -\mathrm{i}\dot{A}_{k,m,n} + 4c_{\mathrm{kin}}\left(\mathbf{A}_k^2\right)_{m,n}, \tag{2.42a}$$

$$v_{1,k,m} = -\mathrm{i}\dot{p}_{k,m} + 4c_{\mathrm{kin}}\left(\mathbf{p}_k^T\mathbf{A}_k\right)_m, \tag{2.42b}$$

$$v_{0,k} = -\mathrm{i}\dot{\gamma}_k + 2\,\mathrm{Tr}\,\mathbf{A}_k + \mathbf{p}_k^T\mathbf{p}_k. \tag{2.42c}$$

The equations can be combined into a matrix equation

$$\mathbf{K}\mathbf{v} = \mathbf{r}, \tag{2.43}$$

where the entries of the matrix $\mathbf{K}$ consist of elements of the form $\langle g_l|x^\alpha y^\beta z^\gamma|g_k\rangle$. The vector $\mathbf{v}$ consist of the $v_{2,k,m,n}$, $v_{1,k,m}$ and $v_{0,k}$, while the vector $\mathbf{r}$ contains the elements of the potential $\langle g_l|\sigma^{l,s}V|g_k\rangle$. By calculating the matrix $\mathbf{K}$ and the vector $\mathbf{r}$ one can calculate the vector $\mathbf{v}$ from the linear system of equations. From the entries of $\mathbf{v}$ the time-derivatives of the variational parameters can be obtained using equation (2.42a).

2.2 Bifurcations and exceptional points

This chapter gives an introduction and recapitulation of bifurcations and exceptional points. The text is focused on the properties which are important for this work.

2.2.1 Bifurcation theory

The behaviour of most systems changes smoothly if their parameters are changed in a continuous way. However, for many systems there exist critical parameter values at which the behaviours of the systems change in a non-continuous way. At such points not only the quantitative but also the qualitative behaviour of the system might change. Such critical parameter values at which for smooth changes of the parameters the system's behaviour changes qualitatively or topologically are called bifurcation points.

Stationary solutions are usually represented by fixed points in differential equations. Let us bring this to a more precise notation. We consider the equations of motions

$$\dot{x} = g(x,\mu), \tag{2.44}$$

where x represents the state vector of the system and μ represents a system parameter. For a given μ the set $L = \{x|g(x,\mu) = 0\}$ represents the stationary solutions for this parameter. For most systems and most parameter ranges small changes in μ result in small changes of the stationary solutions. Especially if μ is changed in a smooth

manner, the solutions also change in a smooth way. However, there are systems and parameter ranges in which this is no longer true.

As an example let us consider the simple equation

$$\dot{x} = g^1(x, \mu) = \mu - x^2. \tag{2.45}$$

Immediately the two stationary solutions (that is $\dot{x} = 0$)

$$x_{1,2} = \pm\sqrt{\mu} \tag{2.46}$$

are found. For real x, solutions exist only for a positive system parameter μ. These solutions vanish at the bifurcation point $\mu = 0$. This bifurcation scenario is the well known tangent bifurcation.

A further important property change, which often occurs at a bifurcation, is the change in stability. A stationary state is stable if small disturbances do not drive the system away from the fixed point. If we consider the differential equation

$$\dot{x} = g^2(x, \mu) = \mu x - x^3, \tag{2.47}$$

which contains a pitchfork bifurcation, one observes the following stationary solutions:

$$x_1 = 0 \text{ and } x_{2,3} = \pm\sqrt{\mu}. \tag{2.48}$$

Again for a real x the solutions $x_{2,3}$ only exist for a positive system parameter μ. However, the solution x_1 exists for all μ. It undergoes a stability change at the bifurcation point $x = 0$. For $x < 0$ the solution is stable while for $x > 0$ the solution is unstable. These stability changes can have a huge impact on systems and therefore a thorough analysis of the bifurcation scenario is required.

2.2.2 Analytical continuation and multivalued functions

Before exceptional points are introduced, we recapitulate the analytical continuation of functions. Especially the construction of this function with Riemann surfaces is important since this construction method leads to multivalued functions of which properties around singularities can be exploited later on [57].

Let us consider a real function $f(x)$ which depends on the real parameter x and returns a real value $f(x)$. This function is intended to be continued to the complex plane, which is possible using a power series. If the power series expanded around the point x_0 has the radius of convergence r_0, one can obtain the values of the complex function $f(z)$ for complex values z by applying the power series to complex values. The function for the whole complex domain can be constructed by compounding power series with overlapping convergence radii. The function surfaces which are constructed in this manner are called Riemann surfaces. If one follows the function value along different parameter paths crossing multiple power series the

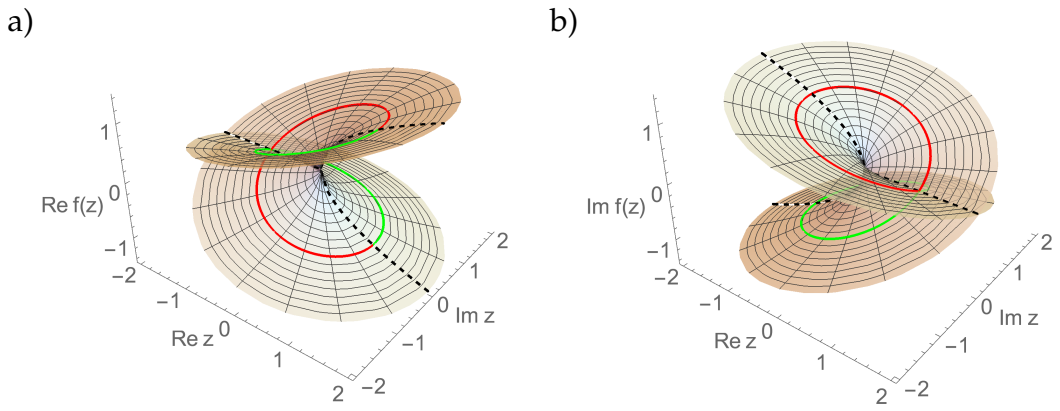

Figure 2.2.: Riemann surfaces of the complex square root function. If the argument of the function starts at $+1$ and follows the unit circle around zero, the function values follow the marked red path. After one complete circle the values $[1, -1]$ are permuted. Only if the circle is followed for one more revolution, the function returns to its original values.

function value at the target parameter has not to be unique. Functions which exhibit this behaviour are called multivalued, while functions where all paths across multiple power series result for every parameter x in the same function value are called single valued function.

One multivalued function often used as the prime example is the complex square root function,

$$f(z) = \sqrt{z}. \tag{2.49}$$

If one examines the Riemann surface shown in figure 2.2 one observes that all values z with the exception of $z = 0$ have two values $f(z)$. As an example we examine the function values for $z = 1$. We start on the surface at $f(1) = 1$. When we follow the path

$$z = \mathrm{e}^{\mathrm{i}\phi} \tag{2.50}$$

for $\phi \in [0, 2\pi]$ the value of the function changes from 1 to -1 (red line). Only if the path is followed for two full circles (red and green line) the function returns to its original value. We observe that the two surfaces are connected. Therefore the two values of the function at $\phi = 0$, that is 1 and -1, are permuted for one circle on the parameter path. This behaviour can only be observed if the path encircles the point $z = 0$. This is the only point at which the "two" surfaces coalesce and the function is single valued. At $z = 0$ the different branches of the function merge. Such a point at which multiple branches of a multivalued function coalesce is called a branch point.

In figure 2.2 the values along the real axes, i.e. $z \in \mathbb{R}$, are marked by a dashed line. If we go back to the previous section 2.2.1, these are the solutions found for the

example system which contained the tangent bifurcation. We see that branch points and bifurcations are closely related.

2.2.3 Exceptional points

In the previous example we learned about multivalued complex functions. Let us consider a linear map $L_\mu(x)$ which depends on the parameter $\mu \in \mathbb{C}$. One can calculate the eigenvalues of this linear map in dependence of the parameter μ by solving the characteristic polynomial

$$\det(L_\mu - \lambda E) = 0. \tag{2.51}$$

Depending on the parameters there can be degeneracies at which eigenvalues appear multiple times. The count of the degeneracy is called the algebraic multiplicity.

All matrices can be transformed to their Jordan normal form. If the Jordan matrix contains nontrivial Jordan blocks the size of the Jordan block is called geometrical multiplicity. If for some isolated value in the parameter space μ the eigenvalues of the linear map form a Jordan block such a point in the parameter space is called an exceptional point. At this point multiple eigenvalues of the characteristic polynomial coalesce. From the discussion of multivalued functions we know that when the exceptional point is encircled in the complex parameter space, the values permute. This is also true for the eigenvectors of the linear map. That is, if an exceptional point is encircled in the parameter space both the eigenvalues and eigenvectors permute. During the encircling of the exceptional point the eigenvectors can pick up an additional phase [58–60]. If the exceptional point is associated with a Jordan block of size n the exceptional point is of the order n [34].

Let us consider a simple two-dimensional example. The linear map is represented by the matrix $\mathbf{A} = \mathbf{A}_0 + k\mathbf{A}_1$, where $\mathbf{A}_1$ is a perturbation

$$A_0 = \begin{pmatrix} 0 & 1 \\ 0 & 0 \end{pmatrix}, \quad A_1 = \begin{pmatrix} 0 & 0 \\ 1 & 0 \end{pmatrix}. \tag{2.52}$$

It is obvious that for $k = 0$ the system is already in Jordan form and has a twofold degenerate eigenvalue. Since the Jordanblock is of size two the algebraic multiplicity is also two. Thus for $k = 0$ this system has a second-order exceptional point.

Instead of examining the block structure of the Jordan matrix we can also examine the behaviour of the eigenvectors and eigenvalues when the system is perturbed. We will follow the parameter path

$$k(\phi) = \mathrm{e}^{\mathrm{i}\phi}. \tag{2.53}$$

The eigenvalues of the system are

$$\lambda = \pm\sqrt{k}. \tag{2.54}$$

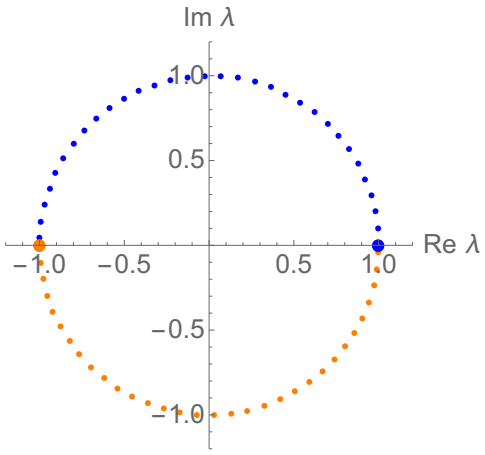

Figure 2.3.: Permutation of the eigenvalues of the linear system (2.52) while the system parameter k follows the path (2.53).

If we follow these eigenvalues from $\phi_i = 0$ to $\phi_f = 2\pi$ the parameter has returned to its original value. It is important that we stay on a continuous branch of the fractional powers (such as in this case the square root) and do not switch to different branches while following the path.

In figure 2.3 we can see the real and imaginary parts of the eigenvalues for different values of ϕ. For a complete path eigenvalue 1 ends at the starting point of eigenvalue 2 and vice versa. To return to the original state up to a phase, the path must be followed twice. The same behaviour can also be observed for the eigenvectors.

Note that this is a completely "mathematical encircling". The parameters are not changed in a physical system over time. If one would try to examine this exchange behaviour in a physical system additional effects would have to be taken into account. They may even prevent the observation of the permutation behaviour. For example additional phase changes may be introduced. In addition, since the states used for the encircling are in a physical context usually resonances and no longer stationary states they decay.

Higher-order exceptional points

If higher-order exceptional points appear in a system the signature may not be as simple as for a second-order exceptional point. Let us consider the system

$$B = B_0 + kB_1 + sB_2 \tag{2.55}$$

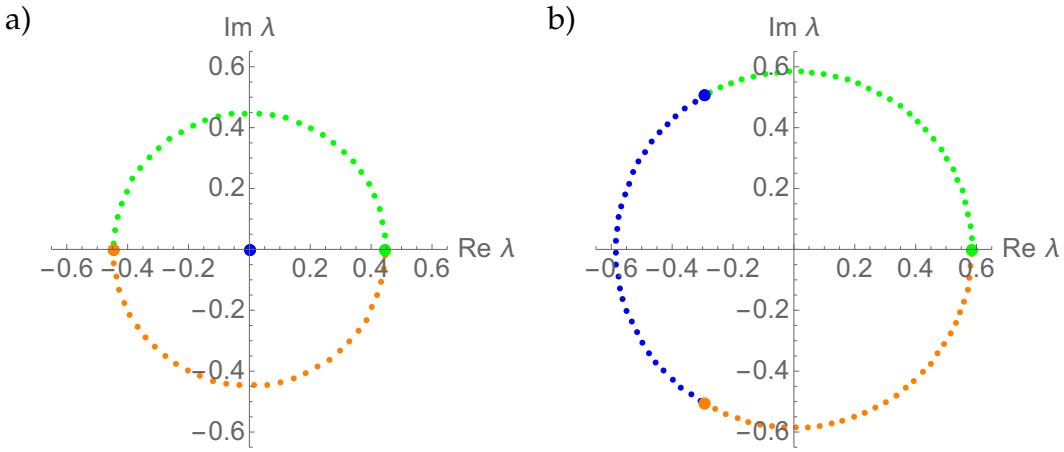

Figure 2.4.: Permutation behaviour of the eigenvalues of the system described in equation (2.55). In a) the permutation is shown in the case that the parameter s is set to zero and the exceptional point is encircled in the complex plane of parameter k. The behaviour if the roles of k and s are exchanged is shown in b). Parameter k is zero and the exceptional point is encircled in the complex parameter plane of parameter s. In a) only the permutation of two eigenvalues can be observed while the third eigenvalue is always zero. By contrast, b) shows the permutation of all three eigenvalues.

with two perturbation parameters k and s, where

$$B_0 = \begin{pmatrix} 0 & 1 & 0 \\ 0 & 0 & 1 \\ 0 & 0 & 0 \end{pmatrix} , \quad B_1 = \begin{pmatrix} 0 & 0 & 0 \\ 1 & 0 & 0 \\ 0 & 0 & 0 \end{pmatrix} , \quad B_2 = \begin{pmatrix} 0 & 0 & 0 \\ 0 & 0 & 0 \\ 1 & 0 & 0 \end{pmatrix} . \tag{2.56}$$

From the matrix structure one directly obtains the Jordan form for $k = s = 0$. The block size is three, and therefore this system contains a third-order exceptional point. One naively expects that, when the exceptional point is encircled in the complex parameter space of a perturbation parameter, one will observe the permutation between three states. While this may be true for many perturbation it is not for all.

As shown in [38] the element $b_{n,1}$, that is the matrix entry in the first column in the last row of the perturbation matrix, must be nonzero. In the example above this is true for the matrix $\mathbf{B}_2$ but not for $\mathbf{B}_1$. Let us examine the eigenvalues for $s = 0$. In figure 2.4 the results for an encircling of the exceptional point with the parameter k is shown. We see that only a square root behaviour similar to that of a second-order exceptional point is observed. If we instead perturb the system with the parameter s and set k to zero, the full permutation behaviour between all three states is observed (see figure 2.4).

Since we cannot simply calculate a Jordan matrix for a Bose-Einstein condensate

described by the Gross-Pitaevskii equation [60], we will search for signatures of exceptional points. If the parameters of a system are changed in such a way that they describe a closed path and for this path the values of the chemical potential and the wave functions of the system are permuted, we know that an exceptional point lies within the area enclosed by the path. It is important that the number of states which permute only gives a lower limit for the order of the exceptional point. Indeed many physical parameters which naturally lend themselves to be used as perturbation parameters do not exhibit the signature of the full order of the exceptional point.

2.3 $\mathcal{PT}$ symmetry

In quantum mechanics physical properties, such as position or momentum, are not necessarily good variables for the precise definition of a state of the system. Instead a physical state is represented by a wave function, a Hilbert space vector, which contains the probability that a certain value for a physical property is measured. These measurements are represented by operators. The possible outcomes of a measurement are the eigenvalues of these operators. Since the physical property has to be represented by a real value this has to be ensured by the formalism. In conventional quantum mechanics Hermitian operators are used to fulfil this requirement. However, there exist other operator classes which have or can have a real eigenvalue spectrum. Bender et al. [61] found that $\mathcal{PT}$-symmetric operators are suitable to fulfil this requirement.

2.3.1 Parity and time-reversal operators

The $\mathcal{PT}$ operator is the combination of the parity operator $\mathcal{P}$ and the time-reversal operator $\mathcal{T}$. The parity operator exchanges the signs of the position and momentum operators, while the time-reversal operator introduces a change in sign for the momentum operator and the imaginary unit, i.e.

$$\mathcal{P}: \quad \hat{\mathbf{x}} \to -\hat{\mathbf{x}}, \quad \hat{\mathbf{p}} \to -\hat{\mathbf{p}}, \tag{2.57a}$$

$$\mathcal{T}: \quad \hat{\mathbf{x}} \to \hat{\mathbf{x}}, \quad \hat{\mathbf{p}} \to -\hat{\mathbf{p}}, \quad \mathrm{i} \to -\mathrm{i}. \tag{2.57b}$$

In order to examine the $\mathcal{PT}$ operator it is important to consider the properties of the $\mathcal{P}$ and $\mathcal{T}$ operators separately. The parity operator is a linear operator, that is

$$\mathcal{P}\left(\lambda|\psi\rangle + \mu|\phi\rangle\right) = \lambda\mathcal{P}|\psi\rangle + \mu\mathcal{P}|\phi\rangle. \tag{2.58}$$

By contrast the time-reversal operator is antilinear, that is the following relation is true,

$$\mathcal{T}\left(\lambda|\psi\rangle + \mu|\phi\rangle\right) = \lambda^*\mathcal{T}|\psi\rangle + \mu^*\mathcal{T}|\phi\rangle. \tag{2.59}$$

Applying the $\mathcal{PT}$ operator twice has no effect. By analysing, with the help of the previously mentioned properties, the effect of the twofold application of the $\mathcal{PT}$ operator has on an eigenfunction $\psi(x)$ with the eigenvalue λ, that is,

$$\mathcal{PT}|\psi\rangle = \lambda|\psi\rangle, \tag{2.60}$$

we obtain

$$|\psi\rangle \stackrel{!}{=} \mathcal{PTPT}|\psi\rangle = \mathcal{PT}\lambda|\psi\rangle = \lambda^*\mathcal{PT}|\psi\rangle = \lambda^*\lambda|\psi\rangle, \tag{2.61}$$

and therefore λ must have the norm one. By applying a global phase to the wave function one can obtain $\lambda = 1$, which is called exact $\mathcal{PT}$ symmetry. In this case the real part of the wave function in position space representation is an even function, while the imaginary part is odd.

2.3.2 Linear $\mathcal{PT}$-symmetric systems

We consider a state $|\psi\rangle$ which is an eigenstate of $\mathcal{H}$ and the $\mathcal{PT}$ operator. Without loss of generality we choose the global phase such that the eigenvalue of $|\psi\rangle$ with respect to the $\mathcal{PT}$ operator is equal to unity. Such a state fulfils the relation

$$\mathcal{H}|\psi\rangle = \mu|\psi\rangle. \tag{2.62}$$

The Hamiltonian $\mathcal{H}$ is $\mathcal{PT}$-symmetric, if $[\mathcal{H}, \mathcal{PT}] = 0$. In position space it is of the form $\mathcal{H} = -\Delta + V(\hat{\mathbf{x}})$. Thus, in order to be $\mathcal{PT}$-symmetric the potential must fulfil the condition

$$V(\hat{\mathbf{x}}) = V^*(-\hat{\mathbf{x}}). \tag{2.63}$$

By application of the $\mathcal{PT}$ operator to both sides of equation (2.62), and by using the relation $[\mathcal{H}, \mathcal{PT}] = 0$ as well as the antilinearity of the $\mathcal{PT}$ operator (2.60), one obtains

$$\begin{aligned} \mathcal{PTH}|\psi\rangle &= \mathcal{PT}\mu|\psi\rangle, \\ \mathcal{HPT}|\psi\rangle &= \mu^*\mathcal{PT}|\psi\rangle, \\ \mathcal{H}|\psi\rangle &= \mu^*|\psi\rangle, \\ \mu|\psi\rangle &= \mu^*|\psi\rangle. \end{aligned} \tag{2.64}$$

Hence, all eigenstates of the $\mathcal{PT}$-operator have real eigenvalues [11, 61]. Such states have unbroken $\mathcal{PT}$ symmetry. If a state does not fulfil $\mathcal{PT}$ symmetry, an eigenvalue, which is not real, will change the norm

$$\|\psi\|^2 = \mathrm{e}^{\frac{2\,\mathrm{Im}\,\mu t}{\hbar}} \tag{2.65}$$

and therefore is not a stationary state. If such a state ψ_a with eigenvalue μ_a exists, the state $\psi_b = \mathcal{PT}\psi_a$ has the complex conjugate eigenvalue $\mu_b = {\mu_a}^*$.

2.3.3 Nonlinear $\mathcal{PT}$-symmetric systems

If the system is nonlinear, that is the Hamiltonian contains a nonlinear part, the analysis has to be extended [62]. Consider a nonlinear equation (such as the Gross-Pitaevskii equation),

$$H_{\text{lin}}|\psi\rangle + f(|\psi\rangle)|\psi\rangle = i\frac{\partial}{\partial t}|\psi\rangle, \tag{2.66}$$

which is composed of the linear, $\mathcal{PT}$-symmetric part H_{lin}, that is $[H_{\text{lin}}, \mathcal{PT}] = 0$, and the nonlinear part $f(\psi)$. In the Gross-Pitaevskii equation the nonlinearity consists of the square modulos, and therefore does not depend on the global phase of $|\psi\rangle$. We assume that f is independent of the global phase, i.e.

$$f(\mathrm{e}^{\mathrm{i}|\phi\rangle}|\psi\rangle) = f(|\psi\rangle). \tag{2.67}$$

A nonlinear system is called $\mathcal{PT}$-symmetric if the relation

$$\mathcal{PT}\left(H_{\text{lin}} + f(|\psi\rangle)\right) = \left(H_{\text{lin}} + f(\mathcal{PT}|\psi\rangle)\right)\mathcal{PT} \tag{2.68}$$

holds true. In addition to a $\mathcal{PT}$-symmetric linear operator the nonlinear part of the equation has to fulfil the condition

$$\mathcal{PT}f(|\psi\rangle)|\psi\rangle = f(\mathcal{PT}|\psi\rangle)\mathcal{PT}|\psi\rangle. \tag{2.69}$$

Thus, nonlinear systems impose additional requirements on $\mathcal{PT}$-symmetric states. For a $\mathcal{PT}$-symmetric system the nonlinearity enforces that the state itself must be $\mathcal{PT}$-symmetric. In this case real eigenvalues are observed.

If μ is an eigenvalue and $|\psi\rangle$ the eigenstate of H, one obtains

$$H_{\text{lin}}|\psi\rangle + f(|\psi\rangle)|\psi\rangle = \mu|\psi\rangle. \tag{2.70}$$

If the $\mathcal{PT}$operator is applied to the equation one obtains

$$\mathcal{PT}\left[H_{\text{lin}}|\psi\rangle + f(|\psi\rangle)\right]|\psi\rangle = \mu\mathcal{PT}|\psi\rangle, \tag{2.71}$$

$$H_{\text{lin}}\mathcal{PT}|\psi\rangle + f(\mathcal{PT}|\psi\rangle)\mathcal{PT}|\psi\rangle = \mu^*\mathcal{PT}|\psi\rangle. \tag{2.72}$$

That is, if $|\psi\rangle$ is an eigenstate with the eigenvalue μ, the state $\mathcal{PT}|\psi\rangle$ is also an eigenstate, but with the eigenvalue μ^*. As for the linear case, if the state is $\mathcal{PT}$-symmetric, i.e., $\mathcal{PT}|\psi\rangle = |\psi\rangle$, the eigenvalue is real.

3 $\mathcal{PT}$-symmetric embedded double-well BEC

In the previous chapter the foundation was laid to understand $\mathcal{PT}$-symmetric systems. It was shown that a $\mathcal{PT}$-symmetric system shows special properties such as a real eigenvalue spectra, even if the Hamiltonian is non-Hermitian. In the first part of this chapter we recapitulate some basic properties of a $\mathcal{PT}$-symmetric double well system [63]. In the next section a two-mode double-well system based on this double-well system is constructed, where each of the two subsystems will serve as the environment of the other. The system itself will be Hermitian. We present different models (see section 3.2), which have different degrees of spatial resolution. The simplest model is a four-dimensional matrix model. For this model analytical solutions are calculated in section 3.3. The bifurcation structures of these solutions and how they differ when compared to the bifurcation diagram of the two-dimensional matrix model is presented in section 3.4. In section 3.5 the probability currents for the different states are shown. In the last section 3.6 of the chapter, the different models from section 3.2 are compared. Most of the results from this chapter are published in [33].

3.1 $\mathcal{PT}$-symmetric double-well system

In the previous section 2.3 the foundation was laid to understand $\mathcal{PT}$-symmetric systems. It was shown that a $\mathcal{PT}$-symmetric system shows special properties such as a real eigenvalue spectra, even if the Hamiltonian is non-Hermitian. In this section the results of one of the simplest possible systems where $\mathcal{PT}$ symmetry can be observed, and which was examined in much detail over the recent years, will be recapitulated. Since systems in the real world are hardly ever completely isolated, the environment must be taken into account. Due to a lack of knowledge about the actual layout of the environment of a system or because the environment is too complicated to be taken into account completely, one can effectively describe such systems as open quantum

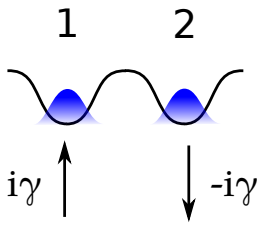

Figure 3.1.: Sketch of a double-well systems coupled to an external reservoir. Particles are incoupled into the left well and outcoupled from the right well.

systems as long as the interaction to the environment is known. Such Hamiltonians are often no longer Hermitian. The interaction with the environment, e.g. gain and loss of the probability amplitude, can be expressed by complex potentials [64]. These Hamiltonians in general do not have a real eigenvalue spectrum.

In [65] it was suggested that $\mathcal{PT}$-symmetry could also be realized in quantum systems, namely in Bose-Einstein condensates. The BEC is supposed to be located in a symmetric double-well potential where particles are gained in one well and lost in the other. This loss and gain can then be described by a complex potential coupling the system to the environment. Figure 3.1 illustrates such a system.

The time-independent solutions of such a $\mathcal{PT}$-symmetric double-well system can, in the simplest possible case, be modeled by the matrix [63]

$$\begin{pmatrix} -g|\psi_1|^2 - \mathrm{i}\gamma & v \\ v & -g|\psi_2|^2 + \mathrm{i}\gamma \end{pmatrix} \begin{pmatrix} \psi_1 \\ \psi_2 \end{pmatrix} = \mu \begin{pmatrix} \psi_1 \\ \psi_2 \end{pmatrix}, \tag{3.1}$$

where ψ_1 and ψ_2 represent the occupations of the two wells with atoms in the condensed phase and μ is the chemical potential. This description can be derived from a non-Hermitian representation of a many-particle Bose-Hubbard dimer [37]. The off-diagonal elements v of the matrix describe the couplings between the wave functions in the two potential wells. The diagonal contains a nonlinear entry introducing the particle-particle interaction described by an s-wave scattering process. Its strength can be changed via the parameter g, which is proportional to the s-wave scattering length, and its physical variation can be achieved close to Feshbach resonances. In comparison to the original model from [63] the replacement $g \to -g$ is introduced to be consistent with the other models in this thesis. In addition the diagonal contains an imaginary term with the parameter γ. This term models a particle gain in one well and a particle loss in the other. This gain and loss is provided by the (not further described) environment. The wave functions consist of two complex values and contain no spatial information. Therefore the parity operator $\mathcal{P}$, which normally exchanges $\hat{x}$ with $-\hat{x}$, exchanges ψ_1 with ψ_2 and vice versa. It is also assumed that the potential

wells are isolated enough such that the nonlinear interaction between ψ_1 and ψ_2 can be neglected.

The system (3.1) is solved analytically [63] for wave function vectors ψ which are normalized to one. The chemical potential reads

$$\mu_s = -\frac{g}{2} \pm \sqrt{v^2 - \gamma^2}, \tag{3.2a}$$

$$\mu_a = -g \pm \gamma \sqrt{\frac{4v^2}{g^2 + 4\gamma^2} - 1}. \tag{3.2b}$$

The values μ_s in (3.2) are the $\mathcal{PT}$-symmetric solutions, and the $\mathcal{PT}$-broken solutions of the system are denoted μ_a. All solutions are shown in figure 3.2. For small γ the system without nonlinearity ($g = 0$) shows only $\mathcal{PT}$-symmetric states with real chemical potential $\mu \in \mathbb{R}$ as can be observed in figure 3.2a. These states pass through a tangent bifurcation at $\gamma = \gamma_c = 1$, and two $\mathcal{PT}$-broken states emerge. For $\gamma > \gamma_c$ only $\mathcal{PT}$-broken states with a complex chemical potential $\mu \in \mathbb{C}$ exist.

For a nonlinearity $g > 0$ the bifurcation, in which the two $\mathcal{PT}$-broken states are created, moves to a smaller value of γ on one of the $\mathcal{PT}$-symmetric branches (compare figure 3.2b). A pitchfork bifurcation is formed. Thus, for nonzero values of g there is an additional parameter region for γ, in which $\mathcal{PT}$-symmetric and $\mathcal{PT}$-broken states exist simultaneously. When the nonlinearity is increased even further ($g > 2$) we see in figure 3.2c that the pitchfork bifurcation is no longer present and the $\mathcal{PT}$-broken states exist for all values of γ. A thorough examination of the bifurcation structure and of the associated exceptional points can be found in [40].

The matrix model does not take the spatial extension of the system into account. In general BECs can be described by the nonlinear Gross-Pitaevskii equation [45]. Often δ functions have been used to gain a deeper insight [13, 14, 66–76]. Therefore a simple model to include spatial effects describes the potential with double-δ functions [77]. In this system two δ-wells exist at the positions $x = \pm b$. While both of these wells have the same real depth they possess antisymmetric imaginary parts. That is, one well has a particle gain and the other has an equally strong particle drain.

The potential fulfils the $\mathcal{PT}$-symmetry condition (2.63). The corresponding Gross-Pitaevskii equation is

$$-\psi''(x) - \left[(1 + \mathrm{i}\gamma)\delta(x + b) + (1 - \mathrm{i}\gamma)\delta(x - b)\right]\psi(x) - g|\psi(x)|^2\psi(x) = \mu\psi(x). \tag{3.3}$$

In this system $\mathcal{PT}$-symmetric solutions and $\mathcal{PT}$-symmetry breaking were found.

In [78, 79] a similar double-well system was examined in much greater detail by using a more realistic potential well shape. The Gross-Pitaevskii equation of such a BEC can be written as

$$(-\Delta + V(x) - g|\psi(x,t)|^2)\psi = \mu\psi \tag{3.4}$$

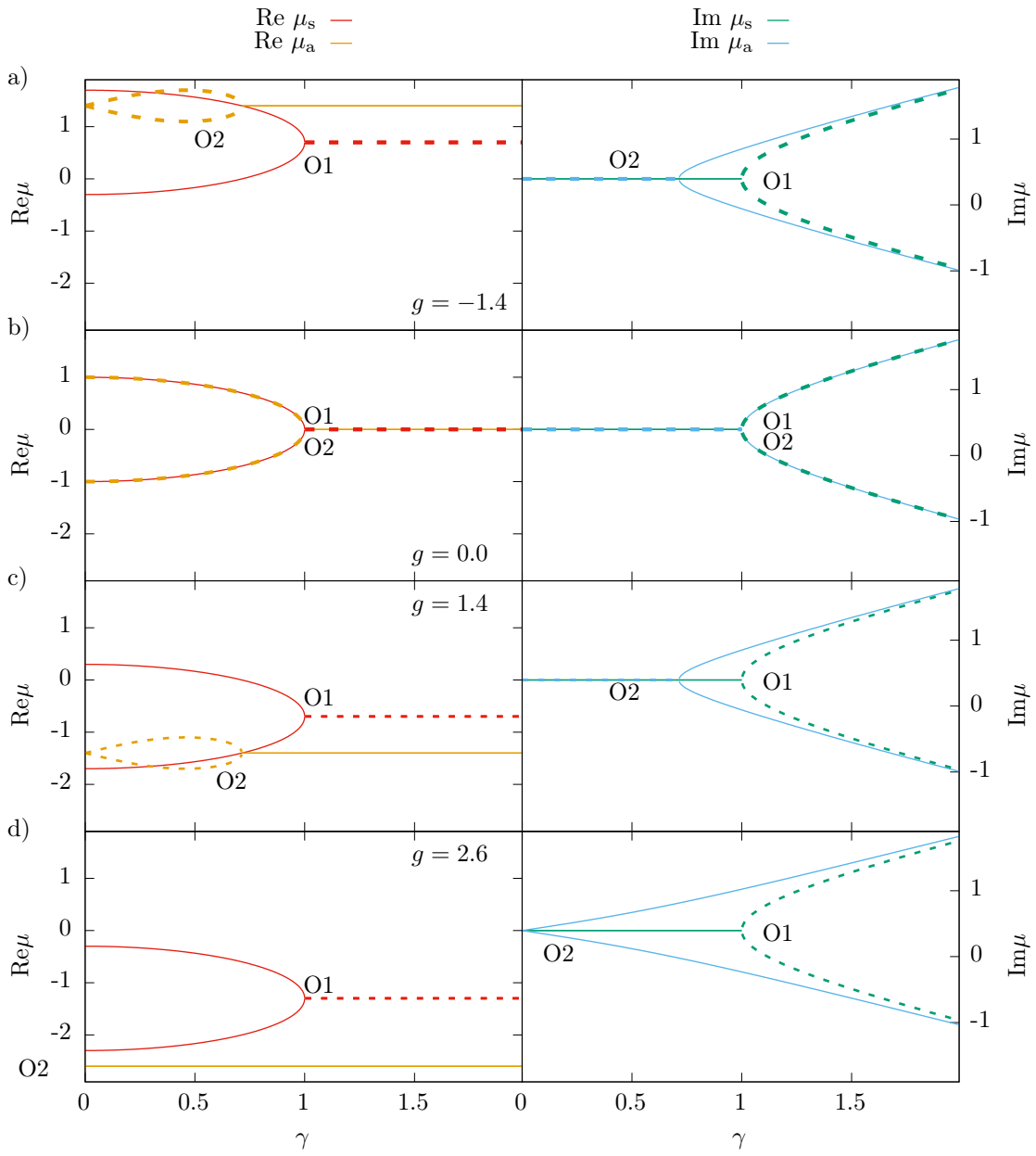

Figure 3.2.: Analytic solutions for the chemical potential (3.2) of the two-dimensional matrix model described in (3.1). The coupling strength $v = 1$, and the nonlinearities $g = -1.4$ in a), $g = 0$ in b), $g = 1.4$ in c) and $g = 2.6$ in d) are used. The analytically continued solutions are plotted using dashed lines.

with the complex potential

$$V(x) = \frac{1}{4}x^2 + V_0^{\mathrm{G}} \mathrm{e}^{-\sigma x^2} + \mathrm{i}\gamma x \mathrm{e}^{-\rho x^2} \quad \text{and } \rho = \frac{\sigma}{2\ln(4V_0^{\mathrm{G}}\sigma)} \tag{3.5}$$

containing the BEC in a harmonic trap divided by a Gaussian potential barrier into two wells. The parameter ρ is chosen in such a way that the maximal coupling between the system and the environment occurs at the minima of the potential wells. The stationary states show the same general behaviour as those in the matrix model.

3.2 Construction of a Hermitian two-mode double-well system

All descriptions so far were focused on complex potentials to effectively describe the environment. Therefore only the $\mathcal{PT}$-symmetric part of the whole system was described in detail while the concrete layout of the environment itself was not specified. We will now discuss how it might be possible to embed such a $\mathcal{PT}$-symmetric two-well system into a larger Hermitian system and therefore explicitly include the environment into our description.

As a first step in this direction a Hermitian four-well model was used [80, 81], where the double-well with in- and outgoing particle fluxes is achieved by embedding it into the larger system. The two outer wells have time-dependent adjustable parameters namely the potential depth and the coupling strength to the inner wells. By lowering and raising these wells a particle gain and loss in the two inner wells can be obtained, which exactly corresponds to the loss and gain in the non-Hermitian two-well model. However, the $\mathcal{PT}$-symmetric subsystem of the inner wells loses its properties when the well which provides the particle gain is depleted. A second possible realization was suggested in [82], where the wave function of a double-well potential was coupled to additional unbound wave functions (e.g. one ingoing and one outgoing) connecting the gain and loss of the system with a reservoir. These auxiliary wave functions replace the previously unknown environment of the system.

Here an additional way of realizing a $\mathcal{PT}$-symmetric two-well system is proposed. By modifying the approach used in [82] we couple two stationary wave functions. Each of them is bound in a double-well system, which has the shape of the $\mathcal{PT}$-symmetric system discussed in section 3.1. The combination results in a Hermitian system. The influx from one system originates from the second and vice versa. By tuning the coupling strength between the two systems we will be able to control the gain and loss in the subsystems. In contrast to [82] our systems are closed and do not require incoming or outgoing wave functions or time-dependent potentials. We will

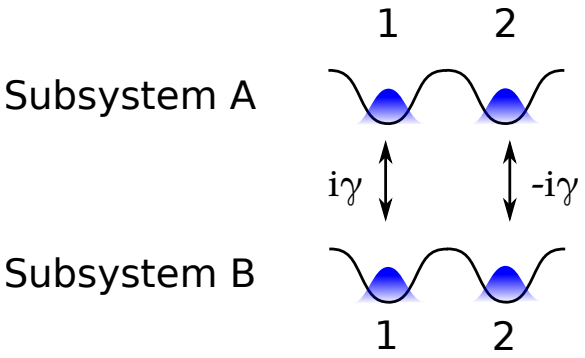

Figure 3.3.: Sketch of two double-well subsystems are combined into a closed Hermitian system. The coupling and description of the wells is given with a varying degree of detail for the different systems discussed in this thesis.

show that for suitable states the subsystems are indeed $\mathcal{PT}$-symmetric, however, also $\mathcal{PT}$-symmetry breaking can be observed.

In figure 3.3 the layout of two coupled two-well systems is sketched. The two subsystems are labelled A and B and each contains two wells with the labels 1 and 2. In the drawing the potentials of the wells are extended. This corresponds to an ansatz as shown in equations (3.4) and (3.5) and will be one of the systems studied in this work. Each of the wells is coupled to its counterpart in the other subsystem. The coupling strength is described by the parameter γ. Since the strength of the in- and outcoupling is also determined by the wave function of the other subsystem, $\mathcal{PT}$-symmetry can only exist for both subsystems. There is no $\mathcal{PT}$-symmetry for arbitrary states but only for states with an appropriate symmetry between the two systems.

From this system also a much simpler four-dimensional matrix model can be derived. For this model it is even possible to find some analytical solutions.

3.2.1 Gross-Pitaevskii equation of the extended two-mode double-well system

In order to construct a two-mode model we now introduce a concrete trap potential for the Gross-Pitaevskii equation (2.25). We also restrict the spatial description to one dimension. We assume that the two modes are contained in a potential similar to (3.5). However the in- and outcoupling of particles due to a complex potential is replaced by terms coupling the two modes to each other. Therefore the remaining

potential consists of a Gaussian well and a harmonic barrier,

$$V(x) = \frac{1}{4}x^2 + V_0^G \mathrm{e}^{-\sigma x^2}. \tag{3.6}$$

The depth of the potential is given by V_0^G, while its width of is described by σ. With this potential the Gross-Pitaevskii equations of the two coupled modes read

$$(-\partial_x^2 + V(x) - g|\psi_A|^2)\psi_A + \mathrm{i}\gamma x \mathrm{e}^{-\rho x^2}\psi_B = \mathrm{i}\partial_t \psi_A, \tag{3.7a}$$

$$(-\partial_x^2 + V(x) - g|\psi_B|^2)\psi_B + \mathrm{i}\gamma x \mathrm{e}^{-\rho x^2}\psi_A = \mathrm{i}\partial_t \psi_B. \tag{3.7b}$$

In these equations the strength of the coupling between the two modes is given by the coupling parameter γ. The coupling is spatially stretched over an area described by a Gaussian and the width of the coupling is given by ρ. In the following the parameters are chosen as

$$\sigma = \frac{1}{2} \quad \text{and} \quad \rho = \frac{1}{12\log 2}. \tag{3.8}$$

Since we only consider one spatial dimension in our description the time-dependent variational principle introduced in section 2.1 can be simplified. The ansatz of coupled Gaussians used to solve the Gross-Pitaevskii equations (3.7) is

$$\psi(x) = \sum_{i=1}^{N} g_i(x) = \sum_{i=1}^{N} \exp\left(a_i x^2 + b_i x + c_i\right). \tag{3.9}$$

Since the equation is one-dimensional the a_i and b_i are simple scalar quantities and no longer matrices or vectors.

One can also use a description of the model which reduces the detail of spatial description of the well by replacing them with δ-functions. While any spatial information from the wells is lost, this description retains a spatial extended wave function, e.g. effects due to an overlap of the wave-functions from different wells still are present. The system is described by

$$\begin{aligned}\Big[-\frac{\partial^2}{\partial x^2} - g|\psi_\mathrm{A}|^2 + V_0^\mathrm{D}(\delta(x-b)+\delta(x+b))\Big]\psi_A \\ +\mathrm{i}\gamma\left[\delta(x-b)\psi_B(b) - \delta(x+b)\psi_B(-b)\right] = \mu_A\psi_A,\end{aligned} \tag{3.10a}$$

$$\begin{aligned}\Big[-\frac{\partial^2}{\partial x^2} - g|\psi_\mathrm{B}|^2 + V_0^\mathrm{D}(\delta(x-b)+\delta(x+b))\Big]\psi_B \\ -\mathrm{i}\gamma\left[\delta(x-b)\psi_A(b) - \delta(x+b)\psi_A(-b)\right] = \mu_B\psi_B,\end{aligned} \tag{3.10b}$$

where the parameter b determines the distance of the delta functions from the center, while the potential depth is given by V_0^D. Results for this model can be found in [83], and we will compare these results with those from equation (3.7).

3.2.2 Derivation of a matrix model with an ansatz of frozen Gaussians

For the general qualitative behaviour we want to derive a matrix model. The derivation of a matrix model from a spatially extended model is performed here for the two-mode model from figure 3.3. However, the simple double-well matrix model can be derived in a similar fashion. We will reduce the parameter count by freezing the shape of the Gaussian functions over time [84, 85].

Starting with the extended description and the ansatz of fixed Gaussians for the wave function we divide each Gaussian function into an amplitude and phase parameter and a term containing the shape, viz.

$$|\psi_i\rangle = \sum_{j=1,2} \underbrace{\phi_{i,j}}_{\text{amplitude and phase}} \underbrace{|s_{i,j}\rangle}_{\text{shape}}, \tag{3.11}$$

with $i = A, B$ and the shape

$$s(x) = \mathrm{e}^{a_{i,j}(x-q_{i,j})^2 + p_{i,j}(x-q_{i,j})}, \tag{3.12}$$

where $a_{i,j} \in \mathbb{C}$ and $p_{i,j}, q_{i,j} \in \mathbb{R}$. In order to derive a matrix model we assume that the shape of the Gaussian function is frozen over time and only the amplitude and phase parameter changes. The system can be rewritten as

$$\left(\underbrace{-\partial_x^2 + \frac{1}{4}x^2 + V_0^G \mathrm{e}^{-\sigma x^2} - g|\psi_A|^2}_{H_A} \right) \psi_A + \underbrace{\mathrm{i}\gamma x \mathrm{e}^{-\rho x^2}}_{H_{AB}} \psi_B = \mathrm{i}\partial_t \psi_A, \tag{3.13}$$

$$\left(\underbrace{-\partial_x^2 + \frac{1}{4}x^2 + V_0^G \mathrm{e}^{-\sigma x^2} - g|\psi_B|^2}_{H_B} \right) \psi_B + \underbrace{\mathrm{i}\gamma x \mathrm{e}^{-\rho x^2}}_{H_{AB}} \psi_A = \mathrm{i}\partial_t \psi_B. \tag{3.14}$$

If the ansatz of fixed Gaussians (3.11) is inserted into the equation and the equation

is multiplied with $\langle s_{A,1}|$ and $\langle s_{A,2}|$ we obtain the matrix equation for mode A

$$\begin{aligned}
&\underbrace{\begin{pmatrix} \langle s_{A,1}|H_A|s_{A,1}\rangle & \langle s_{A,1}|H_A|s_{A,2}\rangle \\ \langle s_{A,2}|H_A|s_{A,1}\rangle & \langle s_{A,2}|H_A|s_{A,2}\rangle \end{pmatrix}}_{G_A} \underbrace{\begin{pmatrix} \phi_{A,1} \\ \phi_{A,2} \end{pmatrix}}_{\phi_A} \\
&\qquad + \underbrace{\begin{pmatrix} \langle s_{A,1}|H_{AB}|s_{B,1}\rangle & \langle s_{A,1}|H_{AB}|s_{B,2}\rangle \\ \langle s_{A,2}|H_{AB}|s_{B,1}\rangle & \langle s_{A,2}|H_{AB}|s_{B,2}\rangle \end{pmatrix}}_{G_{AB}} \underbrace{\begin{pmatrix} \phi_{B,1} \\ \phi_{B,2} \end{pmatrix}}_{\phi_B} \\
&\qquad\qquad = \mathrm{i} \underbrace{\begin{pmatrix} \langle s_{A,1}|s_{A,1}\rangle & \langle s_{A,1}|s_{A,2}\rangle \\ \langle s_{A,2}|s_{A,1}\rangle & \langle s_{A,2}|s_{A,2}\rangle \end{pmatrix}}_{K_A} \partial_t \underbrace{\begin{pmatrix} \phi_{A,1} \\ \phi_{A,2} \end{pmatrix}}_{\phi_A}, \qquad (3.15)
\end{aligned}$$

and in the same manner one obtains for the mode B

$$\begin{aligned}
&\underbrace{\begin{pmatrix} \langle s_{B,1}|H_B|s_{B,1}\rangle & \langle s_{B,1}|H_B|s_{B,2}\rangle \\ \langle s_{B,2}|H_B|s_{B,1}\rangle & \langle s_{B,2}|H_B|s_{B,2}\rangle \end{pmatrix}}_{G_B} \underbrace{\begin{pmatrix} \phi_{B,1} \\ \phi_{B,2} \end{pmatrix}}_{\phi_B} \\
&\qquad + \underbrace{\begin{pmatrix} \langle s_{B,1}|H_{BA}|s_{A,1}\rangle & \langle s_{B,1}|H_{BA}|s_{A,2}\rangle \\ \langle s_{B,2}|H_{BA}|s_{A,1}\rangle & \langle s_{B,2}|H_{BA}|s_{A,2}\rangle \end{pmatrix}}_{G_{BA}} \underbrace{\begin{pmatrix} \phi_{A,1} \\ \phi_{A,2} \end{pmatrix}}_{\phi_A} \\
&\qquad\qquad = \mathrm{i} \underbrace{\begin{pmatrix} \langle s_{B,1}|s_{B,1}\rangle & \langle s_{B,1}|s_{B,2}\rangle \\ \langle s_{B,2}|s_{B,1}\rangle & \langle s_{B,2}|s_{B,2}\rangle \end{pmatrix}}_{K_B} \partial_t \underbrace{\begin{pmatrix} \phi_{B,1} \\ \phi_{B,2} \end{pmatrix}}_{\phi_B}. \qquad (3.16)
\end{aligned}$$

The two equations (3.15) and (3.16) can be combined to

$$\mathrm{i} \begin{pmatrix} K_A & 0 \\ 0 & K_B \end{pmatrix} \begin{pmatrix} \dot{\phi}_A \\ \dot{\phi}_B \end{pmatrix} = \begin{pmatrix} G_A & G_{AB} \\ G_{BA} & G_B \end{pmatrix} \begin{pmatrix} \phi_A \\ \phi_B \end{pmatrix} \qquad (3.17)$$

with the two 2×2-matrices K_i, G_i and the two-dimensional vectors ϕ_i.

For the final matrix model we assume that the overlap between the wave functions in well one and two of a subsystem is small. Therefore we set the off-diagonal elements of K_A and K_B to zero. In principle this can be achieved by a strong barrier. We will verify this assumption in section 3.6. We can choose the norm of the shapes such that the relation

$$\langle s_{i,j}|s_{i,j}\rangle = 1 \qquad (3.18)$$

is fulfilled. Therefore the matrices K_A and K_B become identity matrices. Let us consider the matrices on the right hand side of equation (3.17). The diagonal parts of G_A and G_B consist of terms of the form

$$\left\langle s_{A,1} \middle| -\partial_x^2 + \frac{1}{4}x^2 + V_0^G \mathrm{e}^{-\sigma x^2} \middle| s_{A,1} \right\rangle = \mu_{\text{offset}}, \qquad (3.19)$$

which lead to an offset of the chemial potential (and will be omitted from here on), and terms of the form

$$\left\langle s_{A,1}\middle|-g|\psi_A|^2\middle|s_{A,1}\right\rangle = -\tilde{g}|\phi_A|^2. \tag{3.20}$$

In this case the shape of the wave functions leads to a scaled nonlinearity $\tilde{g}$. For the off-diagonal elements the first terms of the form

$$\left\langle s_{A,1}\middle|-\partial_x^2+\frac{1}{4}x^2+V_0^G\mathrm{e}^{-\sigma x^2}\middle|s_{A,2}\right\rangle = v \tag{3.21}$$

lead to a coupling constant between the two wells and the second part

$$\left\langle s_{A,1}\middle|-g|\psi_A|^2\middle|s_{A,2}\right\rangle = -g|\psi_A|^2\langle s_{A,1}|s_{A,2}\rangle \approx 0 \tag{3.22}$$

is assumed to be zero because of the vanishing overlap.

Last, we analyze the off-diagonal matrices G_{AB} and G_{BA}. The terms of the form

$$\left\langle s_{A,1}\middle|\mathrm{i}\gamma x\mathrm{e}^{-\rho x^2}\middle|s_{B,1}\right\rangle = \mathrm{i}\tilde{\gamma}, \tag{3.23}$$

that is the coupling of the wells of different modes, but at the same x-location, lead to a scaled coupling parameter $\tilde{\gamma}$. The terms of the form

$$\left\langle s_{A,1}\middle|\mathrm{i}\gamma x\mathrm{e}^{-\rho x^2}\middle|s_{B,2}\right\rangle \approx 0, \tag{3.24}$$

are assumed to vanish since the coupling is located in each well and the overlap is small.

Combining all steps lead to the time-dependent matrix model

$$\mathrm{i}\partial_t\psi = \mathbf{M}(|\psi_i|^2)\psi \tag{3.25}$$

with the matrix

$$\mathbf{M} = \begin{pmatrix} -g|\psi_1|^2 & v & \mathrm{i}\gamma & 0 \\ v & -g|\psi_2|^2 & 0 & -\mathrm{i}\gamma \\ -\mathrm{i}\gamma & 0 & -g|\psi_3|^2 & v \\ 0 & \mathrm{i}\gamma & v & -g|\psi_4|^2 \end{pmatrix}. \tag{3.26}$$

We omitted the tilde for the nonlinearity g, and the coupling parameter γ.

3.3 Analytical solutions of the matrix model

In this section we examine possible solutions for the four-dimensional matrix model of equation (3.25). We focus on $\mathcal{PT}$-symmetric solutions, for which analytical expressions can be derived. The time-independent Schrödinger equation for stationary states fulfilling

$$\psi(t) = \mathrm{e}^{-\mathrm{i}\mu t}\psi_0, \tag{3.27}$$

is given by

$$\mu\psi_0 = \mathbf{M}(|\psi_{0,i}|^2)\psi_0. \tag{3.28}$$

In the next section some general observations about stationary states and the influence of the phase between the two modes will be made. It will also be shown how probability currents can be calculated. Thereafter $\mathcal{PT}$-symmetric analytical solutions will be represented. After that we will give expressions for "$\mathcal{PT}$-broken" states, i.e. those corresponding to $\mathcal{PT}$-broken states in the two-dimensional non-Hermitian matrix model.

3.3.1 Probability current

The change of amplitude in the different wells and the associated probability currents are combined in this section to a continuity relation. From equation (3.25) one obtains for the change of the wave function in well i the relation

$$\partial_t\psi_i = -\mathrm{i}\sum_{j=1}^{4} M_{i,j}\psi_j. \tag{3.29}$$

Since the probability in one well is given by $\rho_i = \psi_i\psi_i^*$ one obtains

$$\begin{aligned}\partial_t\rho_i &= \psi_i\partial_t\psi_i^* + (\partial_t\psi_i)\,\psi_i^* = 2\,\mathrm{Re}\left(\psi_i\partial_t\psi_i^*\right)\\ &= 2\,\mathrm{Re}\left(\psi_i\left(-\mathrm{i}\sum_{j=1}^{4} M_{i,j}\psi_j\right)^*\right) = 2\,\mathrm{Im}\left(\sum_{j=1}^{4} M_{i,j}^*\psi_i\psi_j^*\right)\\ &= \sum_{j=1}^{4} J_{j\to i}\end{aligned} \tag{3.30}$$

with the probability current

$$J_{j\to i} = 2\,\mathrm{Im}\left(M_{i,j}^*\psi_i\psi_j^*\right) \tag{3.31}$$

from well j to well i.

3.3.2 No stationary solutions with an empty well

In this section it is shown that no stationary solutions exist if one of the wells is unoccupied. For stationary solutions the change of the probability amplitude (3.30) has to vanish. Therefore one obtains

$$0 = \partial_t \rho_1 = \mathrm{Im}\left(-\psi_1 g|\psi_1|^2)\psi_1^* + \psi_1 v\psi_2^* + \psi_1 \mathrm{i}\gamma\psi_3^*\right), \tag{3.32a}$$

$$0 = \partial_t \rho_2 = \mathrm{Im}\left(-\psi_2 g|\psi_2|^2)\psi_2^* + \psi_2 v\psi_1^* + \psi_2 \mathrm{i}\gamma\psi_4^*\right), \tag{3.32b}$$

$$0 = \partial_t \rho_3 = \mathrm{Im}\left(-\psi_3 g|\psi_3|^2)\psi_3^* + \psi_3 v\psi_4^* + \psi_3 \mathrm{i}\gamma\psi_1^*\right), \tag{3.32c}$$

$$0 = \partial_t \rho_4 = \mathrm{Im}\left(-\psi_4 g|\psi_4|^2)\psi_4^* + \psi_4 v\psi_3^* + \psi_4 \mathrm{i}\gamma\psi_2^*\right), \tag{3.32d}$$

and thus the relations

$$v\,\mathrm{Im}\left(\psi_1\psi_2^*\right) = -\gamma\,\mathrm{Re}\left(\psi_1\psi_3^*\right), \tag{3.33a}$$

$$v\,\mathrm{Im}\left(\psi_2\psi_1^*\right) = \gamma\,\mathrm{Re}\left(\psi_2\psi_4^*\right), \tag{3.33b}$$

$$v\,\mathrm{Im}\left(\psi_3\psi_4^*\right) = \gamma\,\mathrm{Re}\left(\psi_3\psi_1^*\right), \tag{3.33c}$$

$$v\,\mathrm{Im}\left(\psi_4\psi_3^*\right) = -\gamma\,\mathrm{Re}\left(\psi_4\psi_2^*\right) \tag{3.33d}$$

must be fulfilled. Without loss of generality we assume that the empty well is located at the fourth position, that is $\psi_4 = 0$. Since ψ_4 is zero and this is supposed to be a stationary state, also the time derivative of ψ_4 has to vanish. With equation (3.30) one obtains

$$0 = \partial_t \psi_4 = v\psi_3 - \mathrm{i}\gamma\psi_1 \ \text{, that is } \ \psi_3 = \frac{\gamma}{v}\psi_1. \tag{3.34}$$

If this relation is inserted into the previously obtained relation (3.33c), it reads

$$0 = \mathrm{Re}\left(\psi_1\psi_1^*\right), \tag{3.35}$$

and therefore the wave function in the first well vanishes as well. So far we have already shown that there cannot be a single empty well. Futhermore the previous equation shows that ψ_3 and ψ_1 are only scaled by a factor. Thus, since ψ_1 is zero, the same must be true for ψ_3 (because we assumed at the beginning of the section that the parameters γ and v are nonzero). The remaining question is, whether the remaining well can be occupied. If we look at the time derivative of the wave function in the first well we see immediately that also ψ_2 vanishes.

We have therefore shown that there exist no stationary solutions, for which one or more wells are unoccupied.

3.3.3 Phase difference, real solutions and $\mathcal{PT}$-symmetry

If we divide the system into mode A with $\psi_A = \{\psi_1, \psi_2\}$ and mode B with $\psi_B = \{\psi_3, \psi_4\}$ we can write the stationary Schrödinger equation (3.30) as

$$\mu \begin{pmatrix} \psi_A \\ \psi_B \end{pmatrix} = \begin{pmatrix} A & C \\ C^* & B \end{pmatrix} \begin{pmatrix} \psi_A \\ \psi_B \end{pmatrix} \tag{3.36}$$

with the submatrices

$$A = \begin{pmatrix} -g|\psi_1|^2 & v \\ v & -g|\psi_2|^2 \end{pmatrix}, \quad B = \begin{pmatrix} -g|\psi_3|^2 & v \\ v & -g|\psi_4|^2 \end{pmatrix}, \quad C = \begin{pmatrix} \mathrm{i}\gamma & 0 \\ 0 & -\mathrm{i}\gamma \end{pmatrix}. \tag{3.37}$$

If the phase between the two modes is changed, i.e. the wave function for mode B becomes $\psi_B = \mathrm{e}^{\mathrm{i}\phi}\{\psi_3, \psi_4\}$, that is an additional phase ϕ is introduced, the stationary Schrödinger equation reads

$$\mu \begin{pmatrix} \psi_A \\ \psi_B \mathrm{e}^{\mathrm{i}\phi} \end{pmatrix} = \begin{pmatrix} A & C \\ C^* & B \end{pmatrix} \begin{pmatrix} \psi_A \\ \psi_B \mathrm{e}^{\mathrm{i}\phi} \end{pmatrix}. \tag{3.38}$$

It is now possible to multiply the lower equations with $\mathrm{e}^{-\mathrm{i}\phi}$ and to include the term $\mathrm{e}^{\pm\mathrm{i}\phi}$ in the matrix instead of the vectors. The resulting equation is

$$\mu \begin{pmatrix} \psi_A \\ \psi_B \end{pmatrix} = \begin{pmatrix} A & C\mathrm{e}^{\mathrm{i}\phi} \\ C^*\mathrm{e}^{-\mathrm{i}\phi} & B \end{pmatrix} \begin{pmatrix} \psi_A \\ \psi_B \end{pmatrix}. \tag{3.39}$$

If we consider the coupling term between mode A and B as an effective potential for the individual subsystem a phase change between the wave functions of the two modes effectively changes the potential of the subsystem. Therefore we have to restrict the possible phase relation between the two modes if we want to consider stationary states with an effective $\mathcal{PT}$-symmetric potential in the subsystem.

Let us consider the ansatz

$$\psi_A = -\mathrm{i}\psi_B. \tag{3.40}$$

This ansatz leads to decoupled equations for each subsystem and an effective two-dimensional model with the Schrödinger equation

$$\mu \begin{pmatrix} \psi_1 \\ \psi_2 \end{pmatrix} = \begin{pmatrix} -g|\psi_1|^2 - \gamma & v \\ v & -g|\psi_2|^2 - \gamma \end{pmatrix} \begin{pmatrix} \psi_1 \\ \psi_2 \end{pmatrix}. \tag{3.41}$$

This model describes a two-well system where the individual (real) well potentials are either lowered or raised. The norm of the wave function is required to be one. Therefore the ansatz

$$\psi = \frac{1}{\sqrt{2}} \begin{pmatrix} \cos\theta \mathrm{e}^{+i\phi} \\ \sin\theta \mathrm{e}^{-i\phi} \end{pmatrix} \tag{3.42}$$

with $\theta \in [0, \frac{\pi}{2}]$ and $\phi \in [0, 2\pi]$ can be used. It leads to

$$\mu = -g\cos^2\theta - \gamma + v\tan\theta e^{-2\phi}, \tag{3.43a}$$
$$\mu = -g\cos^2\theta + \gamma + v\tan\theta e^{+2\phi}. \tag{3.43b}$$

These equations can be summed up, and by considering only the imaginary parts of the resulting equation one obtains

$$0 = \sin(2\phi)\left(\cot\theta - \tan\theta\right). \tag{3.44}$$

From the two cases fulfilling the equation $\theta = \frac{\pi}{4}$ has no solutions for $\gamma \neq 0$. But $\phi = 0$ leads to

$$\begin{aligned} 0 &= -g\left(\cos^2\theta - \sin^2\theta\right) - 2\gamma - 2v\left(\cot\theta - \cot\theta\right) \\ &= -g\cos 2\theta - 2\gamma - 2v\cot 2\theta, \end{aligned} \tag{3.45}$$

which can be rewritten with the substitution $\theta \to -\frac{\mathrm{i}}{2}\log y$ into a polynomial of degree four,

$$gy^4 + 4(\gamma + \mathrm{i}v)y^3 + 4(\mathrm{i}v - \gamma)y - g = 0. \tag{3.46}$$

The four solutions can then be obtained.

It becomes obvious that these subsystems have no longer an effective $\mathcal{PT}$-symmetric potential. We will therefore restrict our examinations to wave functions which lead to an effective $\mathcal{PT}$-symmetric potential in the subsystems. The most general ansatz which fulfils that the norm is two (that is for a symmetric distribution on the two subsystem, each subsystem has norm one), can be written as

$$\psi = \sqrt{2}\begin{pmatrix} \cos\alpha\ \cos\theta_1\ \mathrm{e}^{+\mathrm{i}\phi_1}\ \mathrm{e}^{+\mathrm{i}\phi_r/2} \\ \cos\alpha\ \sin\theta_1\ \mathrm{e}^{-\mathrm{i}\phi_1}\ \mathrm{e}^{+\mathrm{i}\phi_r/2} \\ \sin\alpha\ \cos\theta_2\ \mathrm{e}^{+\mathrm{i}\phi_2}\ \mathrm{e}^{-\mathrm{i}\phi_r/2} \\ \sin\alpha\ \sin\theta_2\ \mathrm{e}^{-\mathrm{i}\phi_2}\ \mathrm{e}^{-\mathrm{i}\phi_r/2} \end{pmatrix}, \tag{3.47}$$

with $\alpha, \theta_1, \theta_2 \in [0, \frac{\pi}{2}]$ and $\phi_1, \phi_2, \phi_r \in [0, 2\pi]$. In order to obtain $\mathcal{PT}$-symmetric potentials in the subsystems and to have two identical subsystems $\phi_r = 0$ and $\alpha = \frac{\pi}{4}$ are chosen.

3.3.4 $\mathcal{PT}$-symmetric solutions

In the following section we will derive analytical expressions for the $\mathcal{PT}$-symmetric solutions of the matrix model. For the following it is assumed that neither γ nor v are zero, otherwise the matrix will separate into two uncoupled subsystems. With the

restriction from the previous section the ansatz is

$$\psi = \begin{pmatrix} \cos\theta_1 \, \mathrm{e}^{+\mathrm{i}\phi_1} \\ \sin\theta_1 \, \mathrm{e}^{-\mathrm{i}\phi_1} \\ \cos\theta_2 \, \mathrm{e}^{+\mathrm{i}\phi_2} \\ \sin\theta_2 \, \mathrm{e}^{-\mathrm{i}\phi_2} \end{pmatrix}. \tag{3.48}$$

Inserting the ansatz (3.48) into the stationary Schrödinger equation yields

$$\mu = -g\cos^2\theta_1 + v\tan\theta_1 \mathrm{e}^{-2\mathrm{i}\phi 1} + \mathrm{i}\gamma\frac{\cos\theta_2}{\cos\theta_1}\mathrm{e}^{\mathrm{i}(\phi_2-\phi 1)}, \tag{3.49a}$$

$$\mu = -g\sin^2\theta_1 + v\cot\theta_1 \mathrm{e}^{+2\mathrm{i}\phi 1} - \mathrm{i}\gamma\frac{\sin\theta_2}{\sin\theta_1}\mathrm{e}^{\mathrm{i}(\phi_1-\phi 2)}, \tag{3.49b}$$

$$\mu = -g\cos^2\theta_2 + v\tan\theta_1 \mathrm{e}^{-2\mathrm{i}\phi 1} - \mathrm{i}\gamma\frac{\cos\theta_2}{\cos\theta_1}\mathrm{e}^{\mathrm{i}(\phi_1-\phi 2)}, \tag{3.49c}$$

$$\mu = -g\sin^2\theta_2 + v\cot\theta_2 \mathrm{e}^{+2\mathrm{i}\phi 1} + \mathrm{i}\gamma\frac{\sin\theta_2}{\sin\theta_1}\mathrm{e}^{\mathrm{i}(\phi_2-\phi 1)}. \tag{3.49d}$$

From the imaginary parts of equations (3.49) one obtains

$$+v\tan\theta_1 \ \sin(2\phi_1) = +\gamma\frac{\cos\theta_2}{\cos\theta_1} \ \cos(\phi_2-\phi_1), \tag{3.50a}$$

$$-v\cot\theta_1 \ \sin(2\phi_1) = -\gamma\frac{\sin\theta_2}{\sin\theta_1} \ \cos(\phi_2-\phi_1), \tag{3.50b}$$

$$+v\tan\theta_2 \ \sin(2\phi_2) = -\gamma\frac{\cos\theta_1}{\cos\theta_2} \ \cos(\phi_2-\phi_1), \tag{3.50c}$$

$$-v\cot\theta_2 \ \sin(2\phi_2) = +\gamma\frac{\sin\theta_1}{\sin\theta_2} \ \cos(\phi_2-\phi_1). \tag{3.50d}$$

Multiplying equation (3.50a) with (3.50c), and equation (3.50b) with (3.50d) results in

$$v^2\tan\theta_1\tan\theta_2\sin(2\phi_1)\sin(2\phi_2) = -\gamma^2\cos^2(\phi_2-\phi_1), \tag{3.51a}$$

$$v^2\cot\theta_1\cot\theta_2\sin(2\phi_1)\sin(2\phi_2) = -\gamma^2\cos^2(\phi_2-\phi_1), \tag{3.51b}$$

and thus

$$\tan\theta_1\tan\theta_2 = \cot\theta_1\cot\theta_2, \tag{3.52}$$

which can be transformed into

$$\theta_2 = \arccos\tan\theta_1 = \frac{\pi}{2} - \theta_1. \tag{3.53}$$

With the allowed domain of the angles this requires $\theta_1 = \theta_2 = \frac{\pi}{4}$. This already enforces $\mathcal{PT}$-symmetric wave functions. Inserting into equation (3.50) results in

$$v\sin(2\phi_1) = \gamma\cos(\phi_2-\phi_1), \tag{3.54a}$$

$$v\sin(2\phi_2) = -\gamma\cos(\phi_2-\phi_1), \tag{3.54b}$$

and hence $\phi =: \phi_1 = -\phi_2$. The wave function in both subsystems are therefore only mirrored.

Equations (3.49) can be further simplified to

$$\mu = -\frac{g}{2} + (v + \mathrm{i}\gamma)\mathrm{e}^{-2\mathrm{i}\phi},\ \mu = -\frac{g}{2} + (v - \mathrm{i}\gamma)\mathrm{e}^{2\mathrm{i}\phi}. \tag{3.55a}$$

These equations are similar to the equations of the single-mode model. However, they differ in the γ-term. Here the phase ϕ applies to the γ term, which is not the case for the single-mode model. It is not possible to achieve exactly the same in- and outcoupling as in the single-mode model. By substituting $x = \mathrm{e}^{2\mathrm{i}\phi}$ one obtains the equations

$$(v - \mathrm{i}\gamma)\frac{1}{x} = \mu + \frac{g}{2}, \tag{3.56a}$$

$$(v + \mathrm{i}\gamma)x = \mu + \frac{g}{2}, \tag{3.56b}$$

and therefore the following relation for the phase

$$(v - \mathrm{i}\gamma)\frac{1}{x} = (v + \mathrm{i}\gamma)x, \tag{3.57a}$$

$$x = \pm\sqrt{\frac{v - \mathrm{i}\gamma}{v + \mathrm{i}\gamma}}. \tag{3.57b}$$

For the chemical potential one obtains

$$\mu = -\frac{g}{2} \pm \sqrt{v^2 + \gamma^2}. \tag{3.58}$$

Note the difference of the sign under the square root when equation (3.58) is compared to equation (3.2) of the single-mode model.

3.3.5 $\mathcal{PT}$-broken solutions

The question remains whether there exist $\mathcal{PT}$-broken solutions for this system similar to those found for the two-dimensional matrix model. We define $\mathcal{PT}$-broken solutions in this context as solutions that fulfill the matrix equation

$$\begin{pmatrix} \mu\psi_1 \\ \mu\psi_2 \\ \mu^*\psi_3 \\ \mu^*\psi_4 \end{pmatrix} = M\psi. \tag{3.59}$$

That are solutions where the wave function in mode A has an in- or decrease of the probability amplitude and the wave function in mode B behaves exactly opposite.

These are not stationary solutions. They fulfil the equation only for an infinitesimally small time interval.

For the following analysis and calculation we restrict our wave function in the same way as for the search for $\mathcal{PT}$-symmetric solutions. We have seen that the solution of the stationary $\mathcal{PT}$-symmetric states in the two modes have a mirrored phase relation. Therefore using the ansatz

$$\psi = \begin{pmatrix} \cos\theta \mathrm{e}^{+\mathrm{i}\phi} \\ \sin\theta \mathrm{e}^{-\mathrm{i}\phi} \\ \cos\theta \mathrm{e}^{-\mathrm{i}\phi} \\ \sin\theta \mathrm{e}^{+\mathrm{i}\phi} \end{pmatrix} \tag{3.60}$$

and with equations (3.59) we obtain

$$-g\cos^2\theta + v\tan\theta \mathrm{e}^{-2\mathrm{i}\varphi} - \mathrm{i}\gamma \mathrm{e}^{-2\mathrm{i}\varphi} = \mu, \tag{3.61a}$$

$$-g\sin^2\theta + v\cot\theta \mathrm{e}^{+2\mathrm{i}\varphi} + \mathrm{i}\gamma \mathrm{e}^{+2\mathrm{i}\varphi} = \mu. \tag{3.61b}$$

By subtracting the equations from each other, μ can be eliminated and the equation

$$-g(\cos^2\theta - \sin^2\theta) + v\tan\theta \mathrm{e}^{-2\mathrm{i}\varphi} - v\cot\theta \mathrm{e}^{2\mathrm{i}\varphi} - \mathrm{i}\gamma(\mathrm{e}^{-2\mathrm{i}\varphi} + \mathrm{e}^{2\mathrm{i}\varphi}) = 0 \tag{3.62}$$

is obtained. Seperating the real and imaginary parts leads after some further transformations to the relations

$$\sin 2\theta = -\frac{2v}{g}\cos 2\varphi, \tag{3.63a}$$

$$\sin 2\theta = -\frac{v}{\gamma}\tan 2\varphi. \tag{3.63b}$$

Eliminating $\sin 2\theta$ yields

$$\frac{2v}{g}\cos 2\varphi = -\frac{v}{\gamma}\tan 2\varphi \;\Rightarrow\; \cos 2\varphi = \frac{g}{2\gamma}\tan 2\varphi, \tag{3.64}$$

which can be transformed into the polynomial of degree four

$$\frac{x^2+1}{2x} = -\mathrm{i}\frac{g}{2\gamma}\frac{x^2-1}{x^2+1} \;\Rightarrow\; x^4 - 2Ax^3 + 2x^2 + 2Ax + 1 = 0, \tag{3.65}$$

by using the substitution $\phi \to -\frac{\mathrm{i}}{2}\log x$ and $A = -\mathrm{i}\frac{g}{2\gamma}$. A further substitution $z \to x - \frac{1}{x} = \frac{x^2-1}{x}$ results in

$$z^2 - 2Az + 4 = 0. \tag{3.66}$$

The roots of the polynomial are given as

$$z = A \pm \sqrt{A^2 - 4} = -\frac{g\mathrm{i}}{2\gamma} \pm \sqrt{-\frac{g^2}{4\gamma^2} - 4} = -\frac{g\mathrm{i}}{\gamma} \underbrace{\left(\frac{1}{2} \pm \frac{\sqrt{g^2 + 16\gamma^2}}{2g} \right)}_{:=P} = -\frac{g\mathrm{i}}{\gamma} P. \quad (3.67)$$

By back substitution one obtains

$$x = \frac{1}{2}(z \pm \sqrt{4 + z^2}). \quad (3.68)$$

Note that the plus and minus signs in (3.67) and (3.68) are independent, resulting in four different solutions

$$\mu = -\frac{g}{2} \left(2 \mp \sqrt{P + \frac{\gamma^2}{v^2} P^2} - P \right). \quad (3.69)$$

However, ϕ and θ are real parameters. Without an analytical continuation not all states exist for all parameter ranges.

A detailed analysis of the bifurcation structure, the associated bifurcation is given in the next section 3.4 and a comparisons between the matrix model and the spatial extended models is given in section 3.6.

3.4 Bifurcation diagram of the matrix model

In section 3.3 analytical solutions for the matrix model were obtained. In this section these solutions are analysed and compared to the two-dimensional matrix model.

In figure 3.4 the analytical solutions of the matrix model are shown. We have seen in the previous section 3.3.3 that the relative phase between the two modes influences the types of solutions which can be found.

In the following discussion we focus on the $\mathcal{PT}$-symmetric solutions marked by s_1 and s_2 and the $\mathcal{PT}$-broken solutions marked by a_1 and a_2. Only the $\mathcal{PT}$-symmetric solutions are truly stationary solutions. The $\mathcal{PT}$-broken solutions simulate the behaviour of $\mathcal{PT}$-broken solutions in an open quantum system, but only for short times. The nature of a closed Hermitian system obviously prevents infinite exponential growth.

One $\mathcal{PT}$-symmetric state (state s_1) exists for all values of g. This state does not undergo any bifurcation. For increasing g this state has an increasing value of μ. The other $\mathcal{PT}$-symmetric state s_2 is a mirror of the state s_1, but with a decreasing value of μ. In addition for values of g smaller than two, the state participates as central state in a pitchfork bifurcation with the two $\mathcal{PT}$-broken states.

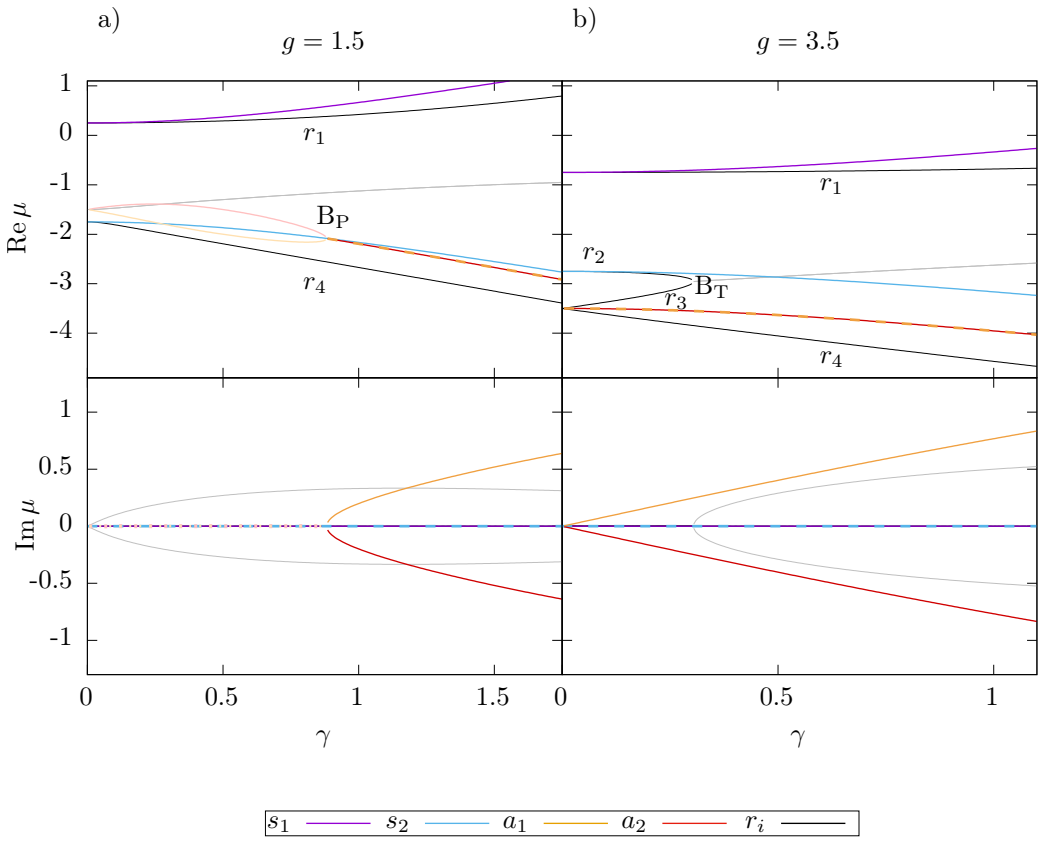

Figure 3.4.: Analytical solutions for the chemical potential of the matrix model are shown. The $\mathcal{PT}$-symmetric states (equation (3.58)) are denoted by s_1 and s_2. $\mathcal{PT}$-broken states (equation (3.69)) are labelled with a_1 and a_2. Solutions of the effective system (3.41) are labelled with r_i. The states r_2 and r_3 only exist if the absolute square of the nonlinearity g is greater than 2. In figure a) g is set to 1.5, while in figure b) g is set to 3.5. The pitchfork bifurcation between a_1, a_2 and s_2 which occurs in a) is labelled with B_P and occurs at $\gamma \approx 0.882$. The tangent bifurcation between states r_2 and r_3 in b) is marked by B_T. The solutions which occur only in the analytically continued system are plotted using lighter colours.

If $\mathcal{PT}$-symmetric states are compared with the open single-mode matrix model the obvious difference is the missing bifurcation between the $\mathcal{PT}$-symmetric states. If we compare the $\mathcal{PT}$-symmetric solutions from equation (3.58) with equation (3.2) one notes the difference in the sign under the square root. While the minus sign in the single-mode model leads to a tangent bifurcation, the plus sign in the two-mode model leads to an ever increasing difference between the chemical potential of the two states for an increasing coupling parameter γ.

As in the single-mode model, however, a bifurcation between the $\mathcal{PT}$-broken and one $\mathcal{PT}$-symmetric state occurs. This bifurcation occurs at different values of γ and moves along the $\mathcal{PT}$-symmetric s_2 branch. The bifurcation point moves to smaller values of γ for increasing nonlinearity g. At $g = 2$ the pitchfork bifurcation is replaced by a tangent bifurcation between the two $\mathcal{PT}$-broken states. The $\mathcal{PT}$-symmetric state s_2 does no longer participate in the bifurcation.

3.5 Probability currents in the matrix model

In this section we consider the probability currents for the different states presented in the previous section. The probability current for the $\mathcal{PT}$-symmetric and $\mathcal{PT}$-broken states are shown for values of g below and above $g = 2$.

The probability current for the $\mathcal{PT}$-symmetric states is nonzero. A circular current can be observed. This behaviour is similar for both $\mathcal{PT}$-ymmetric states above and below $g = 2$ (compare figures 3.5 and 3.6 (and in the appendix A, figures A.1 and A.2). A current from well 0 to well 1, to well 3, to well 2, and back to well 0 can be observed. Since these are stationary states one also observes a balanced in- and outflux in each well, that is the probability amplitudes are constant. The current in the single-mode model where particles are in- and outcoupled [37], is replaced by a circular probability amplitude current.

Figures 3.7 (and figures A.3 to A.5 in appendix A) show the probability current for the $\mathcal{PT}$-broken states. These states also show a circular current, but the strength of the current varies between the different wells. These states are not stationary as can be seen from the unbalanced in- and outflux for the individual wells. The closer to the bifurcation with the state s_2 (for nonlinearities $g < 2$) the smaller is the imbalance. For larger nonlinearities $g > 2$ the probability current vanishes if the $\mathcal{PT}$-broken states approach the tangent bifurcation at $\gamma = 0$.

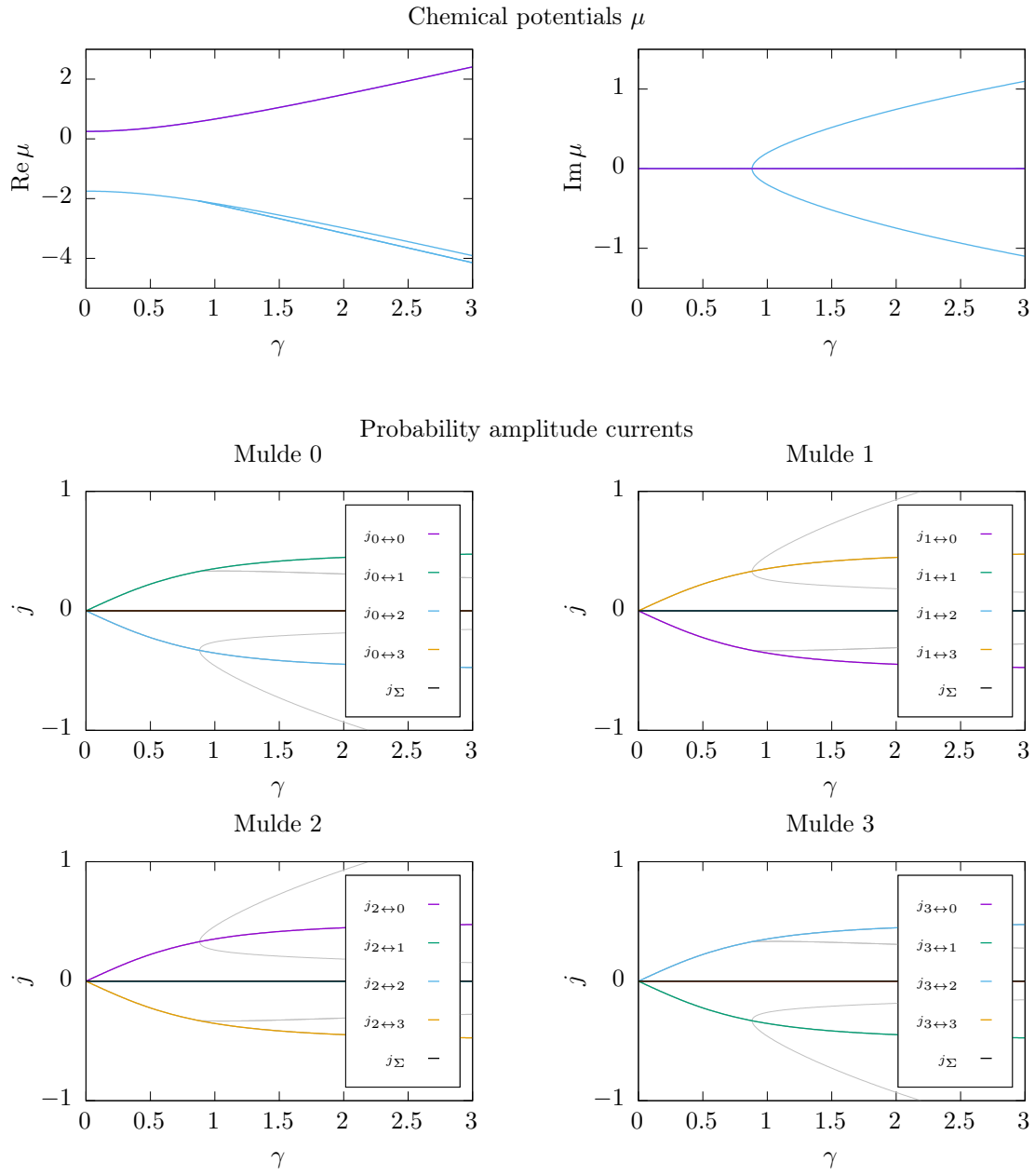

Figure 3.5.: Probability currents between the different modes for the $\mathcal{PT}$-symmetric state s_1. The value of the nonlinearity is $g = 1.5$.

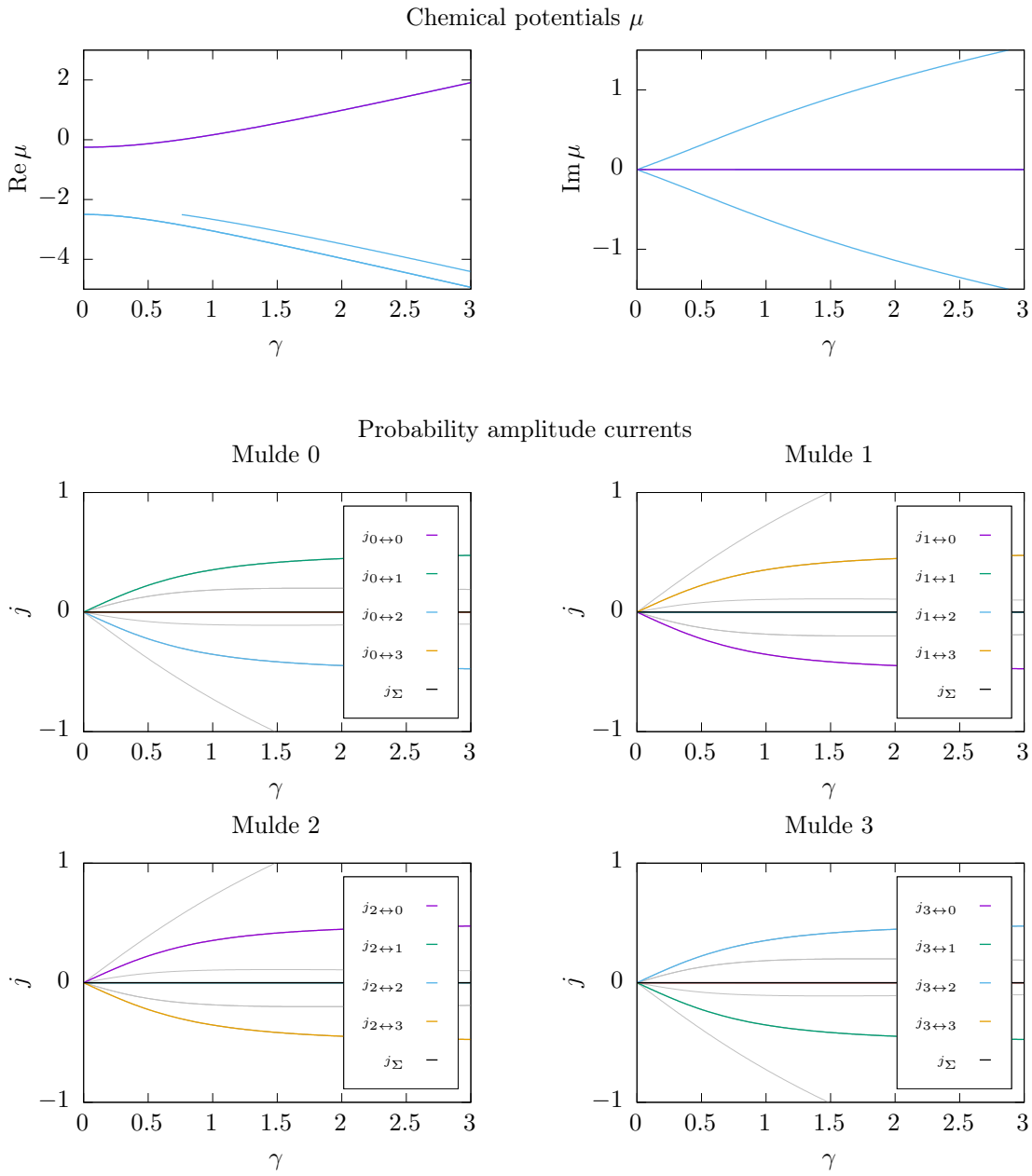

Figure 3.6.: Same as figure 3.5 but for $g = 2.5$.

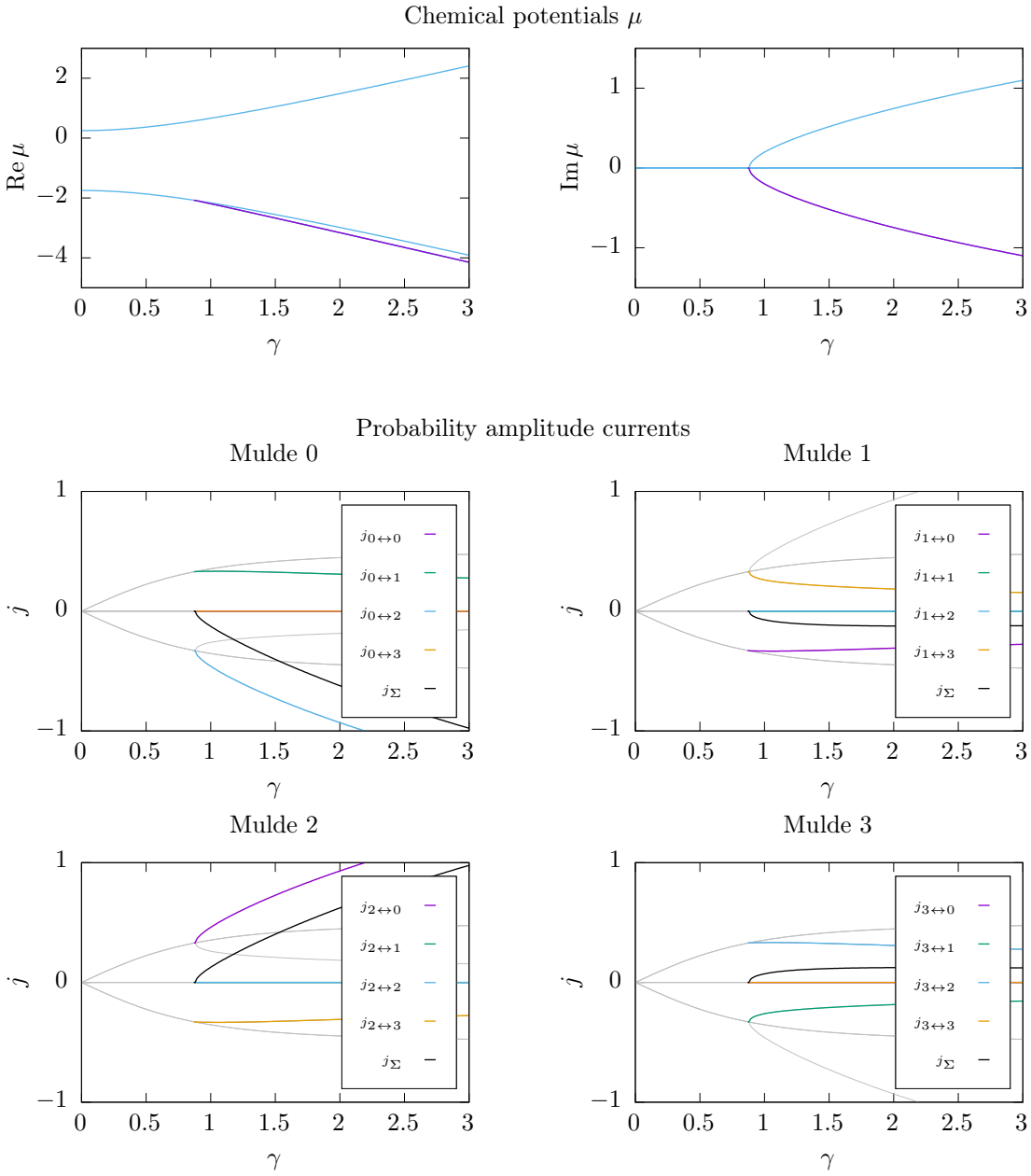

Figure 3.7.: Same as figure 3.5 but for the $\mathcal{PT}$-broken state a_1 for $g = 1.5$.

3.6 Comparison of the spatially extended model with the matrix model

.

The results of the system with the double-δ potentials are given in figure 3.8 in comparison with those of the matrix model. To be able to compare the two models the parameters in the matrix model are replaced by $g \to g/g_0$ and $\gamma \to \gamma/\gamma_0$. Also a shift $\Delta\mu$ in the chemical potential is introduced. Then the parameters γ_0, g_0, v and $\Delta\mu$ are fitted to the results of the double-δ model. How these parameters are connected to the extended model can be seen in section 3.2.2.

In contrast to the matrix model the double-δ system includes spatial properties of the wave functions. In figure 3.9 the wave functions for the parameters marked in figure 3.8 are shown. One can clearly observe the non-differentiability of the wave functions at the locations $x = \pm b$ of the δ-potentials. It is also clearly visible that the states with complex chemical potential are $\mathcal{PT}$-broken (see figure 3.9c). The two wave functions for the subsystems A and B fulfil the condition $\psi_A(x) = \psi_B^*(x)$, which ensures that loss and gain in each subsystem are balanced by the gain and loss in the other subsystem and the $\mathcal{PT}$-symmetry of the potential is maintained. Furthermore the wave function of the ground state (figure 3.9a) is much more localized in the potential wells than the wave function of the excited state (figure 3.9b).

When we compare the solutions of the matrix model with those of the model with the double-δ potential we observe that the qualitative bifurcation structure of the states is the same for both models but some quantitative deviations can be seen. Before we continue our investigation of the cause of these differences we take a look at the influence of the phase difference ϕ_r between the two subsystems.

To examine the influence of the phase difference on the bifurcation scenario we show in figure 3.8c the case where the phase difference between the subsystems is set to $\phi_r = 0.03$. The pitchfork bifurcation B_P in figure 3.8c turns into a cusp bifurcation B_C. While the central ($\mathcal{PT}$-symmetric) state s_1 exists on both sides of the bifurcation point, the two outer ($\mathcal{PT}$-broken) states $a_{1,2}$ are created in the bifurcation of figure 3.8a. In the cusp bifurcation of figure 3.8c one of the outer states (depending on the sign of ϕ_r) merges with the central state and the other outer state performs a continuous transition to the central state for smaller values of γ. Also the $\mathcal{PT}$-symmetry of all states is broken. The asymmetry increases for the central state for increasing values of ϕ_r.

If we introduce the phase difference $\exp(i\phi_r)$ between the two subsystems explicitly into the stationary Gross-Pitaevskii equation (3.25) for the matrix model we obtain

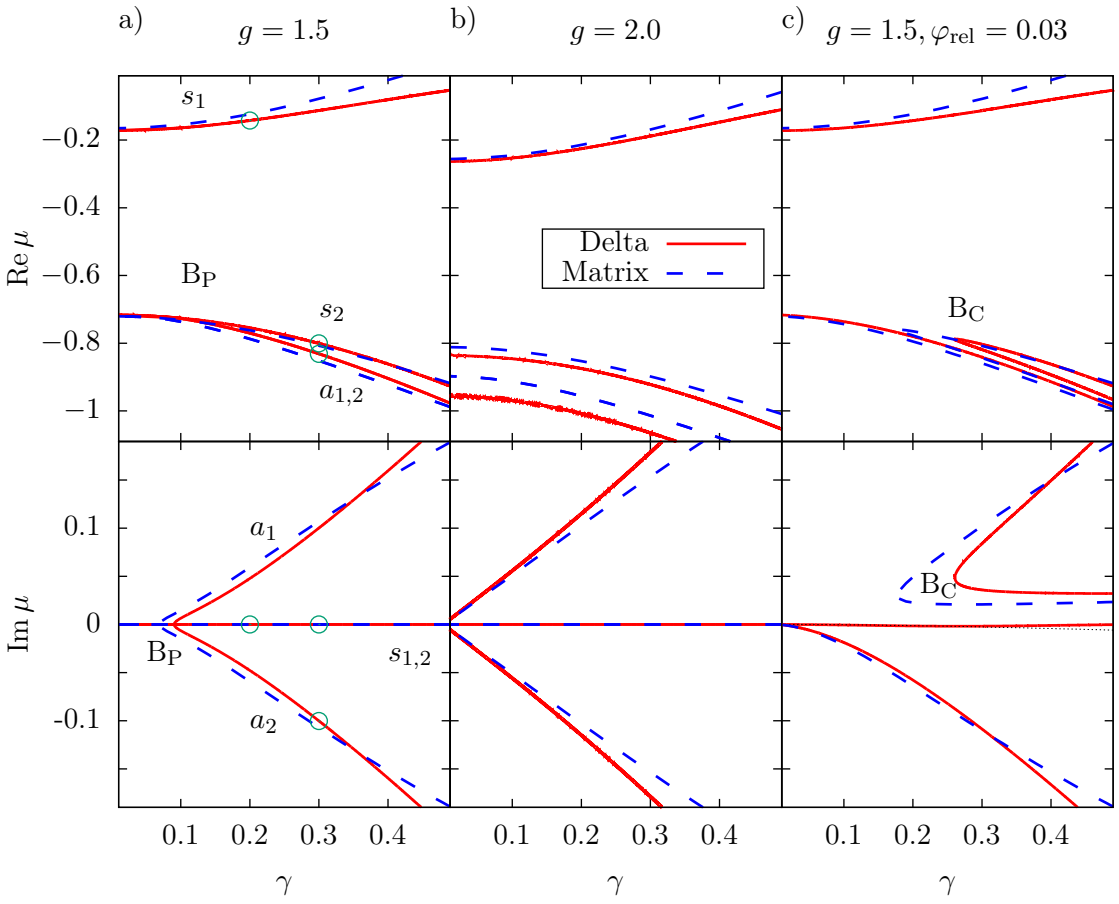

Figure 3.8.: Chemical potential $\mu = \mu_{\mathrm{A}} = \mu_{\mathrm{B}}^*$ for the matrix model (3.25) (blue dashed lines). The parameters of the matrix used for all three plots are $g_0 = 2.75$, $v = 0.28$ and $\gamma_0 = 1.27$. The shift of the chemical potential of the matrix model is $\Delta\mu = -0.17$. For both figures a) and b) the phase difference φ_{rel} was set to zero. Figure a) was calculated for a nonlinearity of $g = 1.5$. The different states are denoted by $s_{1,2}$, $a_{1,2}$. In plot b) a nonlinearity of $g = 2.0$ was used. For plot c) the same nonlinearity as in plot a) was used but the phase difference was set to $\varphi_{\mathrm{rel}} = 0.03$. The figure also contains the results for the double-δ-system (red solid lines). For the coupling of the two subsystems V_0^{D} was set to 1.0 and the δ-potentials were located at $b = \pm 1.1$. The same nonlinearities as for the matrix model were used. In figure a) the parameters for which the wave functions are shown in figure 3.9 are marked by green circles. A pitchfork bifurcation between the states s_2 and $a_{1,2}$ is denoted by $\mathrm{B_P}$. An additional cusp bifurcation appearing in the case φ_{rel} is marked by $\mathrm{B_C}$. Data for the δ-model from [83].

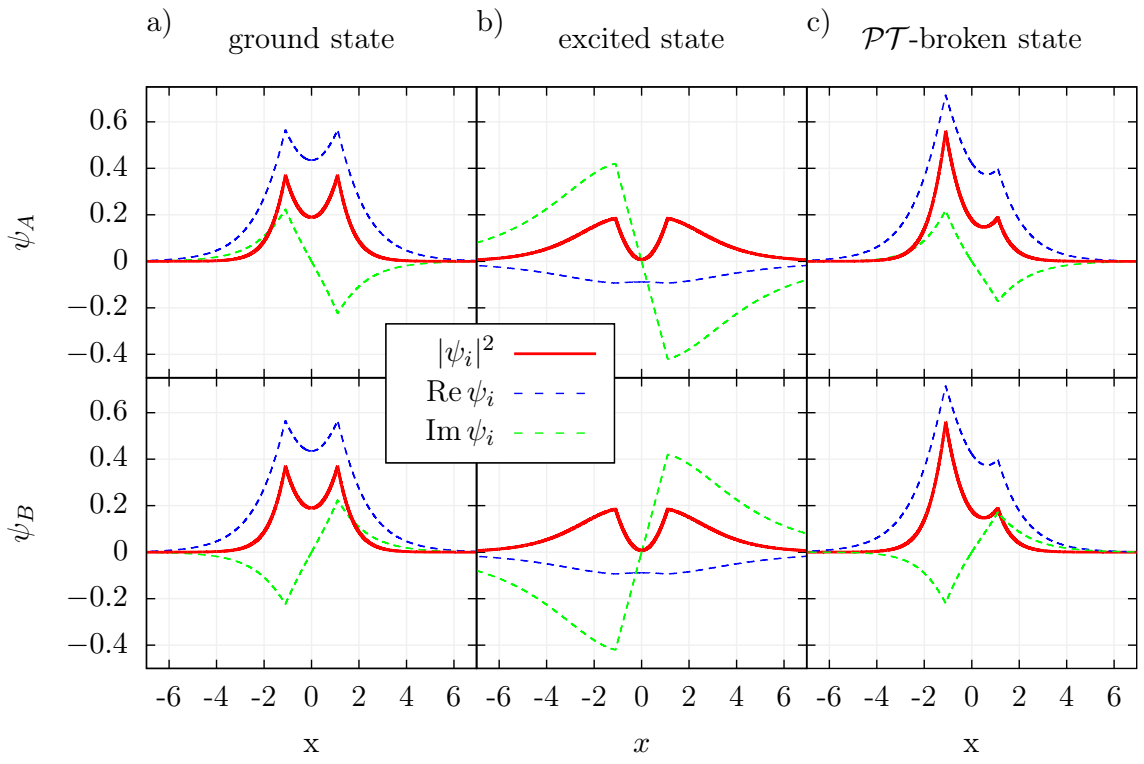

Figure 3.9.: Wave functions of the double-δ potential system for the parameter sets marked in figure 3.8a. a) Wave function of the $\mathcal{PT}$-symmetric ground state. b) Wave function of the $\mathcal{PT}$-symmetric excited state. In c) the broken symmetry of the $\mathcal{PT}$-broken state can be recognized. Data for the δ-model from [83].

for the subsystem A

$$\begin{aligned}\mu_A\psi_{\mathrm{A},1} &= -g|\psi_{\mathrm{A},1}|^2\psi_{\mathrm{A},2} + v\psi_{\mathrm{A},2} + \sin(\phi_\mathrm{r})\gamma\psi_{\mathrm{B},1} - \mathrm{i}\cos(\varphi_\mathrm{r})\gamma\psi_{\mathrm{B},1},\\ \mu_A\psi_{\mathrm{A},1} &= -g|\psi_{\mathrm{A},1}|^2\psi_{\mathrm{A},2} + v\psi_{\mathrm{A},1} - \underbrace{\sin(\phi_\mathrm{r})\gamma\psi_{\mathrm{B},2}}_{\text{asym. pot.}} + \underbrace{\mathrm{i}\cos(\phi_\mathrm{r})\gamma\psi_{\mathrm{B},2}}_{\text{gain or loss}}.\end{aligned} \tag{3.70}$$

We see that a phase difference between the two subsystems leads to different contributions to the real and imaginary part of the effective potential of each subsystem. The real part of the effective potential can therefore become asymmetric (this not only depends on the phase difference ϕ_r but also on the phase value of the wave function in the other subsystem).

The influence of an asymmetric double-well potential on the bifurcation structure has been discussed previously [86]. For an asymmetric potential there is no longer a pitchfork bifurcation but a tangent bifurcation. We can compare this to the well known normal forms of the two-parameter bifurcation theory [87]. The normal form of the cusp bifurcation is

$$0 = \dot{x} = f_\mathrm{C}(x) = \beta + \alpha x - x^3 \tag{3.71}$$

with the bifurcation parameters α and β. In our model the role of the second parameter β is taken by the phase difference ϕ_r between the two subsystems. A constant $\phi_\mathrm{r} = 0$ (which is equivalent with $\beta = 0$) defines a line in the ϕ_r-γ parameter space. On this line the pitchfork bifurcation scenario emerges.

We have seen that the phase difference between the two modes is critical to obtain a $\mathcal{PT}$-symmetric system, and the breaking of this symmetry changes the bifurcation structure. Only for $\phi_\mathrm{r} = 0$ $\mathcal{PT}$-symmetric states are observed.

In the system (3.7) the two modes are coupled over a spatially extended range and therefore the continuous change of the phase in the wave functions may play a role. In figure 3.10 we show the stationary states of the matrix model (3.25) in comparison with those of the smooth potential system (3.7). The parameters of the matrix model (g_0,γ_0 and v) and a shift of the chemical potential $\Delta\mu$ were adjusted to the solution of the model (3.7) but remained the same for all calculations in figure 3.10 with different values for g and ϕ_r.

Since the two wells in the extended model have a finite depth, the Gaussian wave functions in each well have an overlap which is neglected in the matrix model. For further investigation one can increase the distance between the wells or deepen them. One might expect that the stationary states then would be in a better agreement with the matrix model. We compare the results for the extended model for potentials with different barrier heights (figure 3.11a and 3.11b). For a lower potential barrier the asymmetry of the two states becomes more pronounced.

Taking a closer look at the states of the matrix model one discovers that the upper and lower states are symmetric with respect to $-g/2$ as can be seen in equation (3.58).

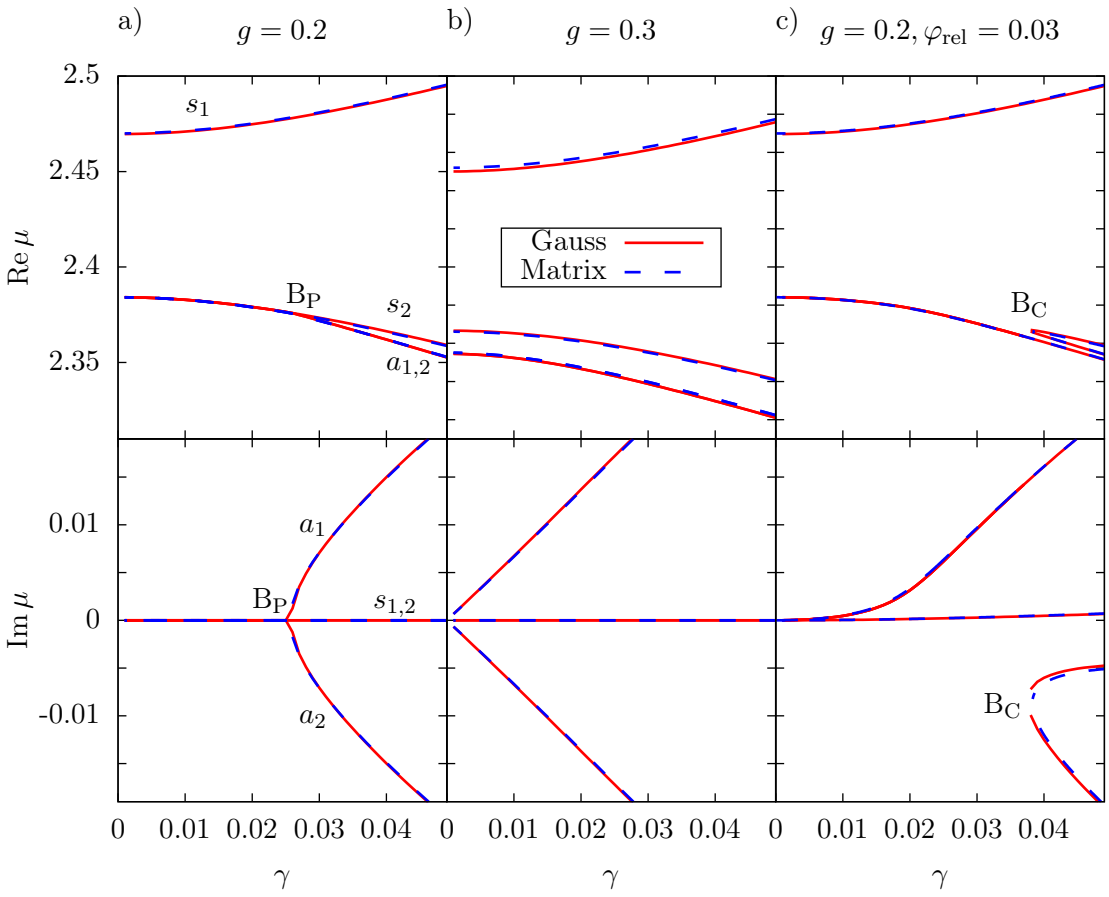

Figure 3.10.: Comparison of the eigenvalues of the matrix model (3.25) (blue dashed lines) with the eigenvalues of the system (3.7) (red solid lines), in which the BEC is trapped in a smooth harmonic potential separated into two wells by a Gaussian potential barrier. The fit parameters for the matrix model are $g_0 = 2.78$, $v = 0.043$ and $\gamma_0 = 0.92$ and are used for all cases a)-c). The chemical potential of the matrix model is shifted by $\Delta\mu = 2.463$. The height of the Gaussian potential barrier in system (3.7) is $V_0^{\mathrm{G}} = 0.25$ with the width $\sigma = 0.5$. Figures a) and c) contain the results for $g = 0.2$, while figure b) is plotted for $g = 0.3$. In figure c) the phase difference is non-zero ($\phi_{\mathrm{r}} = 0.03$).

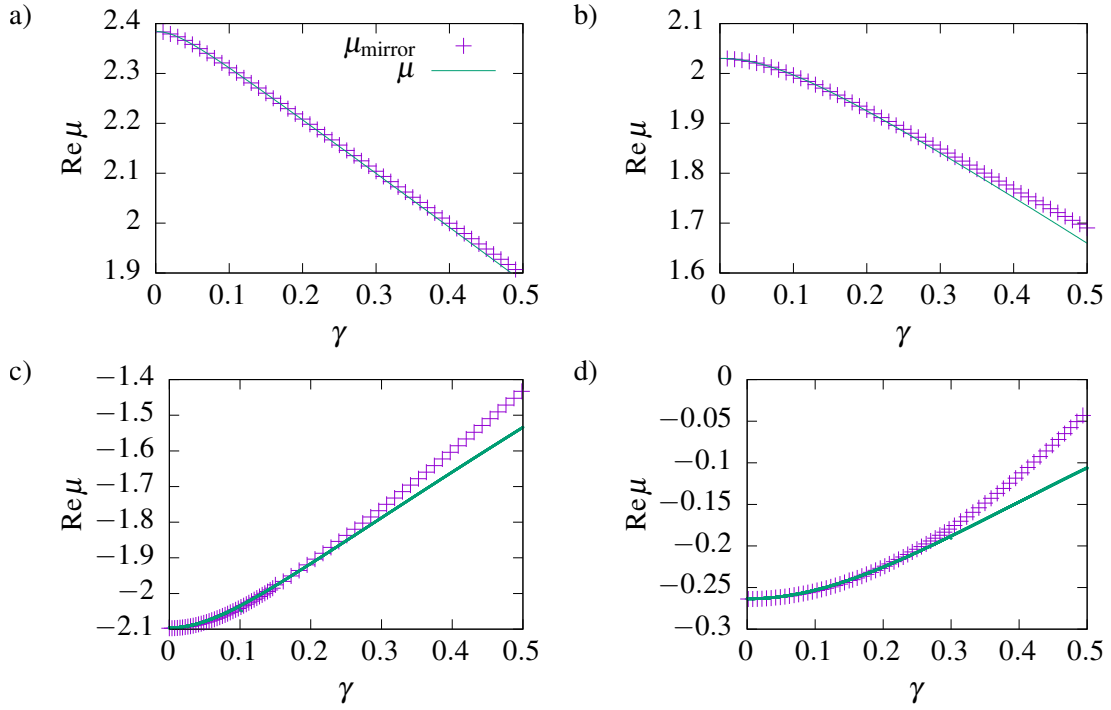

Figure 3.11.: Ground state and mirrored excited state ($\mu_{\text{mirror}} = \mu_0 - \mu$). The states are not symmetric. Figures a) and b) show the results for the Gaussian model (3.7) with $g = 0.2$ and $\mu_0 = 4.854$ and $\mu_0 = 4.2733$, respectively. Figures c) and d) show the results of the double-δ model (3.10) with $g = 2.0$ and $\mu_0 = -4.5$ and $\mu_0 = -1.1$, respectively. In the Gaussian model the hight of the potential barrier between the two wells in each subsystem is changed. For a) the barrier hight is $V_0^{\text{G}} = 4.0$, for b) it is $V_0^{\text{G}} = 2.5$. In the case of the δ-model the (real) depth of the potentials is lowered from $V_0^{\text{D}} = 1.0$ in a) to $V_0^{\text{G}} = 2.5$ in b).

Table 3.1.: Fit parameters of the matrix model used for the comparison with the spatially extended models in figures 3.8 and 3.10.

Comparison with	g_0	v	γ_0	$\Delta\mu$	V_0^{G}	σ	V_0^{D}	b
double-δ model	2.75	0.28	1.27	-0.17	—	—	1.0	1.1
smooth potential	2.78	0.043	0.92	2.463	2.5	0.5	—	—

This is no longer true for the models with a spatial description. To make this asymmetry visible we examine figure 3.11, in which one state is mirrored onto the other, e.g. for one state

$$\mu_{\mathrm{mirror}} = \mu_0 - \mu \tag{3.72}$$

is plotted and μ_0 is the average value of the chemical potentials of both states at $\gamma = 0$. One observes that the deviation is much more pronounced in the model with δ-wells than for that with smooth potentials (3.7).

The wave functions for the different parameter sets are shown in figure 3.12. Here the probability density of the ground and excited state for the smooth potential model with different heights for the potential barrier can be seen. One observes a higher probability density in the overlap region around $x = 0$ for the excited states. This overlap increases for a lower potential barrier. Thus, we can conclude that the matrix model captures all relevant information of the bifurcation scenario and the $\mathcal{PT}$-symmetric properties as long as the different potential wells are sufficiently separated. A larger overlap leads to quantitative changes and the loss of a mirror symmetry of pairs of values for the chemical potential in the (μ, γ)-diagram (see figure 3.11), however, it does not affect the generic structure of the states.

In section 3.5 the probability current for the two mode matrix model were discussed. In this section the probability current in the extended model is shown. In the figures 3.13 and 3.14 (and in the appendix A, figures A.6 and A.7) the current in the spatial model is shown. We concentrate on the current in one mode. It can be seen that the strength of the current varies for different positions. However, if we define the current at $x = 0$ as the current from one well to the other and compare the result to the matrix model the qualitatively same behaviour emerges.

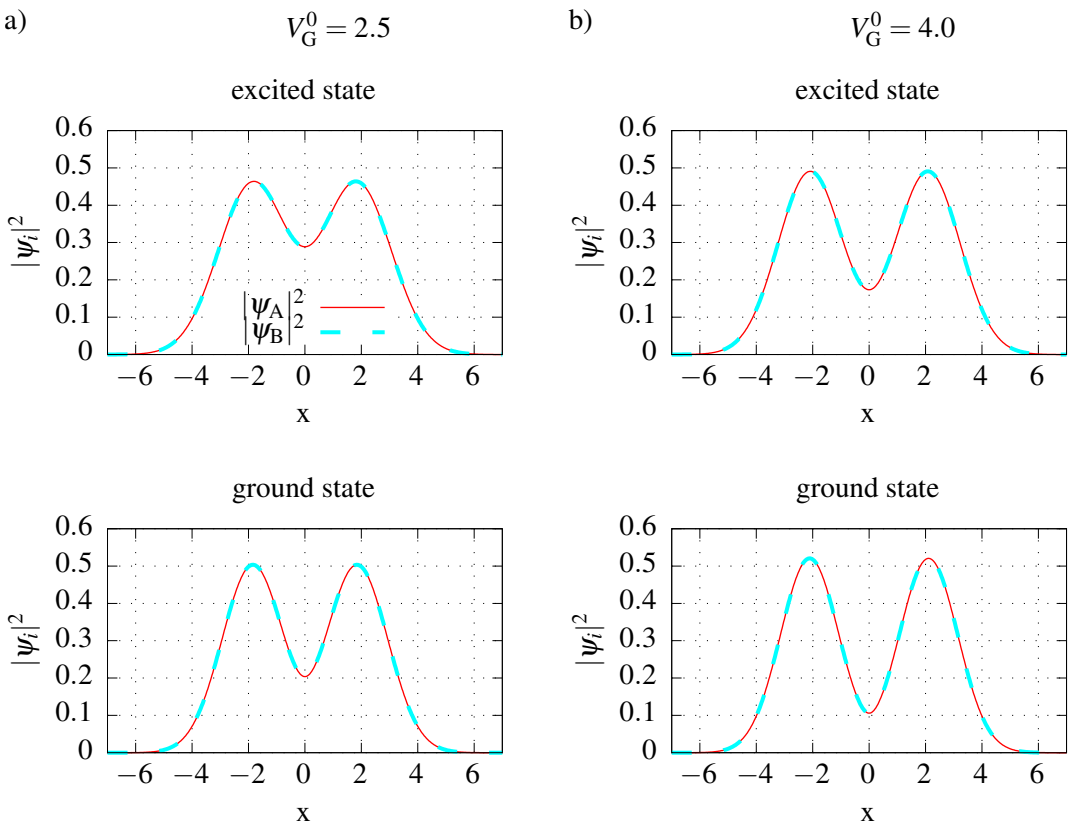

Figure 3.12.: Wave functions for the ground and excited states in the Gaussian model for different potential barriers (in a) $V_0^G = 2.5$, in b) $V_0^G = 4.0$) for a nonlinearity of $g = 0.2$. The overlap of the Gaussians at $x = 0$ is much higher for the lower potential barrier in a) and for the excited states.

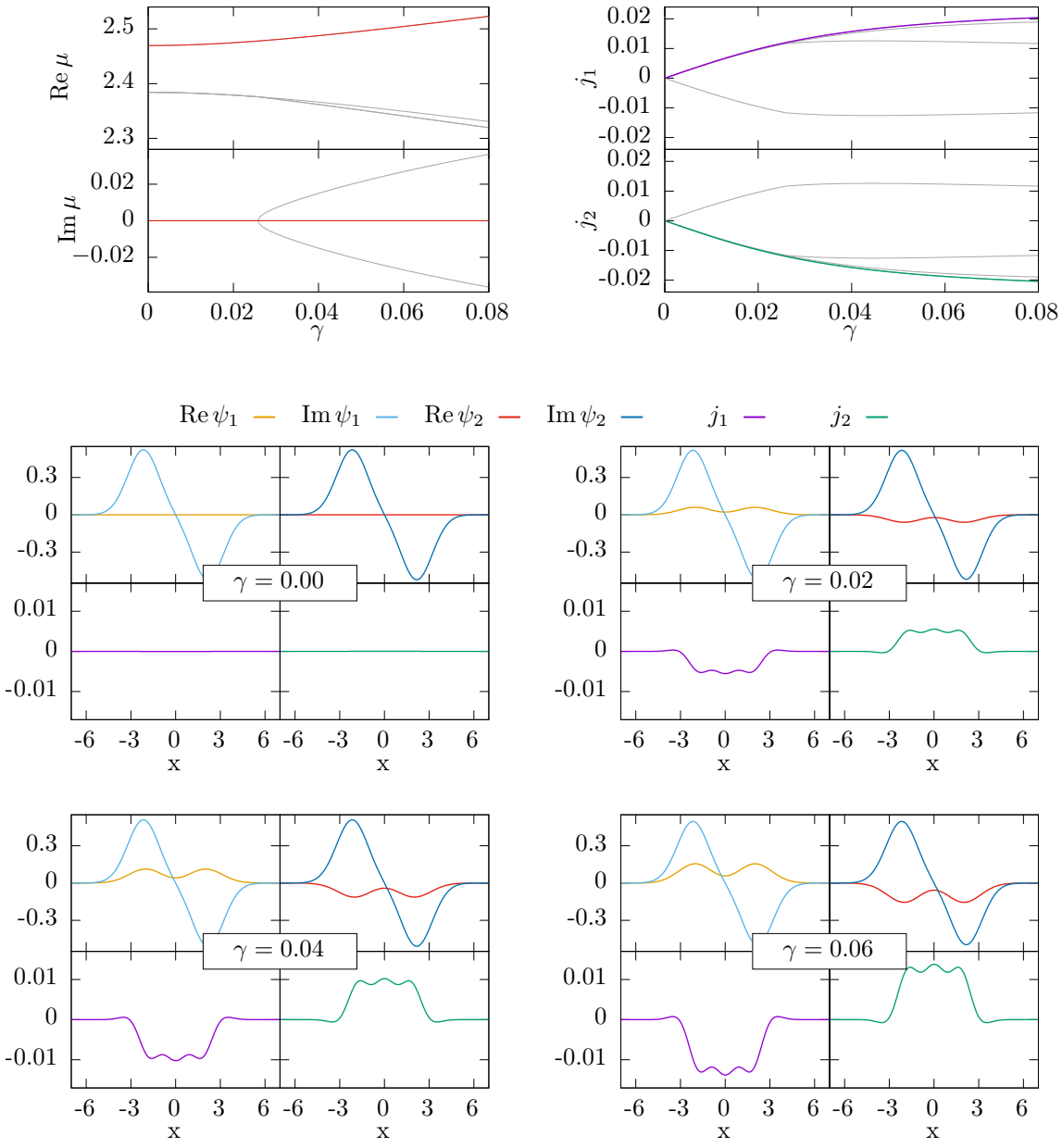

Figure 3.13.: Probability current in the two-modes for the stationary state s_1 in the spatially extended model (3.7).

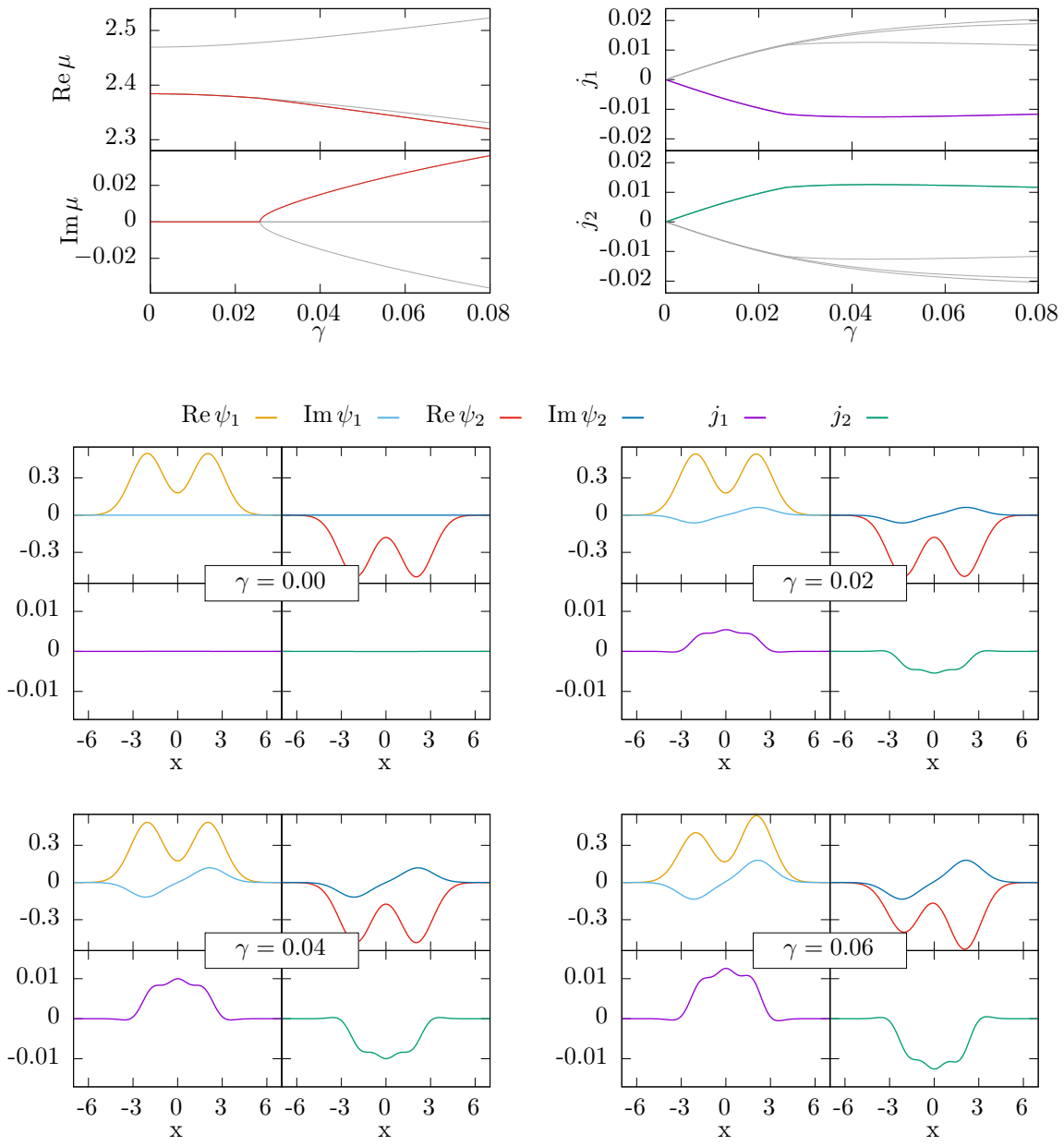

Figure 3.14.: Same as figure 3.13 but for the $\mathcal{PT}$-broken solution a_1.

4 Exceptional points in a dipolar $\mathcal{PT}$-symmetric BEC

In this chapter the order and occurence of exceptional points in $\mathcal{PT}$-symmetric dipolar Bose-Einstein condensates is examined. The bifurcation scenario discovered in [42] already hinted that in this particular double-well system exceptional points of higher order might exist. To examine these points it is neccessary to perform an analytical continuation of the Gross-Pitaevskii equation (2.25) which was derived in chapter 2. The neccessary mathematical tools, that is bicomplex numbers, are introduced in section 4.1. With these numbers it is possible to obtain a representation of the analytical continued equations which allows for an efficient numerical implementation (see section 4.2). Finally we are able to obtain a bifurcation diagram where all (mathematical) branches of the bifurcations are present (see section 4.3). It is then also possible, to examine the order of the associated exceptional points by encircling them in the now complex parameter space. It becomes clear that an encircling in the parameter space may not reveal the actual order of an exceptional point, but only an encircling in the parameter space of a particular parameter is necessary. Most of the results of this chapter are published in [88].

4.1 Analytic continuation and bicomplex numbers

In section 2.2 it was shown how real functions can be analytically continued. The non-analyticity of the Gross-Pitaevskii equation, due to the square modulus of the wave function, prevents us from examining the exchange behaviour of an exceptional point. In this section we will provide the tools neccessary to perfrome an analytical continuation of the complex Gross-Pitaevskii equation using bicomplex numbers.

4.1.1 Analytic continuation of complex functions

In order to create an analytical continuation of a complex function $f(z)$ we first split the function and it's parameters into their real and imaginary parts. Then we obtain for the function $f(z) \in \mathbb{C}$ with the complex parameter $z \in \mathbb{C}$ the following equivalent notation,

$$f(x,y) = f_R(x,y) + \mathrm{i} f_I(x,y) \tag{4.1}$$

with the real parameters $x, y \in \mathbb{R}$ and the two real functions $f_R, f_I \in \mathbb{R}$. The equation

$$0 = f(z) \tag{4.2}$$

can therefore be splitted into two real equations, viz.

$$0 = f_R(x,y), \tag{4.3a}$$
$$0 = f_I(x,y). \tag{4.3b}$$

Now f_R and f_I can be analytically continued as described in section 2.2. The continuation results in the two complex functions $f_R, f_I \in \mathbb{C}$ depending on the complex parameters $x, y \in \mathbb{C}$.

However, the Gross-Pitaevskii equation contains a nonlinear part. We first have to discuss how the nonlinear part of the equation has to be treated. Let us consider the equation

$$f(\psi) = |\psi|^2 = \psi\psi^* \tag{4.4}$$

containing the absolute value square with $f, \psi \in \mathbb{C}$. In order to analytically continue the equation we apply the following steps:

1. The first step is to split all complex values into their real and imaginary parts. Thus, f now has the form

$$\begin{aligned} 0 = f(\psi_\mathrm{r}, \psi_\mathrm{i}) &= (\psi_\mathrm{r} + \mathrm{i}\psi_\mathrm{i})\,(\psi_\mathrm{r} - \mathrm{i}\psi_\mathrm{i}) \\ &= \underbrace{\psi_\mathrm{r}^2 + \psi_\mathrm{i}^2}_{=:f_\mathrm{r}(\psi_\mathrm{r},\psi_\mathrm{i})} + \underbrace{\mathrm{i}\,0}_{=:f_\mathrm{i}(\psi_\mathrm{r},\psi_\mathrm{i})}. \end{aligned} \tag{4.5}$$

2. In the next step the equations are split into double the number of equations. We obtain

$$0 = f_\mathrm{r}(\psi_\mathrm{r}, \psi_\mathrm{i}) = \psi_\mathrm{r}^2 + \psi_\mathrm{i}^2, \tag{4.6a}$$
$$0 = f_\mathrm{i}(\psi_\mathrm{r}, \psi_\mathrm{i}) = 0. \tag{4.6b}$$

   These to equations are functions depending on the real values $\psi_\mathrm{r}, \psi_\mathrm{i} \in \mathbb{R}$.

3. The function can be expressed as a Taylor series and can be analytically continued. Therefore the functions and their arguments are now complex values $f_\mathrm{r}, f_\mathrm{i}, \psi_r, \psi_i \in \mathbb{C}$.

4. To simplify the equations one can combine both equations to one bicomplex equation with $f, \psi \in \mathbb{BC}$. However, this requires the introduction of a new imaginary unit. Bicomplex numbers will be introduced in much greater detail in the next section.

4.1.2 Bicomplex numbers

There exists a whole class of algebras with multiple imaginary units. Well known are for example quaternions, which can be used to represent rotations. In the previous section we have seen how a complex equation can be systematically continued. We now have to choose the appropriate type of hypercomplex numbers, which has the multiplication rules [89] allowing us to rewrite the analytically continued equations from the preceeding section as a bicomplex equation. In table 4.1 the multiplication rules for bicomplex numbers $\mathbb{BC}$ are shown. The imaginary units of bicomplex numbers fulfil the relations

$$\mathrm{i}^2 = \mathrm{j}^2 = -1, \qquad \mathrm{k}^2 = 1, \qquad \mathrm{ij} = \mathrm{ji} = \mathrm{k}. \tag{4.7}$$

×	1	i	j	k
1	1	i	j	k
i	i	-1	k	-j
j	j	k	-1	-i
k	k	-j	-i	1

Table 4.1.: With $\mathrm{i}^2 = -1$, $\mathrm{k}^2 = 1$ and $\mathrm{ji} = \mathrm{ij} = \mathrm{k}$ the multiplication table for the imaginary units can be obtained.

The bicomplex numbers form an algebra over $\mathbb{C}$ of dimension two. Since $\mathbb{C}$ is an algebra of dimension two over $\mathbb{R}$, the bicomplex numbers are an algebra of dimension four over $\mathbb{R}$. We can use these properties to rewrite the process of the analytical continuation as follows. Again the complex equation

$$0 = f \tag{4.8}$$

is split into it's real and imaginary parts,

$$0 = \underbrace{\underbrace{f_R}_{\in\mathbb{R}} + \mathrm{i}\,\underbrace{f_I}_{\in\mathbb{R}}}_{\in\mathbf{C}}. \tag{4.9}$$

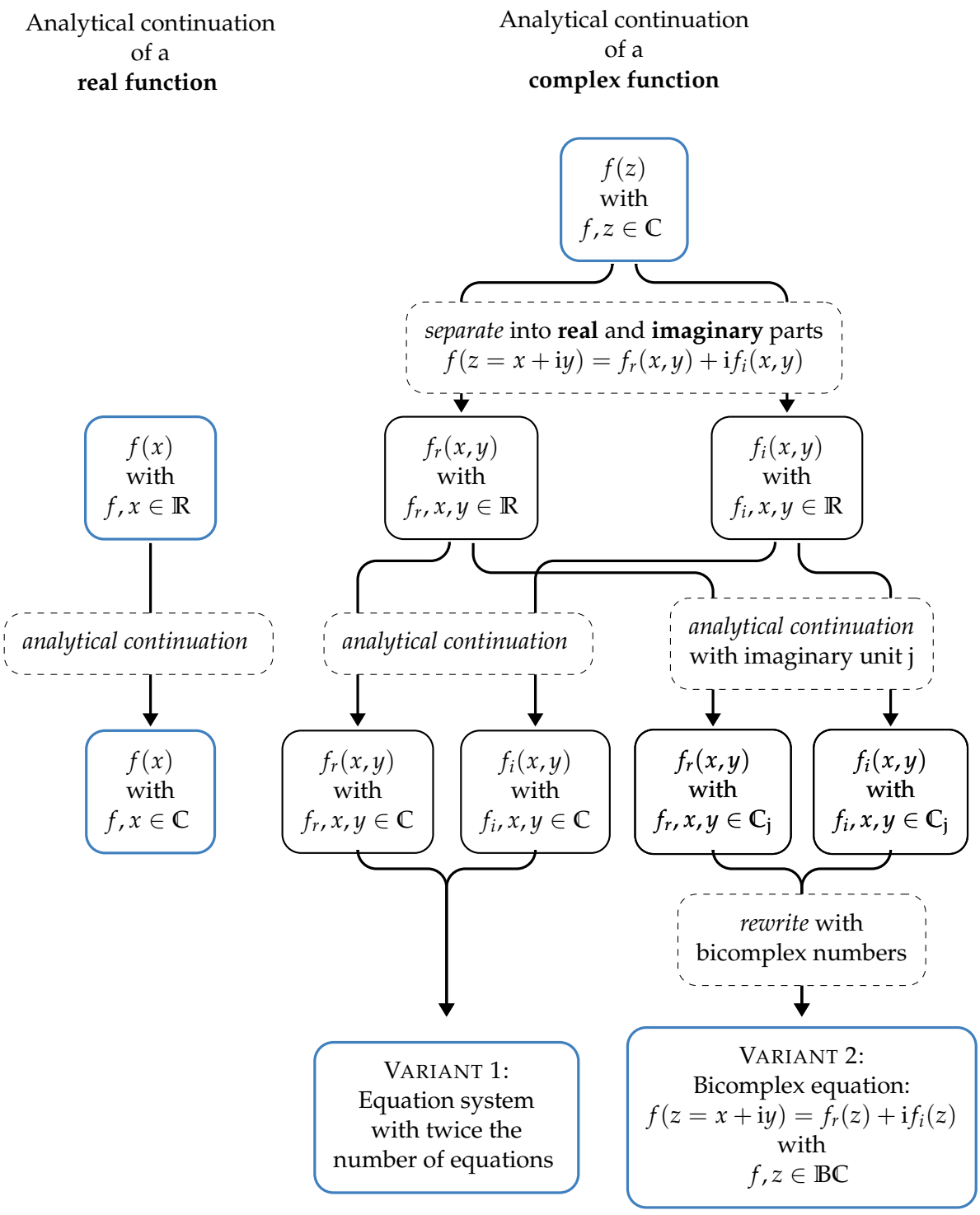

Figure 4.1.: The different steps, which are necessary to analytically continue either a real or a complex equation, are illustrated.

Instead of dividing the equation into two real equations the individual real functions are analytically continued, but the imaginary unit j is used instead of i. This leads to the equation

$$0 = \underbrace{\underbrace{\left(\underbrace{f_0}_{\in\mathbb{R}} + \mathrm{j}\underbrace{f_1}_{\in\mathbb{R}}\right)}_{=f_R\in\mathbb{C}_\mathrm{j}} + \mathrm{i}\underbrace{\left(\underbrace{f_2}_{\in\mathbb{R}} + \mathrm{j}\underbrace{f_3}_{\in\mathbb{R}}\right)}_{=f_I\in\mathbb{C}_\mathrm{j}}}_{\in\mathbb{BC}}. \tag{4.10}$$

The complex numbers $\mathbb{C}_\mathrm{j}$ with the imaginary unit j are isomorphous to the complex numbers $\mathbb{C}_\mathrm{i}$.

4.1.3 The idempotent elements of bicomplex numbers

A bicomplex number $z \in \mathbb{BC}$ can be represented in the form

$$z = z_0 + \mathrm{j}z_1 + \mathrm{i}z_2 + \mathrm{k}z_3, \tag{4.11}$$

with the four real components $z_i \in \mathbb{R}$. However, there exists a representation using an idempotent basis. We will see that this representation simplifies the calculation of the basic arithmetic operations. It will also allow us to implement the analytical continuation of the Gross-Pitaevskii equation very efficiently.

Let us consider the idempotent elements [89]

$$\mathrm{e}^{\oplus} = \frac{1+\mathrm{k}}{2}, \tag{4.12a}$$

$$\mathrm{e}^{\ominus} = \frac{1-\mathrm{k}}{2}. \tag{4.12b}$$

These elements fulfil the relations

$$(\mathrm{e}^{\oplus})^2 = \mathrm{e}^{\oplus}, \tag{4.13a}$$

$$(\mathrm{e}^{\ominus})^2 = \mathrm{e}^{\ominus}, \tag{4.13b}$$

$$\mathrm{e}^{\oplus}\mathrm{e}^{\ominus} = 0. \tag{4.13c}$$

These properties allow us to decompose every bicomplex number into two complex numbers either in $\mathbb{C}_\mathrm{i}$ or in $\mathbb{C}_\mathrm{j}$. The two possible decompositions will be discussed later on. First we have to introduce the necessary notations.

4.1.4 Complex conjugation and notation

For the bicomplex numbers with their three imaginary units i, j and k there are various "complex conjugations", that is, operations which change the sign of the imaginary units. For the bicomplex number

$$z = z_0 + \mathrm{j}z_1 + \mathrm{i}z_2 + \mathrm{k}z_3 \tag{4.14}$$

the three complex conjugations [90], which are compatible with the relation (4.7), are

$$\mathrm{conj}_1 z = z_0 - \mathrm{j}z_1 - \mathrm{i}z_2 + \mathrm{k}z_3, \tag{4.15a}$$
$$\mathrm{conj}_2 z = z_0 - \mathrm{j}z_1 + \mathrm{i}z_2 - \mathrm{k}z_3, \tag{4.15b}$$
$$\mathrm{conj}_3 z = z_0 + \mathrm{j}z_1 - \mathrm{i}z_2 - \mathrm{k}z_3. \tag{4.15c}$$

If we consider conj_3, we obtain for

$$\begin{aligned} &[z_0 + \mathrm{j}z_1 + \mathrm{i}z_2 + \mathrm{k}z_3]\ \mathrm{conj}_3\left([z_0 + \mathrm{j}z_1 + \mathrm{i}z_2 + \mathrm{k}z_3]\right) \\ &= [(z_0 + \mathrm{j}z_1) + \mathrm{i}(z_2 + \mathrm{j}z_3)]\,[(z_0 + \mathrm{j}z_1) - \mathrm{i}(z_2 + \mathrm{j}z_3)] \\ &= \left[(z_0 + \mathrm{j}z_1)^2 + (z_2 + \mathrm{j}z_3)^2\right] + \mathrm{i}\,0 \end{aligned} \tag{4.16}$$

a quadratic form. Please note that the result is still an element of $\mathbb{C}_\mathrm{j}$. A similar calculation can be done for conj_2, this however leads to a quadratic form with a result from $\mathbb{C}_\mathrm{i}$.

We will only use the complex conjugation conj_3, which changes the sign in front of the imaginary units i and k. This conjugation is required for the analytical continuation. If a complex function containing a complex conjugation is analytically continued using bicomplex numbers, the complex conjugation can simply be replaced by conj_3 to obtain the appropriate signs in our application.

However, we use not only bicomplex numbers, but also complex numbers. In order to avoid any confusion about the complex conjugation used in a particular equation we introduce for the conjugations used in this work the following notions, dependent whether the complex conjugation acts on the bicomplex number space or the complex conjugation acts on a complex number space.

Complex conjugation on bicomplex numbers $z \in \mathbb{BC}$ are denoted and defined by

$$\langle z|_{\mathbb{BC}} = z^* := z_0 + \mathrm{j}z_1 - \mathrm{i}z_2 - \mathrm{k}z_3. \tag{4.17}$$

Complex conjugation on complex spaces The complex conjugation which acts on elements from either $\mathbb{C}_\mathrm{i}$ or $\mathbb{C}_\mathrm{j}$ is defined as

$$\langle z| = \overline{z} = \overline{(a + \mathrm{i}b)} := a - \mathrm{i}b \tag{4.18}$$

for $z \in \mathbb{C}_\mathrm{i}$ or as

$$\langle w| = \overline{w} = \overline{(c + \mathrm{j}d)} := c - \mathrm{j}d \tag{4.19}$$

for $w \in \mathbb{C}_\mathrm{j}$ with $a, b, c, d \in \mathbb{R}$.

4.1.5 Decomposition of bicomplex numbers

With the bicomplex idempotent elements $e^{\oplus}$ and $e^{\ominus}$ a bicomplex number can be decompositioned into

$$z = z^{\oplus}e^{\oplus} + z^{\ominus}e^{\ominus}. \tag{4.20}$$

The numbers $z^{\oplus}$ and $z^{\ominus}$ are complex numbers. They can be chosen to be either elements of $\mathbb{C}_i$ (decomposition A) or $\mathbb{C}_j$ (decomposition B). If one imaginary unit is chosen the decomposition is unique. For

$$z = z_0 + jz_1 + iz_2 + kz_3 = z^{\oplus}e^{\oplus} + z^{\ominus}e^{\ominus} \tag{4.21}$$

with $z \in \mathbb{BC}$ and $z_{1-4} \in \mathbb{R}$ the decompositioned values have the form

$$z^{\oplus} = (z_0 + z_3) + i(z_2 - z_1), \qquad z^{\ominus} = (z_0 - z_3) + i(z_2 + z_1), \tag{4.22a}$$

$$z^{\oplus} = (z_0 + z_3) + j(z_1 - z_2), \qquad z^{\ominus} = (z_0 - z_3) + j(z_1 + z_2), \tag{4.22b}$$

with

$$z^{\oplus}, z^{\ominus} \in \mathbb{C}_i, \tag{4.23a}$$

$$z^{\oplus}, z^{\ominus} \in \mathbb{C}_j. \tag{4.23b}$$

These two decompositions have some notable different properties concerning the complex conjugation of bicomplex numbers introduced previously,

$$z^* = z_0 + jz_1 - iz_2 - kz_3 = z^{*\oplus}e^{\oplus} + z^{*\ominus}e^{\ominus}. \tag{4.24}$$

The decomposition of leads to

$$z^{*\oplus} = (z_0 - z_3) + i(-z_2 - z_1) = \overline{z^{\ominus}}, \qquad z^{*\ominus} = (z_0 + z_3) + i(-z_2 + z_1) = \overline{z^{\oplus}}, \tag{4.25a}$$

$$z^{*\oplus} = (z_0 - z_3) + j(z_2 + z_1) = z^{\ominus}, \qquad z^{*\ominus} = (z_0 + z_3) + j(z_2 - z_1) = z^{\oplus}. \tag{4.25b}$$

There are also special relations between the $z^{\oplus}$ and $z^{\ominus}$ if the bicomplex number z contains only certain imaginary units. If $z = z_0 + iz_2$ is only composed of a real part z_0 and an imaginary part z_2i the decomposition reads

$$z^{\oplus} = z_0 + iz_2 = z^{\ominus}, \qquad z^{\ominus} = z_0 + iz_2 = z^{\oplus}, \tag{4.26a}$$

$$z^{\oplus} = z_0 - jz_2 = \overline{z^{\ominus}}, \qquad z^{\ominus} = z_0 + jz_2 = \overline{z^{\oplus}}. \tag{4.26b}$$

By contrast a bicomplex number $z = z_0 + jz_1$ with only a real part z_0 and an imaginary part z_1j leads to the decomposition

$$z^{\oplus} = z_0 - iz_1 = \overline{z^{\ominus}}, \qquad z^{\ominus} = z_0 + iz_1 = \overline{z^{\oplus}}, \tag{4.27a}$$

$$z^{\oplus} = z_0 + jz_1 = z^{\ominus}, \qquad z^{\ominus} = z_0 + jz_1 = z^{\oplus}. \tag{4.27b}$$

For the purpose of this work decomposition A is used. Therefore all parameters of the decompositions $z^{\oplus}, z^{\ominus}$ are elements of the complex numbers $\mathbb{C}_{\mathrm{i}}$ with the imaginary unit i.

If the "bra-ket" notation is used, the left "bra" has a different meaning, depending on whether it is applied to an element of the bicomplex numbers $\mathbb{BC}$ or on $\mathbb{C}_{\mathrm{i}}$.

$$\langle z|_{\mathbb{BC}} := z^* \,, \qquad \langle w_{R,I}| := \overline{w_{R,I}} \tag{4.28}$$

with $z \in \mathbb{BC}$ and $w \in \mathbb{C}_{\mathrm{i}}$. Choosing decomposition A allows us to write a bicomplex bra-vector as follows

$$\langle z|_{\mathbb{BC}} = \langle w_R|\mathrm{e}^{\oplus} + \langle w_I|\mathrm{e}^{\ominus}. \tag{4.29}$$

4.1.6 Decomposition of bicomplex functions

The properties of the idempotent basis allows also for an easy decomposition of functions, which are composed of the basic arithmetic operations mentioned above. For example, all integrals for the analytical continued function $f_{\mathbb{BC}}$ can be written in terms of the original function f.

$$\int f(z)_{\mathbb{BC}} dz = \int f(z^{\oplus})\, dz^{\oplus}\mathrm{e}^{\oplus} + \int f(z^{\ominus})\, dz^{\ominus}\mathrm{e}^{\ominus}. \tag{4.30}$$

We will make extensive use of this property to implement the analytically continued Gross-Pitaevskii equation.

We started in this chapter with an example about the analytical continuation of the absolute square, and we will conclude this chapter with some properties of the norm. Let us consider the decomposition of the bicomplex analytical continuation of the norm:

$$\begin{aligned}
\langle\psi|\psi\rangle_{\mathbb{BC}} &= \psi^*\psi \\
&= \left(\psi^{*\oplus}\mathrm{e}^{\oplus} + \psi^{*\ominus}\mathrm{e}^{\ominus}\right)\left(\psi^{\oplus}\mathrm{e}^{\oplus} + \psi^{\ominus}\mathrm{e}^{\ominus}\right) \\
&= \left(\overline{\psi^{\ominus}}\mathrm{e}^{\oplus} + \overline{\psi^{\oplus}}\mathrm{e}^{\ominus}\right)\left(\psi^{\oplus}\mathrm{e}^{\oplus} + \psi^{\ominus}\mathrm{e}^{\ominus}\right) \\
&= \overline{\psi^{\ominus}}\psi^{\oplus}\mathrm{e}^{\oplus} + \overline{\psi^{\oplus}}\psi^{\ominus}\mathrm{e}^{\ominus} \\
&= \langle\psi^{\ominus}|\psi^{\oplus}\rangle\mathrm{e}^{\oplus} + \langle\psi^{\oplus}|\psi^{\ominus}\rangle\mathrm{e}^{\ominus}.
\end{aligned} \tag{4.31}$$

This is also the norm which was real before the analytic continuation was applied. For bicomplex numbers this leads to

$$\begin{aligned}\langle\psi|\psi\rangle_{\mathbb{BC}} &= \underbrace{\langle\psi^{\ominus}|\psi^{\oplus}\rangle}_{=:C=\alpha+\mathrm{i}\beta}\mathrm{e}^{\oplus} + \underbrace{\langle\psi^{\oplus}|\psi^{\ominus}\rangle}_{=:\overline{C}=\alpha-\mathrm{i}\beta}\mathrm{e}^{\ominus} \\ &= \frac{1}{2}\left[(\alpha+\mathrm{i}\beta)(1+\mathrm{k})+(\alpha-\mathrm{i}\beta)(1-\mathrm{k})\right] \\ &= \frac{1}{2}\left[\alpha+\mathrm{i}\beta+\mathrm{k}\alpha+\mathrm{i}\mathrm{k}\beta+\alpha-\mathrm{i}\beta-\mathrm{k}\alpha+\mathrm{i}\mathrm{k}\beta\right] \\ &= \alpha-\mathrm{j}\beta, \end{aligned} \tag{4.32}$$

and therefore the norm is now an element of $\mathbb{C}_{\mathrm{j}}$. The same applies to other real values as the meanfield energy or the chemical potential.

4.2 Analytical continuation in presence of long-range interactions

In the previous chapters no long-range interaction between the constituents of a Bose-Einstein condensate were considered. However, there exist various elements and molecules which possess dipolar moments. This long-range interaction can introduce completely new effects. They also have a huge impact on the bifurcation structure which can be observed [42]. It might be possible that in these condensates exceptional points of higher order can be found. The bifurcation scenario in [42] only contains physical stationary states, and is mathematically incomplete, in the sense that states from an analytical continued equation are missing. To examine the full mathematical properties of the associated Gross-Pitaevskii equation the equation has to be analytically continued. Only then all mathematical properties can be examined. In order to extend the Gross-Pitaevskii equation bicomplex numbers are used.

Bicomplex numbers were introduced in section 4.1. In this chapter we will show how the Gross-Pitaevskii equation with long-range interactions can be analytically continued.

4.2.1 Potentials

In section 2.1 the Gross-Pitaevskii equation (2.25) was introduced. In this section we will discuss the potentials, which will be used further on.

As already discussed, we use s-wave scattering for the contact interaction between two atoms in equation (2.26). Since we only consider s-wave scattering the interaction is isotropic and the strength of the interaction is determined by the scattering length a_{sc}.

The other molecular interaction which we consider is the dipole-dipole interaction (see equation (2.27)).

As a potential term an external trap is introduced. The trap has a double-well structure. In addition one well of this structure is used to incouple particles from an external reservoir while particles are removed from the other well. This is modelled using a complex $\mathcal{PT}$-symmetric potential of the form

$$V_{\text{ext}}(\mathbf{r}) = \underbrace{-(V_0 - \mathrm{i}\Gamma)}_{=:c_{g,1}} g^+ \underbrace{-(V_0 + \mathrm{i}\Gamma)}_{=:c_{g,2}} g^-, \tag{4.33}$$

where V_0 determines the potential depth and Γ the strength of the in- and outcoupling. The shape is given by two Gaussian wells with

$$g^{\pm} = \exp\left(-\frac{x^2}{2L_x^2} - \frac{y^2}{2L_y^2} - \frac{(z \pm l/2)^2}{2L_z^2}\right). \tag{4.34}$$

By using appropriate dimensionless units [50, 55] one obtains the equation

$$\mathrm{i}\frac{d}{dt}\psi(\mathbf{r},t) = \left[-\Delta + V_{\text{ext}} + c_{sc}|\psi(\mathbf{r},t)|^2 + c_d \int d^3\mathbf{r}' \frac{1 - 3\cos^2\theta}{|\mathbf{r} - \mathbf{r}'|^3}|\psi(\mathbf{r}',t)|^2\right]\psi(\mathbf{r},t). \tag{4.35}$$

To simplify the equations all relevant pre factors are combined into c_{sc}, containing the scattering length, and c_d, containing the dipole-dipole interaction strength.

As discussed in section 2.1, the time-dependent variational principle (TDVP) can be used to numerically calculate solutions for the GPE. The ansatz of coupled Gaussians (2.35) leads to the variational parameters $\mathbf{A}_k$, $\mathbf{p}_k$ and γ_k. The number of Gaussian parameters can be further reduced. If we consider a condensate which is strongly confined in one direction (in this case the y-direction), we can eliminate A_{xy}, A_{yz}, and p_z. That is no rotational and translational degrees of freedom in the direction of the confinement are allowed. If no rotational degrees of freedom are allowed at all also A_{xz} can be set to zero.

4.2.2 Equations of motion

We have seen in section 2.1 that the equations of motion rely on solving the linear system of equations

$$\mathbf{K}\mathbf{v} = \mathbf{r}. \tag{4.36}$$

Using the bicomplex numbers introduced in chapter 4.1 we can now analytically continue the system of linear equations. Therefore the matrix and vectors are introduced as elements of the bicomplex vector spaces $\mathbf{K} \in \mathbb{BC}^{N\times N}$, $\mathbf{v}, \mathbf{r} \in \mathbb{BC}^N$. Using the two idempotent elements $\mathrm{e}^{\oplus}$ and $\mathrm{e}^{\ominus}$ we can decompose the equation into

$$\mathbf{K}^{\oplus}\mathbf{v}^{\oplus}\mathrm{e}^{\oplus} + \mathbf{K}^{\ominus}\mathbf{v}^{\ominus}\mathrm{e}^{\ominus} = \mathbf{r}^{\oplus}\mathrm{e}^{\oplus} + \mathbf{r}^{\ominus}\mathrm{e}^{\ominus}. \tag{4.37}$$

Thus, instead of solving the bicomplex equations directly, we can obtain the solution by solving the two complex linear equation systems

$$\mathbf{K}^{\oplus}\mathbf{v}^{\oplus} = \mathbf{r}^{\oplus}, \tag{4.38a}$$
$$\mathbf{K}^{\ominus}\mathbf{v}^{\ominus} = \mathbf{r}^{\ominus}. \tag{4.38b}$$

In the following sections we will decompose the vector $\mathbf{r}$ and the matrix $\mathbf{K}$ into their plus and minus components.

Abbreviations

Similar to [55] we introduce the following abbreviations. However, great care must be applied whenever a complex conjugation occurs.

$$\begin{aligned}
\mathbf{A}_{kl}{}^{\oplus} &= \overline{\mathbf{A}_l{}^{\ominus}} + \mathbf{A}_k{}^{\oplus}, & \mathbf{p}_{kl}{}^{\oplus} &= \overline{\mathbf{p}_l{}^{\ominus}} + \mathbf{p}_k{}^{\oplus}, & \gamma_{kl}{}^{\oplus} &= \overline{\gamma_l{}^{\ominus}} + \gamma_k{}^{\oplus}, \\
\mathbf{A}_{kl}{}^{\ominus} &= \overline{\mathbf{A}_l{}^{\oplus}} + \mathbf{A}_k{}^{\ominus}, & \mathbf{p}_{kl}{}^{\ominus} &= \overline{\mathbf{p}_l{}^{\oplus}} + \mathbf{p}_k{}^{\ominus}, & \gamma_{kl}{}^{\ominus} &= \overline{\gamma_l{}^{\oplus}} + \gamma_k{}^{\ominus}.
\end{aligned} \tag{4.39}$$

Note that in these combinations of the matrices, vectors, and phases of the Gaussian parameters of the ansatz, the plus and minus components from the bicomplex decomposition are mixed. This leads to a coupling of the two systems of linear equations (4.38). Also the special structure of the equations lead to the relations

$$\mathbf{A}_{kl}{}^{\oplus} = \overline{\mathbf{A}_{lk}{}^{\ominus}}, \qquad \mathbf{p}_{kl}{}^{\oplus} = \overline{\mathbf{p}_{lk}{}^{\ominus}}, \qquad \gamma_{kl}{}^{\oplus} = \overline{\gamma_{lk}{}^{\ominus}}. \tag{4.40}$$

Similarly the four-component abbreviations are obtained. For the plus component they read

$$\mathbf{A}_{klij}{}^{\oplus} = \overline{\mathbf{A}_l{}^{\ominus}} + \mathbf{A}_k{}^{\oplus} + \overline{\mathbf{A}_j{}^{\ominus}} + \mathbf{A}_i{}^{\oplus} = \mathbf{A}_{kl}{}^{\oplus} + \mathbf{A}_{ij}{}^{\oplus}, \tag{4.41a}$$
$$\mathbf{p}_{klij}{}^{\oplus} = \overline{\mathbf{p}_l{}^{\ominus}} + \mathbf{p}_k{}^{\oplus} + \overline{\mathbf{p}_j{}^{\ominus}} + \mathbf{p}_i{}^{\oplus} = \mathbf{A}_{kl}{}^{\oplus} + \mathbf{A}_{ij}{}^{\oplus}, \tag{4.41b}$$
$$\gamma_{klij}{}^{\oplus} = \overline{\gamma_l{}^{\ominus}} + \gamma_k{}^{\ominus} + \overline{\gamma_j{}^{\ominus}} + \gamma_i{}^{\oplus} = \gamma_{kl}{}^{\oplus} + \gamma_{ij}{}^{\oplus}, \tag{4.41c}$$

while the abbreviations for the minus components read

$$\mathbf{A}_{klij}{}^{\ominus} = \overline{\mathbf{A}_l{}^{\oplus}} + \mathbf{A}_k{}^{\ominus} + \overline{\mathbf{A}_j{}^{\oplus}} + \mathbf{A}_i{}^{\ominus} = \mathbf{A}_{kl}{}^{\ominus} + \mathbf{A}_{ij}{}^{\ominus}, \tag{4.42a}$$
$$\mathbf{p}_{klij}{}^{\ominus} = \overline{\mathbf{p}_l{}^{\oplus}} + \mathbf{p}_k{}^{\ominus} + \overline{\mathbf{p}_j{}^{\oplus}} + \mathbf{p}_i{}^{\ominus} = \mathbf{A}_{kl}{}^{\ominus} + \mathbf{A}_{ij}{}^{\ominus}, \tag{4.42b}$$
$$\gamma_{klij}{}^{\ominus} = \overline{\gamma_l{}^{\oplus}} + \gamma_k{}^{\ominus} + \overline{\gamma_j{}^{\oplus}} + \gamma_i{}^{\ominus} = \gamma_{kl}{}^{\ominus} + \gamma_{ij}{}^{\ominus}. \tag{4.42c}$$

Same as for the two-component abbreviations, these fulfil some symmetry relations:

$$\mathbf{A}_{klij}{}^{\oplus} = \overline{\mathbf{A}_l{}^{\ominus}} + \mathbf{A}_k{}^{\oplus} + \overline{\mathbf{A}_j{}^{\ominus}} + \mathbf{A}_i{}^{\oplus} = \overline{\mathbf{A}_l{}^{\ominus} + \overline{\mathbf{A}_k{}^{\oplus}} + \mathbf{A}_j{}^{\ominus} + \overline{\mathbf{A}_i{}^{\oplus}}} = \overline{\mathbf{A}_{lkji}{}^{\ominus}}, \tag{4.43a}$$
$$\mathbf{p}_{klij}{}^{\oplus} = \overline{\mathbf{p}_l{}^{\ominus}} + \mathbf{p}_k{}^{\oplus} + \overline{\mathbf{p}_j{}^{\ominus}} + \mathbf{p}_i{}^{\oplus} = \overline{\mathbf{p}_l{}^{\ominus} + \overline{\mathbf{p}_k{}^{\oplus}} + \mathbf{p}_j{}^{\ominus} + \overline{\mathbf{p}_i{}^{\oplus}}} = \overline{\mathbf{p}_{lkij}{}^{\ominus}}, \tag{4.43b}$$
$$\gamma_{klji}{}^{\oplus} = \overline{\gamma_l{}^{\ominus}} + \gamma_k{}^{\oplus} + \overline{\gamma_j{}^{\ominus}} + \gamma_i{}^{\oplus} = \overline{\gamma_l{}^{\ominus} + \overline{\gamma_k{}^{\oplus}} + \gamma_j{}^{\ominus} + \overline{\gamma_i{}^{\oplus}}} = \overline{\gamma_{lkji}{}^{\ominus}}. \tag{4.43c}$$

As described in section 4.1 the bar denotes the complex conjugation in the complex subspace.

Decomposition of the matrix K

The elements of **K** have the form $\langle g_l|\alpha^n\beta^m|g_k\rangle_{\mathbb{BC}}$ with the bicomplex functions g_l, gk and the real $\alpha = x, y, z$ and $\beta = x, y, z$. We now start to decompose the elements of the matrix into the idempotent basis. With the decomposition

$$\langle g_l|\alpha^n\beta^m|g_k\rangle_{\mathbb{BC}} = \langle {g_l}^{\ominus}|\alpha^n\beta^m|{g_k}^{\oplus}\rangle \mathrm{e}^{\oplus} + \langle {g_l}^{\oplus}|\alpha^n\beta^m|{g_k}^{\ominus}\rangle \mathrm{e}^{\ominus} \tag{4.44}$$

one obtains for the matrix components

$$K^{\oplus}{}_{lk} = \langle {g_l}^{\ominus}|\alpha^n\beta^m|{g_k}^{\oplus}\rangle = I_{\alpha^m\beta^m}({\mathbf{A}_{kl}}^{\oplus}, {\mathbf{p}_{kl}}^{\oplus}, {\gamma_{kl}}^{\oplus}), \tag{4.45a}$$

$$K^{\ominus}{}_{lk} = \langle {g_l}^{\oplus}|\alpha^n\beta^m|{g_k}^{\ominus}\rangle = I_{\alpha^m\beta^m}({\mathbf{A}_{kl}}^{\ominus}, {\mathbf{p}_{kl}}^{\ominus}, {\gamma_{kl}}^{\ominus}). \tag{4.45b}$$

The evaluation of the Gaussian integrals $I_{\alpha^m\beta^m}$ can be found in [55]. Note that the form of the integrals for the plus and minus components are the same, only the function arguments have changed. The elements of the $\mathbf{K}^{\oplus}$ and $\mathbf{K}^{\ominus}$ also fulfil a symmetry relation,

$$\begin{aligned} K^{\oplus}{}_{lk} = \langle {g_l}^{\ominus}|\alpha^n\beta^m|{g_k}^{\oplus}\rangle &= \overline{\langle {g_k}^{\oplus}|\alpha^n\beta^m|{g_l}^{\ominus}\rangle} = \overline{K^{\ominus}{}_{kl}} \\ \Rightarrow \mathbf{K}^{\oplus} &= \overline{\mathbf{K}^{T\ominus}}. \end{aligned} \tag{4.46}$$

Decomposition of the vector r

The elements of the vector **r** are of the form

$$r_l = \sum_k^N \underbrace{\langle g_l|\alpha^n\beta^m V(x)|g_k\rangle_{\mathbb{BC}}}_{=: r_{lk}} \tag{4.47}$$

with $\alpha, \beta = x, y, z$ and $V(x) = V_{\mathrm{ext}} + V_{\mathrm{c}} + V_{\mathrm{d}}$. It is important to keep in mind that the potential $V(x)$ is in general not a real number and has also to be decomposed accordingly. This makes the treatment of the vector **r** more complicated than that of the matrix **K**.

Therefore a decomposition of **r** leads to

$$\begin{aligned} r_{lk} &= \langle g_l|\alpha^n\beta^m V(x)|g_k\rangle_{\mathbb{BC}} \\ &= \underbrace{\left\langle {g_l}^{\ominus}\middle|\alpha^n\beta^m V(x)^{\oplus}\middle|{g_k}^{\oplus}\right\rangle}_{=: {r_{lk}}^{\oplus}} \mathrm{e}^{\oplus} + \underbrace{\left\langle {g_l}^{\oplus}\middle|\alpha^n\beta^m V(x)^{\ominus}\middle|{g_k}^{\ominus}\right\rangle}_{=: {r_{lk}}^{\ominus}} \mathrm{e}^{\ominus}. \end{aligned} \tag{4.48}$$

These expression can be further separated into

$$\begin{aligned} r_{lk}{}^{\oplus} &= \langle g_l{}^{\ominus} | \alpha^n \beta^m V^{\oplus} | g_k{}^{\oplus} \rangle \\ &= \langle g_l{}^{\ominus} | \alpha^n \beta^m V_{\text{ext}}{}^{\oplus} | g_k{}^{\oplus} \rangle + \langle g_l{}^{\ominus} | \alpha^n \beta^m V_{\text{c}}{}^{\oplus} | g_k{}^{\oplus} \rangle + \langle g_l{}^{\ominus} | \alpha^n \beta^m V_{\text{d}}{}^{\oplus} | g_k{}^{\oplus} \rangle \end{aligned} \tag{4.49}$$

and

$$\begin{aligned} r_{lk}{}^{\ominus} &= \langle g_l{}^{\oplus} | \alpha^n \beta^m V^{\ominus} | g_k{}^{\ominus} \rangle \\ &= \langle g_l{}^{\oplus} | \alpha^n \beta^m V_{\text{ext}}{}^{\ominus} | g_k{}^{\ominus} \rangle + \langle g_l{}^{\oplus} | \alpha^n \beta^m V_{\text{c}}{}^{\ominus} | g_k{}^{\ominus} \rangle + \langle g_l{}^{\oplus} | \alpha^n \beta^m V_{\text{d}}{}^{\ominus} | g_k{}^{\ominus} \rangle. \end{aligned} \tag{4.50}$$

In the following we will individually address the different parts of the potential.

The contact potential describes the s-wave scattering between the atoms of the BEC. It contains the norm of the wave function of the condensate and therefore must be decomposed with care. For the component of $\mathrm{e}^{\oplus}$ we obtain

$$\begin{aligned} \langle g_l{}^{\ominus} | \alpha^n \beta^m V_{\text{c}}{}^{\oplus} | g_k{}^{\oplus} \rangle &= \left\langle g_l{}^{\ominus} \middle| \alpha^n \beta^m c_{\text{sc}}{}^{\oplus} \sum_{i,j} \langle g_j{}^{\ominus} | g_i{}^{\oplus} \rangle \middle| g_k{}^{\oplus} \right\rangle \\ &= c_{\text{sc}}{}^{\oplus} \sum_{i,j} \langle g_l{}^{\ominus} g_j{}^{\ominus} | \alpha^n \beta^m | g_i{}^{\oplus} g_k{}^{\oplus} \rangle \\ &= c_{\text{sc}}{}^{\oplus} \sum_{i,j} I_{\alpha^m \beta^m}(\mathbf{A}_{klij}{}^{\oplus}, \mathbf{p}_{klij}{}^{\oplus}, \gamma_{klij}{}^{\oplus}) \end{aligned} \tag{4.51}$$

and for $\mathrm{e}^{\ominus}$ the result reads

$$\begin{aligned} \langle g_l{}^{\oplus} | \alpha^n \beta^m V_{\text{c}}{}^{\ominus} | g_k{}^{\ominus} \rangle &= \left\langle g_l{}^{\oplus} \middle| \alpha^n \beta^m c_{\text{sc}}{}^{\ominus} \sum_{i,j} \langle g_j{}^{\oplus} | g_i{}^{\ominus} \rangle \middle| g_k{}^{\ominus} \right\rangle \\ &= c_{\text{sc}}{}^{\ominus} \sum_{i,j} \langle g_l{}^{\oplus} g_j{}^{\oplus} | \alpha^n \beta^m | g_i{}^{\ominus} g_k{}^{\ominus} \rangle \\ &= c_{\text{sc}}{}^{\ominus} \sum_{i,j} I_{\alpha^m \beta^m}(\mathbf{A}_{klij}{}^{\ominus}, \mathbf{p}_{klij}{}^{\ominus}, \gamma_{klij}{}^{\ominus}). \end{aligned} \tag{4.52}$$

In general the scattering length a is real and therefore also the parameter c_{sc}. However, the examination of exceptional points requires the encircling of the parameter point in the complex space. Therefore (as for other parameters) we extend c_{sc} into the complex plane. It is important to note that, since our complex continuation of the Gross-Pitaevskii equation was realized using the complex unit j, c_{sc} is a member of $\mathbb{C}_{\text{j}}$. Since the parameter has the form $c_{\text{sc}} = c_{\text{sc},0} + \mathrm{j} c_{\text{sc},1}$ the relation

$$a^{\oplus} = \overline{a^{\ominus}} \tag{4.53}$$

as mentioned in section 4.1 applies. With this relation we obtain the symmetry relations for $\mathbf{A}_{klij}$, $\mathbf{p}_{klij}$ and γ_{klij} as follows:

$$\begin{aligned}\left\langle {g_l}^{\ominus}\middle|\alpha^n\beta^m {V_\mathrm{c}}^{\oplus}\middle|{g_k}^{\oplus}\right\rangle &= {c_\mathrm{sc}}^{\oplus}\sum_{i,j} I_{\alpha^m\beta^m}({\mathbf{A}_{klij}}^{\oplus}, {\mathbf{p}_{klij}}^{\oplus}, {\gamma_{klij}}^{\oplus}) \\ &= \overline{{c_\mathrm{sc}}^{\ominus}}\sum_{i,j} I_{\alpha^m\beta^m}(\overline{{\mathbf{A}_{lkji}}^{\ominus}}, \overline{{\mathbf{p}_{lkji}}^{\ominus}}, \overline{{\gamma_{lkji}}^{\ominus}}) \\ &= \overline{{c_\mathrm{sc}}^{\ominus}\sum_{i,j} I_{\alpha^m\beta^m}({\mathbf{A}_{lkji}}^{\ominus}, {\mathbf{p}_{lkji}}^{\ominus}, {\gamma_{lkji}}^{\ominus})} \\ &= \overline{\left\langle {g_k}^{\oplus}\middle|\alpha^n\beta^m {V_\mathrm{c}}^{\ominus}\middle|{g_l}^{\ominus}\right\rangle}. \end{aligned} \tag{4.54}$$

The trap potential consists of Gaussian shaped wells. They can be decomposed into the components

$$\begin{aligned}&\left\langle {g_l}^{\ominus}\middle|\alpha^n\beta^m {V_h}^{\oplus}\exp\left(-(\mathbf{r}^T\mathbf{A}_h^T\mathbf{r}+\mathbf{p}_h^T\mathbf{r}+\gamma_h)\right)\middle|{g_k}^{\oplus}\right\rangle \\ &\qquad = {V_h}^{\oplus} I_{\alpha^n\beta^m}\left({\mathbf{A}_{lkij}}^{\oplus}+\mathbf{A}_h, {\mathbf{p}_{lkij}}^{\oplus}+\mathbf{p}_h, {\gamma_{lkij}}^{\oplus}+\gamma_h\right), \end{aligned} \tag{4.55a}$$

$$\begin{aligned}&\left\langle {g_l}^{\oplus}\middle|\alpha^n\beta^m {V_h}^{\ominus}\exp\left(-(\mathbf{r}^T\mathbf{A}_h^T\mathbf{r}+\mathbf{p}_h^T\mathbf{r}+\gamma_h)\right)\middle|{g_k}^{\ominus}\right\rangle \\ &\qquad = {V_h}^{\ominus} I_{\alpha^n\beta^m}\left({\mathbf{A}_{lkij}}^{\ominus}+\mathbf{A}_h, {\mathbf{p}_{lkij}}^{\ominus}+\mathbf{p}_h, {\gamma_{lkij}}^{\ominus}+\gamma_h\right) \end{aligned} \tag{4.55b}$$

with $A_h \in \mathbb{R}^{3\times3}$, $p_h \in \mathbb{R}^3$ and $g_h \in \mathbb{R}$. These are again Gaussian integrals. The potential strength $V_h = V_0 \pm \mathrm{i}\Gamma$ is a bicomplex number since both the original real potential depth V_0 and the original real in- and outcoupling strength Γ are extended using the imaginary unit j. In combination with the imaginary unit i all imaginary units can occur. Therefore no similar symmetry relation as for the previous potentials can be found. Only the following relation can be used

$$\begin{aligned}&I_{\alpha^n\beta^m}\left({\mathbf{A}_{lkij}}^{\oplus}+\mathbf{A}_h, {\mathbf{p}_{lkij}}^{\oplus}+\mathbf{p}_h, {\gamma_{lkij}}^{\oplus}+\gamma_h\right) \\ &\qquad = \overline{I_{\alpha^n\beta^m}\left({\mathbf{A}_{klji}}^{\ominus}+\mathbf{A}_h, {\mathbf{p}_{klji}}^{\ominus}+\mathbf{p}_h, {\gamma_{klji}}^{\ominus}+\gamma_h\right)}. \end{aligned} \tag{4.56}$$

The dipole-dipole interaction can be decomposed into its plus and minus component similar to the contact interaction

$$\begin{aligned}&\left\langle {g_l}^{\ominus}\middle|\alpha^n\beta^m {c_\mathrm{d}}^{\oplus}\sum_{i,j}\int d^3\mathbf{r}'\frac{1-3\cos^2\theta}{|\mathbf{r}-\mathbf{r}'|^3}\overline{g_i(r')^{\ominus}}g_j(r')^{\oplus}\middle|{g_k}^{\oplus}\right\rangle \\ &\qquad = {c_\mathrm{d}}^{\oplus}\sum_{i,j} I^{\mathrm{D}}_{\alpha^n,\beta^m}\left({A_{kl}}^{\oplus}, {A_{ij}}^{\oplus}, {p_{kl}}^{\oplus}, {p_{ij}}^{\oplus}, \gamma^{\oplus}, \gamma^{\oplus}\right), \end{aligned} \tag{4.57a}$$

$$\left\langle {g_l}^{\oplus} \middle| \alpha^n \beta^m {c_\mathrm{d}}^{\ominus} \sum_{i,j} \int d^3\mathbf{r}' \frac{1-3\cos^2\theta}{|\mathbf{r}-\mathbf{r}'|^3} \overline{g_i(r')^{\oplus}} \left(g_j(r')\right)^{\ominus} \middle| {g_k}^{\ominus} \right\rangle$$
$$= {c_\mathrm{d}}^{\ominus} \sum_{i,j} I^{\mathrm{D}}_{\alpha^n,\beta^m} \left({A_{kl}}^{\ominus}, {A_{ij}}^{\ominus}, {p_{kl}}^{\ominus}, {p_{ij}}^{\ominus}, {\gamma}^{\ominus}, {\gamma}^{\ominus}\right). \quad (4.57b)$$

All previous Gaussian integrals can be calculated very fast. However, the calculation of the dipolar Integral is numerical expensive and complex. In [55] many techniques were discussed, how this calculation can be accelerated. During these calculations the auxiliary integrals $J_{\sigma,ijkl}$ are calculated. For permutation of the indices i, j, k, l symmetry relations exist. However, using bicomplex numbers these symmetry relations have to be adjusted accordingly.

Exchanging the index pairs (i, j) with (k, l) one obtains the same relation as initially introduced

$${J_{\sigma,ijkl}}^{\oplus} = s_\sigma {J_{\sigma,klij}}^{\oplus}, \quad {J_{\sigma,ijkl}}^{\ominus} = s_\sigma {J_{\sigma,klij}}^{\ominus} \quad (4.58)$$

with the sign $s_\sigma = \pm 1$. Since complex conjugation is involved no modification is necessary. However, if the indices in each pair are exchanged, one obtains the relations

$${J_{\sigma,ijkl}}^{\oplus} = s_\sigma \overline{{J_{\sigma,jilk}}^{\ominus}}, \quad {J_{\sigma,ijkl}}^{\ominus} = s_\sigma \overline{{J_{\sigma,jilk}}^{\oplus}}, \quad (4.59)$$

where due to the complex conjugation the plus components can be expressed by the minus components and vice versa. Finally, if the pairs are permuted and the indices in each pair are exchanged, one obtains

$${J_{\sigma,ijkl}}^{\oplus} = \overline{{J_{\sigma,lkji}}^{\ominus}}, \quad {J_{\sigma,ijkl}}^{\ominus} = \overline{{J_{\sigma,lkji}}^{\oplus}}. \quad (4.60)$$

This optimization decreases the number of auxiliary integrals which have to be calculated.

4.3 Bifurcations and exceptional points with long-range interactions

After introducing the Gross-Pitaevskii equation (section 2.1), the equation was analytically continued (section 4.2) with the help of bicomplex numbers (section 4.1). This is the prerequisite to be able to examine the bifurcation scenario more closely and determine the order and exchange behaviour of the associated exceptional points. The resulting equations pose some numerical difficulties. How they can be solved was discussed in the previous chapter. In this chapter the results will be presented and discussed.

4.3.1 Bifurcations

The calculations for the Gross-Pitaevskii equation (2.25), which was analytically continued in section 4.2, reveals the bifurcation structure of the system. In addition to the known stationary states, which exist in the complex domain new states, which are truly bicomplex, are found. With these new states all (mathematical) branches of a bifurcation are present.

In figure 4.2 the meanfield energies E_{mf} for states with a scattering parameter $c_{\mathrm{sc}} = -0.9$ are shown. First one notices that the states which are purely complex (solid lines) and are already known from [42] fulfil the relation

$$E_{\mathrm{mf}}{}^{\oplus} = E_{\mathrm{mf}}{}^{\ominus}. \tag{4.61}$$

These states have only two real independent components in the meanfield energy $E_{\mathrm{mf}}{}^{\oplus}$ and $E_{\mathrm{mf}}{}^{\ominus}$, or respectively in the chemical potential $\mu^{\oplus}$ and $\mu^{\ominus}$ (see figure 4.3).

This is no longer the case for the states living in bicomplex space (dashed lines). In contrast to [55] all branches of the bifurcations are now present, there exist six states for the whole parameter range of Γ. Since the chemical potential exhibits the same qualitative bifurcation behaviour as the meanfield energy, we only show the plus component of the meanfield energy in the following discussion.

In figure 4.2 different bifurcations are observed. They are marked with the labels B1, B2 and B3. These bifurcations change for different values of the scattering parameter. One observes mergers and at these mergers changes occur. Amongst others the contributing branches may change. Figure 4.4 gives a general overview of the bifurcations for different scattering length values while figure 4.5 and figure 4.6 provide a detailed view of the mergers.

For small values of Γ the states s1 and s2 show the typical behaviour also known from Bose-Einstein condensates without long-range interactions. They merge in a tangent bifurcation B1. Up to this point the states also exist without the analytical continuation and were already observed in [42]. But for larger Γ they become bicomplex. This qualitative behaviour is largely independent of the scattering length, and only the critical point is slightly shifted.

The bifurcation B2 undergoes multiple behaviour changes for different scattering lengths. Also this bifurcation does not always exist (see figure 4.4(a)). For smaller scattering lengths the bifurcation appears at $\Gamma = 0$. This is a pitchfork bifurcation between the states s1, s3 and s6. The bifurcation moves along the state s1 to larger Γ as the scattering length is decreased (see figure 4.4(b) and (c)). At a critical scattering length $c_{\mathrm{sc,crit,1}} = -0.93063$ the bifurcation merges with the bifurcation B1 (see figure 4.5(b)). For even smaller scattering lengths the bifurcation moves back to $\Gamma = 0$ along the state s2. The pitchfork bifurcation is now formed between the states s2, s3 and s6 (see figure 4.5(c)). However, before the bifurcation reaches $\Gamma = 0$ another critical scattering length is reached. At $c_{\mathrm{sc,crit,2}} = -0.93365$ the bifurcation B2 merges with

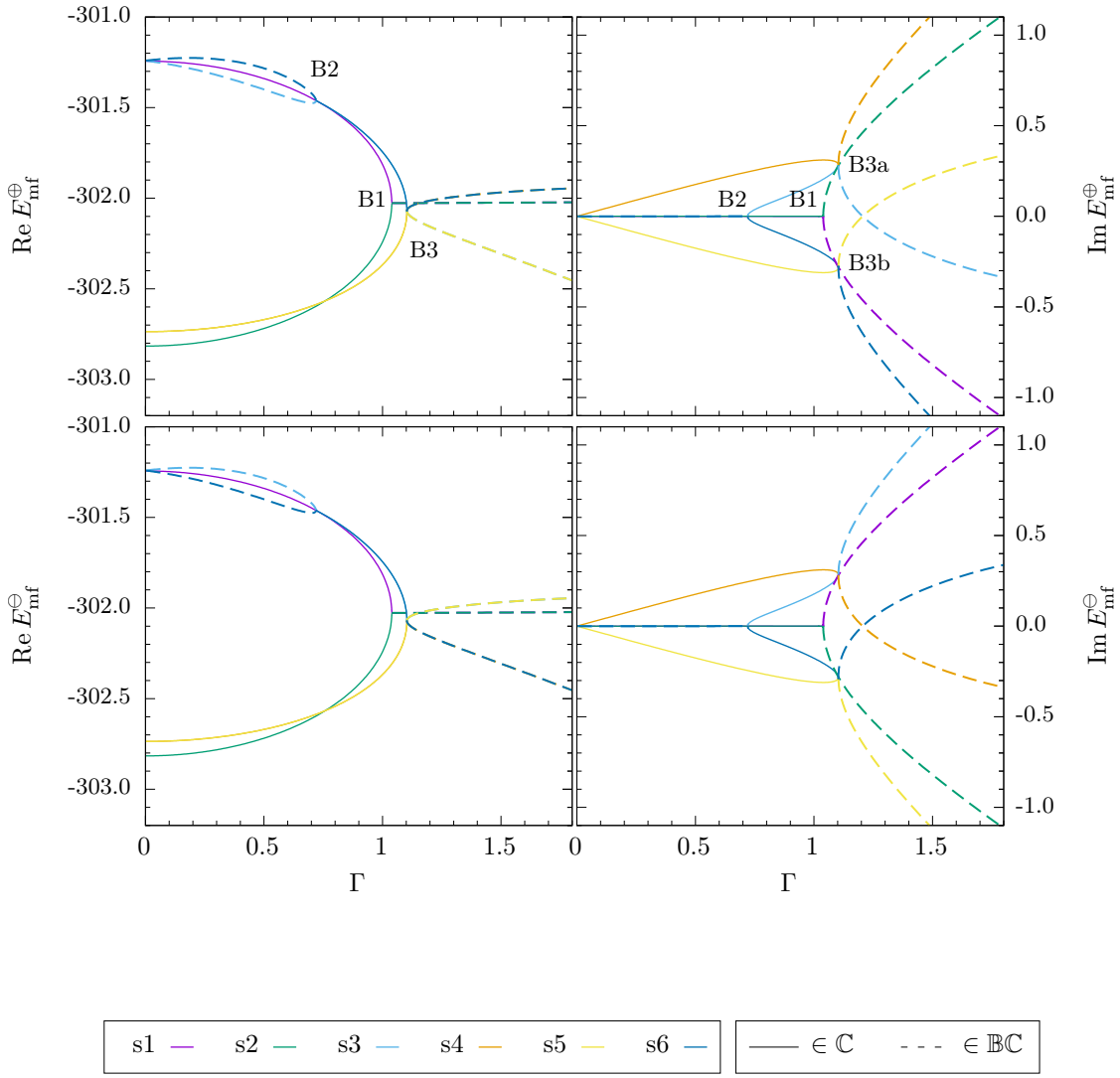

Figure 4.2.: Real and imaginary parts of the plus and minus components of the bicomplex meanfield energy in a dipolar Bose-Einstein condensate with scattering length $c_{\mathrm{sc}} = -0.9$. The meanfield energy is composed as $E_{\mathrm{mf}} = {E_{\mathrm{mf}}}^{\oplus}\mathrm{e}^{\oplus} + {E_{\mathrm{mf}}}^{\ominus}\mathrm{e}^{\ominus}$. States which exist without the analytical continuation into bicomplex values must obey ${E_{\mathrm{mf}}}^{\oplus} = {E_{\mathrm{mf}}}^{\ominus}$ and are shown as solid lines. States which exist only in the bicomplex domain are shown as dashed lines. The four bifurcations which occur between the states are marked with B1 to B4. As discussed in [42] states s1 and s2 obey $\mathcal{PT}$-symmetry from $\Gamma = 0$ up to the bifurcation B1. Beyond this point the states are $\mathcal{PT}$-broken.

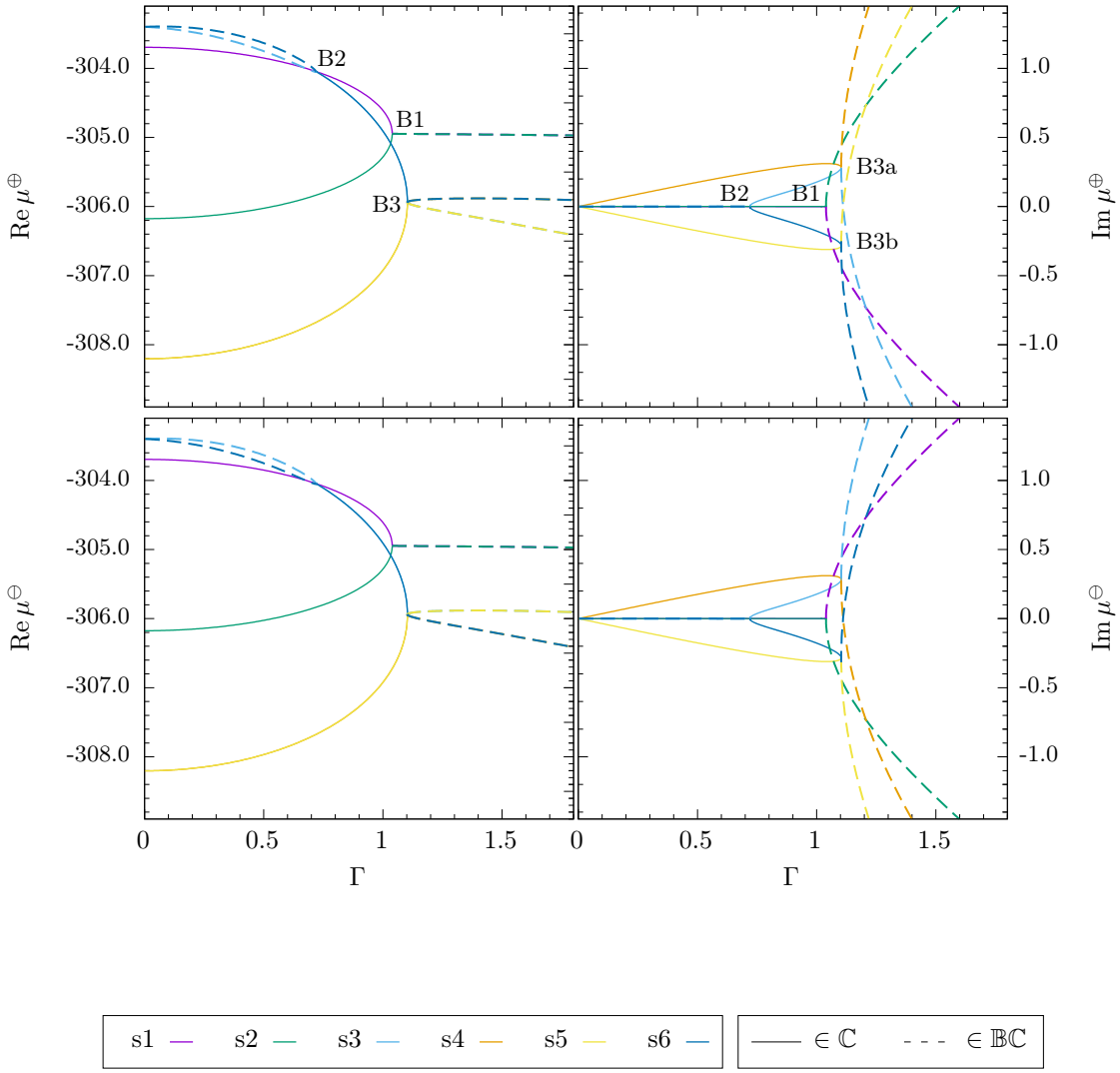

Figure 4.3.: Real and imaginary parts of the plus and minus components of the bicomplex chemical potential of a dipolar Bose-Einstein condensate with scattering length $c_{sc} = -0.9$. The chemical potential is composed as $\mu = \mu^{\oplus}e^{\oplus} + \mu^{\ominus}e^{\ominus}$. States which exist without the analytical continuation into bicomplex values must obey $\mu^{\oplus} = \mu^{\ominus}$ and are shown as solid lines. States which exist only in the bicomplex domain are shown as dashed lines. The four bifurcations which occur between the states are marked with B1 to B4. As discussed in [42] states s1 and s2 obey $\mathcal{PT}$-symmetry from $\Gamma = 0$ up to the bifurcation B1. Beyond this point the states are $\mathcal{PT}$-broken.

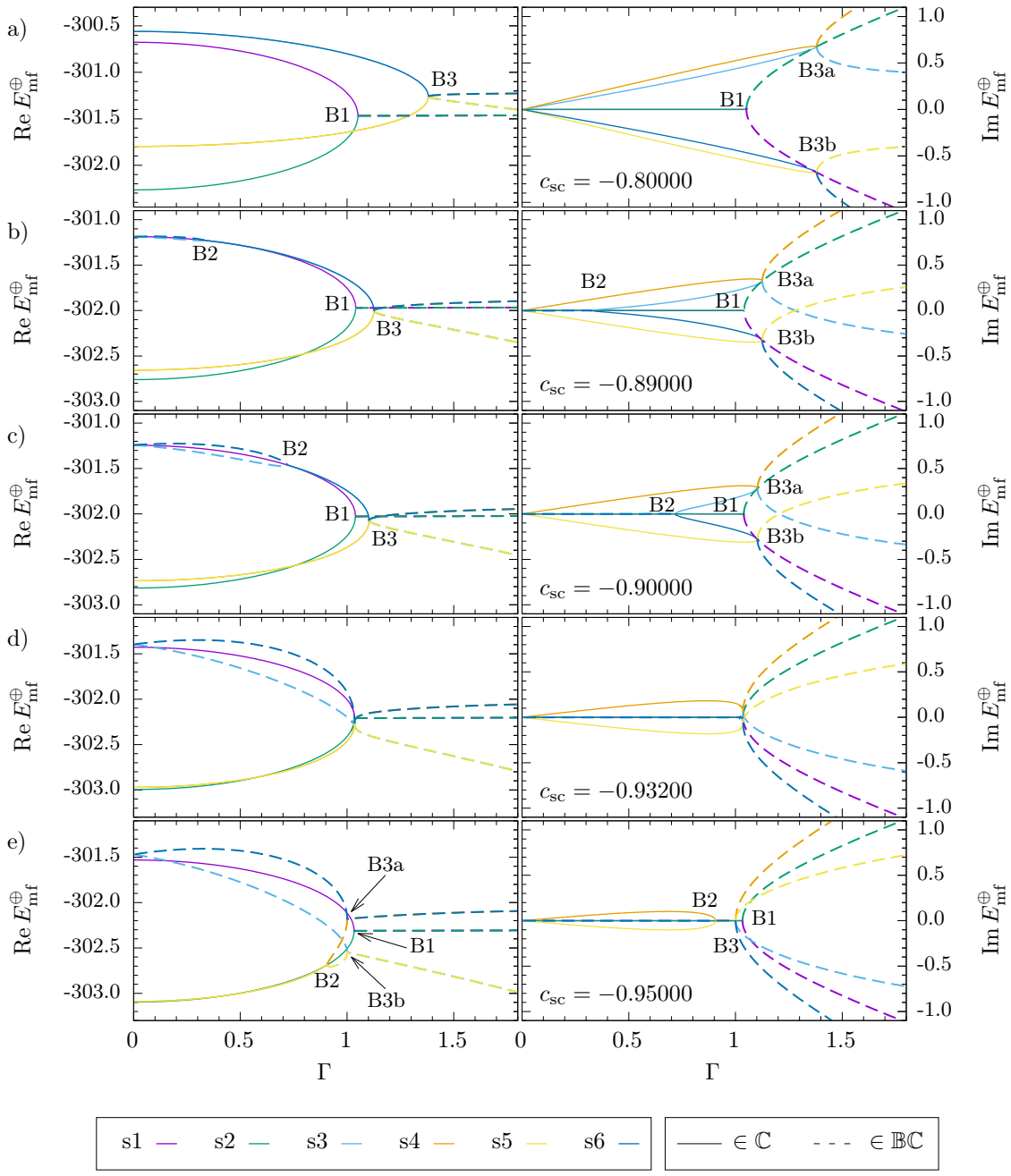

Figure 4.4.: Meanfield energies $E_{\mathrm{mf}}{}^{\oplus}$ for different values of c_{sc}. The different bifurcation points are denoted by B1, B2, B3a and B3b. When the bifurcations B3a and B3b coincide they are marked by B3. The bifurcation B2 does not exist in (a).

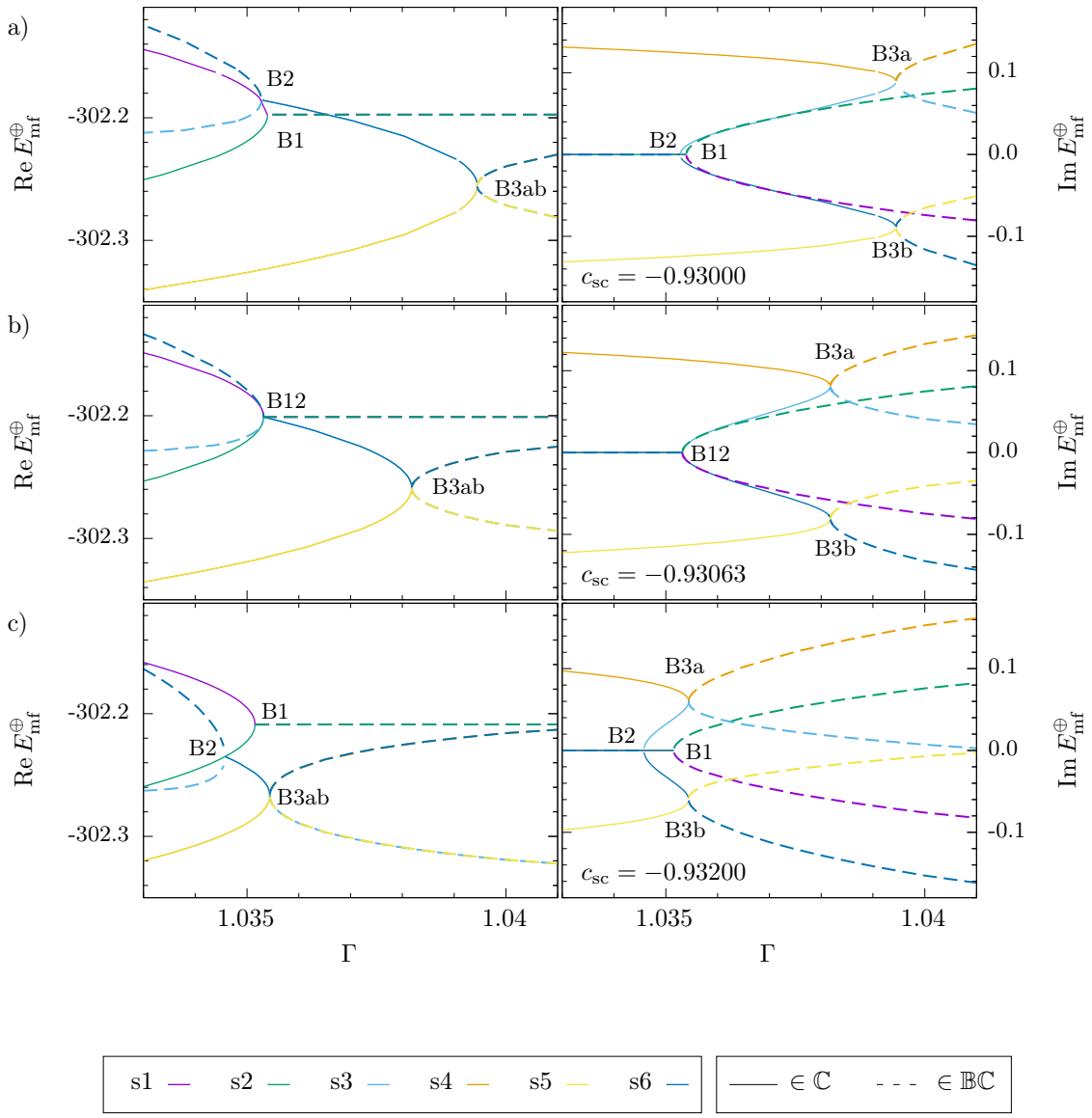

Figure 4.5.: For a scattering length of $c_{\mathrm{sc,crit,1}} = -0.93063$ the bifurcations and EP2s B1 and B2 merge. This can be seen in b) and the resulting bifurcation is marked as B12. In a) the bifurcations can be seen for a slightly larger and in b) for a slightly smaller scattering length.

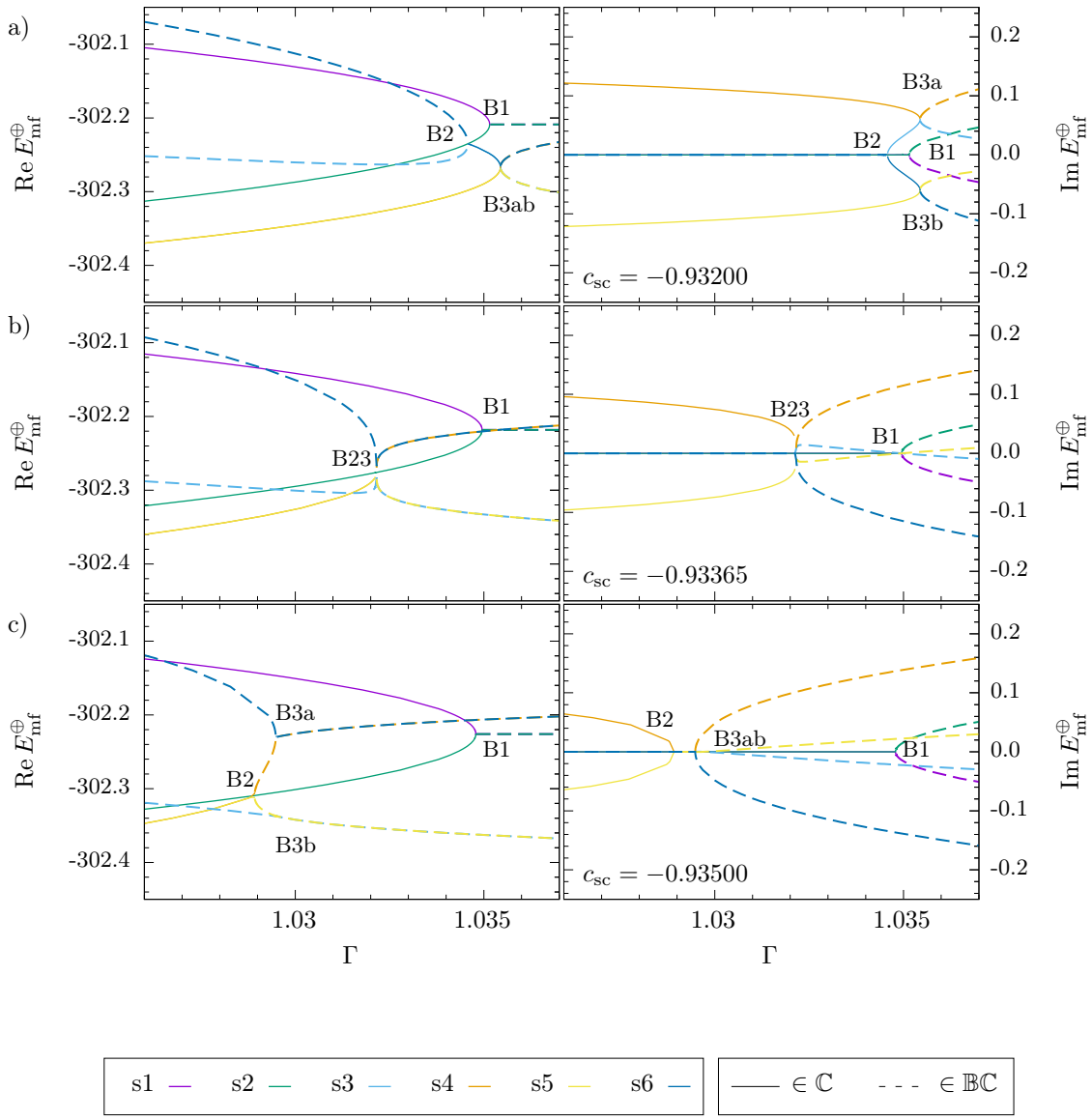

Figure 4.6.: In b) the EPs and bifurcations B2, B3a and B3b merge for the critical scattering length $c_{\mathrm{sc,crit,2}} = -0.93365$ into a higher order exceptional point which is denoted by B23. In a) the bifurcations can be seen for a slightly larger and in b) for a slightly smaller scattering length.

the bifurcations B3a and B3b (see figure 4.6(b)). At this point the behaviour of the bifurcation is altered.

For larger scattering lengths at smaller Γ all participating states of the bifurcation exist only in the bicomplex equation (see figure 4.6(a)). Thus, in these parameter regions the bifurcation could not be observed previously. However, for larger Γ some of the states exist already in the complex Gross-Pitaevskii equation (see figure 4.6(c)) without the bicomplex extension. So the bifurcation could be observed previously, but some states were missing.

If the scattering length is smaller than $c_{\mathrm{sc,crit,2}}$ this behaviour is mirrored with respect to the Γ-axis. Until the bifurcation vanishes for smaller scattering lengths at $\Gamma = 0$ it is composed of the states s2, s4 and s5. If the bifurcation B2 is compared with the bifurcation O2 of the Bose-Einstein condensate without long-range interactions (see figure 3.2), the first change (the merger of B1 and B2) can also be observed. However, the second change in behaviour is a new effect since the bifurcations B3a and B3b do not exist without long-range interactions.

We have seen that the merger of the bifurcations B2, B3a and B3b changes the behaviour of bifurcation B2. The properties of the tangent bifurcations B3a and B3b are altered. For scattering lengths greater than $c_{\mathrm{sc,crit,2}}$ the bifurcations B3a and B3b are bicomplex for larger Γ (i.e., the states have components of the imaginary units j and k). However, for Γ below the critical value only the real component and the component with complex unit i is nonzero (see figure 4.6(a)). For smaller values of the scattering lengths the states in both Γ regions are bicomplex, i.e., they only exist as solutions of the analytically continued Gross-Pitaevskii equation (see figure 4.6(c)).

We have found that the critical scattering length parameters dividing the parameter regions with different behaviours are related with the merger of multiple bifurcations. In figure 4.7 the parameter pairs of the scattering length c_{sc} and Γ are shown at which the different bifurcations occur. One observes three points at which the parameters of two different bifurcations become identical. Point P3 is not special, the states which are involved in the two bifurcations (B1 and B3) have different eigenvalues and wave functions. Therefore just two independent bifurcations occur at the same parameter pair. By contrast at P2 the bifurcations B1 and B2 are joined into one bifurcation. The bifurcation scenario is shown in figure 4.5(b). Another bifurcation merger appears for the parameters at point P1. The resulting bifurcation, which consists of B2, B3a and B3b is shown in figure 4.6(b). These merger points are also of special interest because they have the prerequisites necessary that exceptional points of higher order can appear.

4.3.2 Exchange behaviour of the states around the exceptional points

We now examine which signatures of exceptional points can be observed. In [38, 43] it was discussed that a complex encircling of a higher-order exceptional point does not have to exhibit an exchange of all states involved in the exceptional point. Using

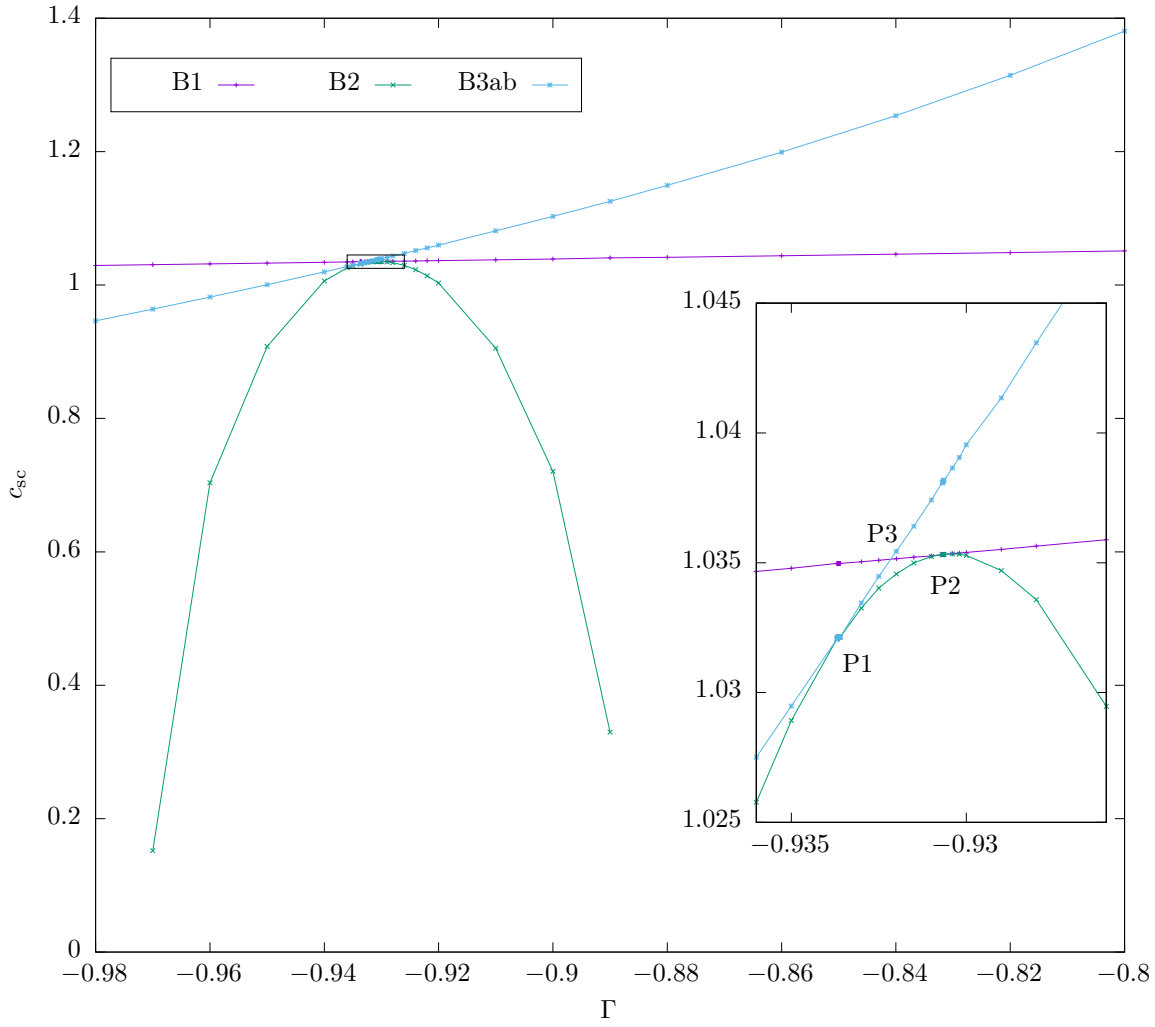

Figure 4.7.: Positions of the bifurcations and exceptional points in the Γ-c_{sc}-parameter space. In the inset the mergers of multiple bifurcations can be observed. Note that at the point P3 no merger occurs. There merely exist two bifurcations between different states at the same point in parameter space.

different parameters to encircle the exceptional point can show different exchange behaviours.

The second-order exceptional points of the tangent bifurcations B1, B3a and B3b show the expected square root behaviour by exchanging each state with the other (see figure 4.8(a,c,d)) when the point is encircled in the complex parameter. The path on which the point is encircled is parameterized as

$$\Gamma(\phi) = \Gamma_{\text{center}} + r\mathrm{e}^{\mathrm{i}\phi} \tag{4.62}$$

where ϕ starts at zero and ends at $\phi = 2\pi$. On the other hand the third-order exceptional point at the bifurcation B2 only shows the exchange of two states. For the encircling in the complex Γ-space a cubic root exchange behaviour cannot be observed (see figure 4.8(b)).

In figure 4.9a) we show the exchange behaviour of the states involved in P2 where the bifurcations B1 and B2 merge. When encircling the exceptional point in a complex Γ plane (see figure 4.9b) an exchange within pairs of states is found, however, these two exchanges are separated and no exchange between all four states can be observed. Therefore it is unclear whether these are two second-order exceptional points or one fourth-order exceptional point.

Also a circle around the critical point in the complex plane of the scattering length (see figure 4.9d)) does not change the qualitative behaviour (see figure 4.9c)), again only two states exchange. To prove that this must be indeed an exceptional point of order four, one must search for further complex perturbation parameters. However, there is a further possibility to gain information. Since for an exceptional point of order n, all n eigenvalues and eigenstates must coalesce [34] we examine the wave functions of the participating states and they all coalesce at the critical point (which means that for the ansatz of coupled Gaussians all Gaussian parameters must be the same, which is indeed the case).

The same examination can be performed for the merger of the bifurcations B2, B3a and B3b (point P1). At this critical point five eigenvalues coalesce. A circle in the complex Γ plane (see figure 4.10b)) reveals the signature of four exchanging states (see figure 4.10a)). Again the circle can be repeated in the complex plane of the scattering length (figure 4.10cd)) resulting in the same exchange behaviour. In this case the question arises whether this is an exceptional point of order four or of order five. The exchange behaviour proves that the order of the exceptional point must be at least four. All wave functions of the participating states coalesce at the critical point, however, to finally decide whether this is a fifth-order exceptional point a further perturbation parameter must be examined.

We introduce a new asymmetry parameter s in the Gross-Pitaevskii equation (2.25), which lifts or lowers the potential wells (see equation (4.33)) and breaks the symmetry of the wells,

$$c_{\mathrm{g},1} = (V_0 + s) + \mathrm{i}\Gamma\,, \;\; c_{\mathrm{g},2} = (V_0 - s) + \mathrm{i}\Gamma. \tag{4.63}$$

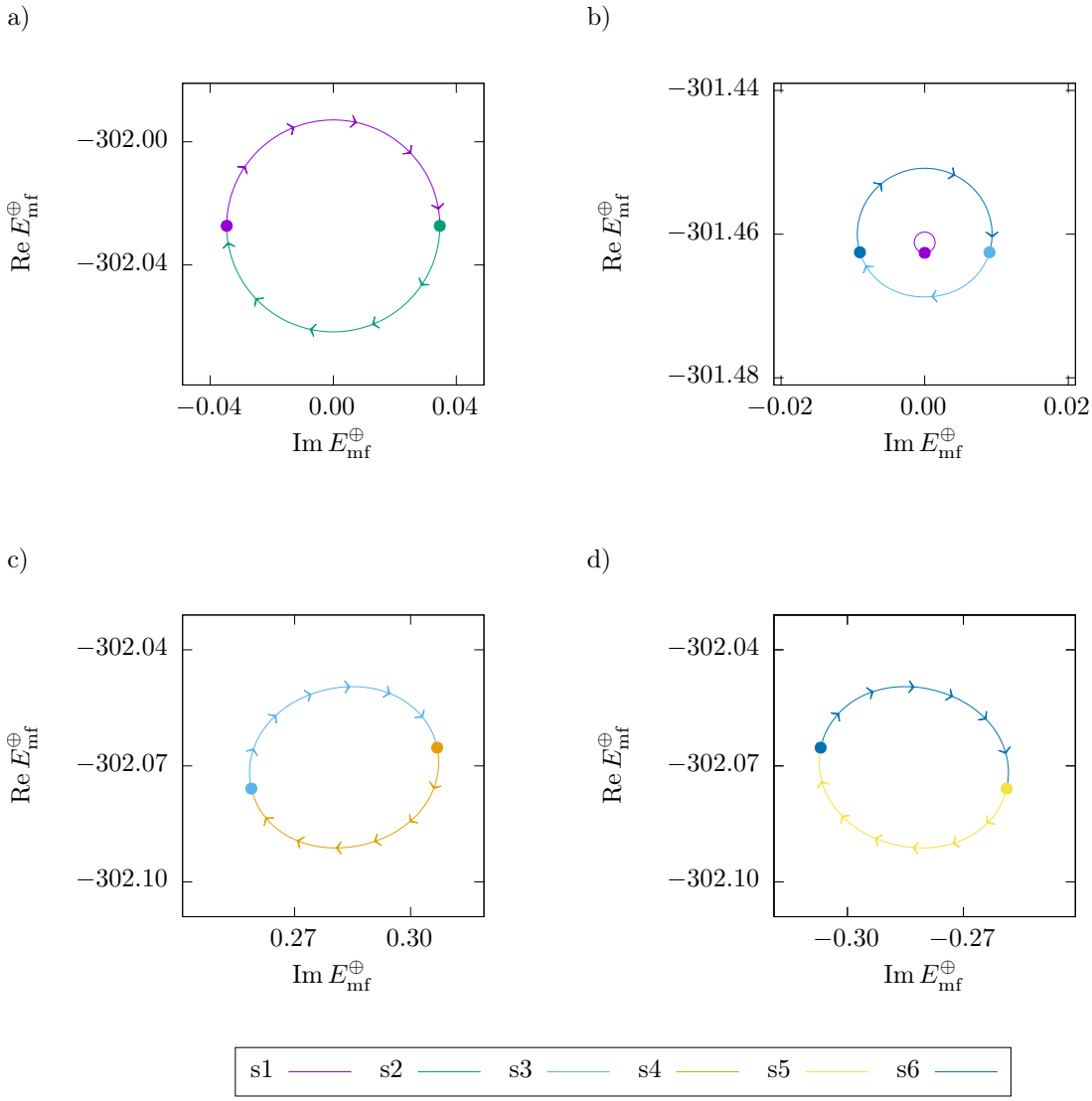

Figure 4.8.: Characteristic exchange of states when an exceptional point is encircled in the complex parameter space. In this case the bifurcation B1 (a), $\Gamma_{\mathrm{center}} = 1.03904$, $r = 10^{-3}$), bifurcation B2 (b), $\Gamma_{\mathrm{center}} = 0.71967$, $r = 2 \times 10^{-3}$), bifurcation B3a (c), $\Gamma_{\mathrm{center}} = 1.10296$, $r = 10^{-4}$) and bifurcation B3b (d), $\Gamma_{\mathrm{center}} = 1.10296$, $r = 10^{-4}$) are encircled on the parameter path $\Gamma(\phi) = \Gamma_{\mathrm{center}} + re^{\mathrm{j}\phi}$ for $\phi \in [0, 2\pi]$. All plots were calculated for a scattering length of $c_{\mathrm{sc}} = -0.9$. The starting positions are marked by a points.

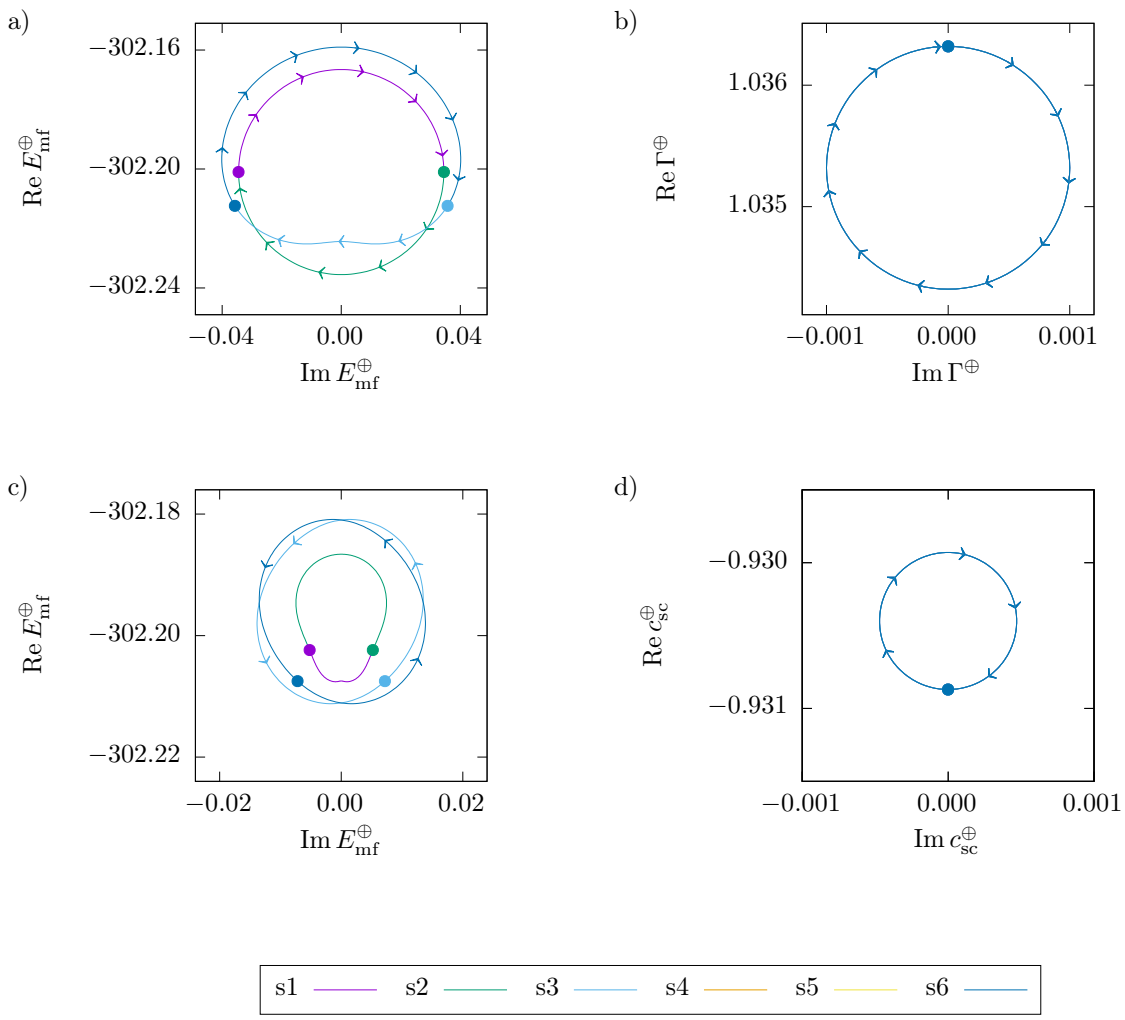

Figure 4.9.: Exchange behaviour of the eigenvalues when the exceptional point at $c_{\mathrm{sc,crit,1}} = -0.93063$ and $\Gamma = 1.03531$ is encircled. a) shows the energy eigenvalues if the exceptional point is encircled on a path b) in the complex Γ-plane. c) shows the energy eigenvalues if the exceptional point is encircled on a path d) in the complex c_{sc}-plane.

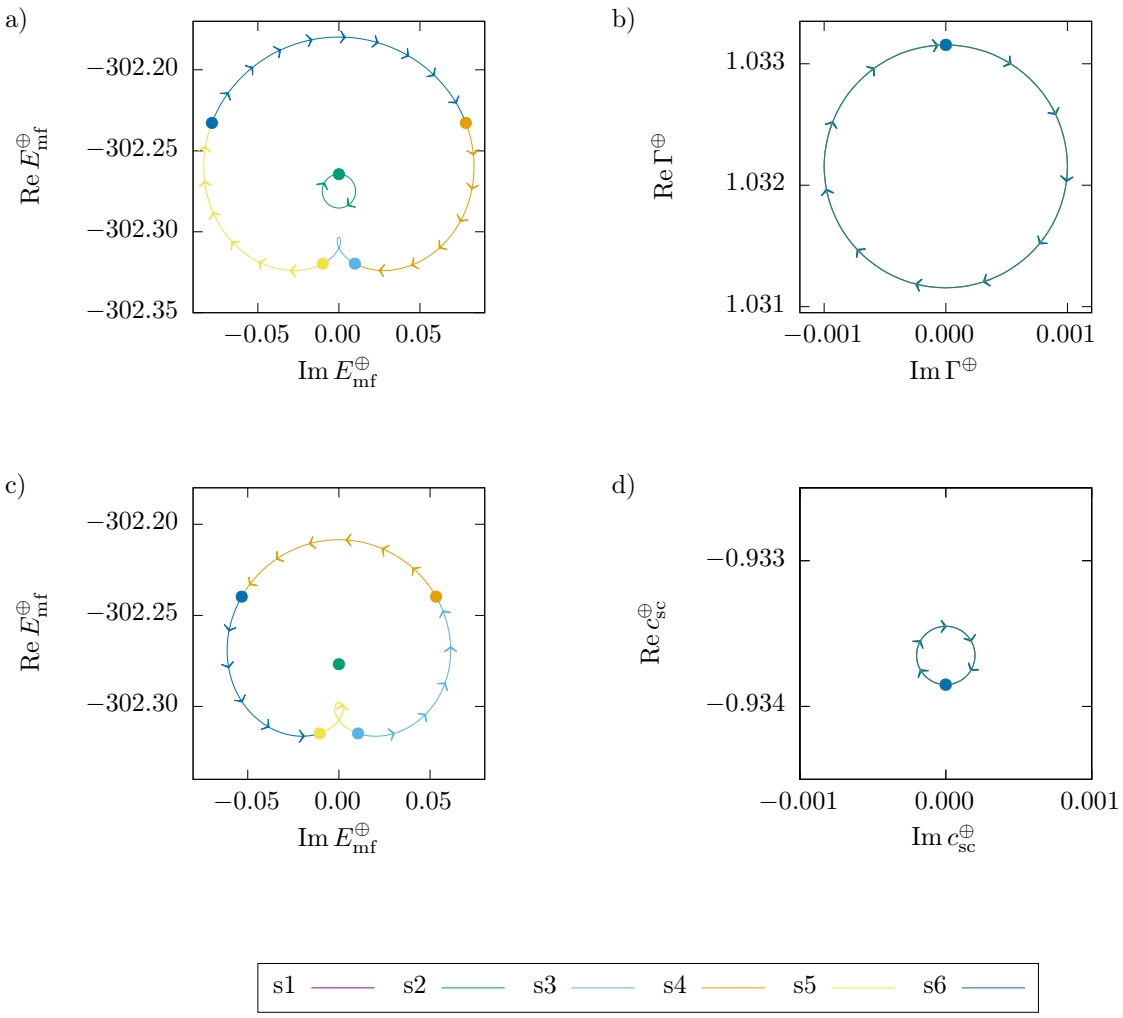

Figure 4.10.: Exchange behaviour of the eigenvalues when the exceptional point at $c_{\mathrm{sc,crit,1}} = -0.93365$ and $\Gamma = 1.03215$ is encircled. a) shows the energy eigenvalues if the exceptional point is encircled on a path b) in the complex Γ-plane. c) shows the energy eigenvalues if the exceptional point is encircled on a path d) in the complex c_{sc}-plane.

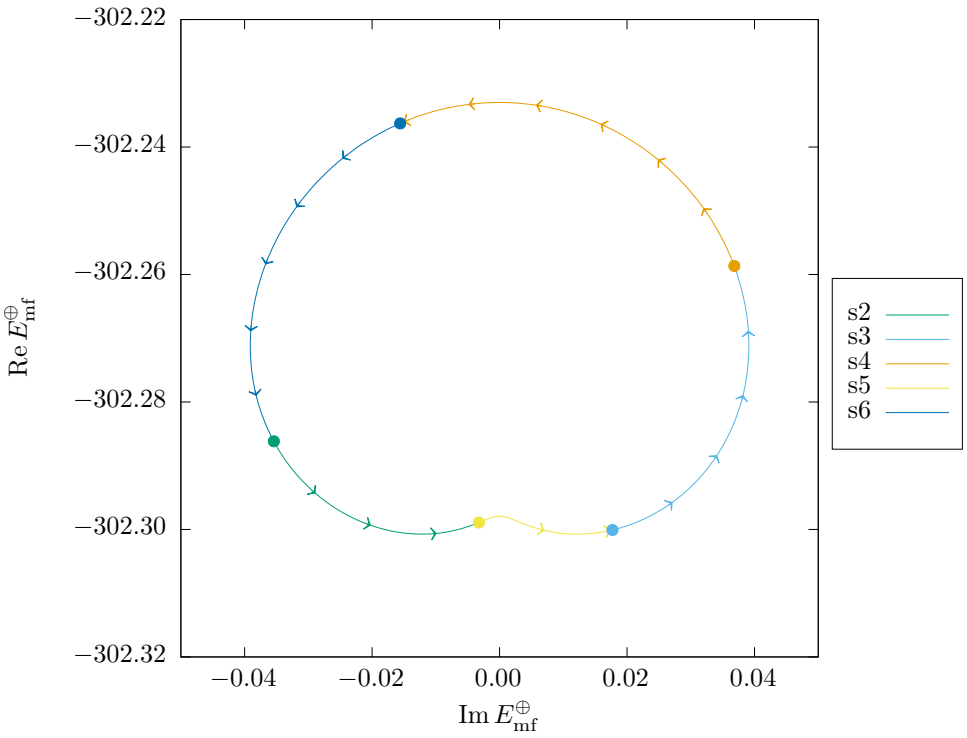

Figure 4.11.: Mean-field energies ${E_{\mathrm{mf}}}^{\oplus}$ when the exceptional point where the bifurcations B2, B3a and B3b coalesce is encircled in the complex asymmetry-parameter space s from equation (4.64).

The new parameter s allows us to break the remaining trap symmetry of the system, e.g. one potential well is deepened, while the other is flattened. We encircle the bifurcation for the scattering length $c_{\mathrm{sc,crit,2}} = -0.93365$ and the coupling parameter $\Gamma = 1.03215$ on the path

$$s = 5 \times 10^{-5} \mathrm{e}^{\mathrm{j}\phi} \text{ for } \phi \in [0, 2\pi] \tag{4.64}$$

and observe a permutation of all five states with each other (see figure 4.11). Thus, we have proven the existence of an exceptional point of order five in this system.

5 Summary and outlook

For an experimental realization of a $\mathcal{PT}$-symmetric double-well potential the explicit description of a physical environment, which implements the gain and loss, often described by a complex potential, is an important prerequisite. By combining two double-well subsystems into one closed Hermitian system we have come one step closer to such a realization (chapter 3).

For the four-dimensional matrix model without a phase difference between the two subsystems analytical solutions for all $\mathcal{PT}$-symmetric and $\mathcal{PT}$-broken states were found. Although the four-dimensional matrix model showed a new and different bifurcation scenario in comparison with the two-dimensional matrix model from [63] some generic features remained the same.

The matrix model showed the same qualitative bifurcation scenario as the two spatially extended models. Deviations could be observed when the two wells of the systems were not sufficiently isolated, such that the wave functions different wells had a significant overlap. In this case the solutions from the systems with a spatially resolved wave function differed from those of the matrix model. A larger overlap leads to quantitative changes and the loss of a mirror symmetry of pairs of energy eigenvalues in the (μ, γ)-diagram, however, it does not affect the generic structure of the states.

The influence of the phase difference between the two subsystems was also examined. While the coupling strength γ between the two subsystems took the role of one bifurcation parameter, the phase difference ϕ_r took the role of another, leading to a two-parametric cusp bifurcation. This bifurcation degenerated for $\phi_\mathrm{r} = 0$ into a pitchfork bifurcation. Only in this case $\mathcal{PT}$-symmetric states could be observed which makes the phase difference between the subsystems critical for the $\mathcal{PT}$-symmetric properties of the system.

The matrix model can be investigated further. Under the assumption that the two wells of the system are sufficiently isolated the matrix model reduces the descrip-

tion of the system to a small number of key parameters. Therefore, the analytically accessible matrix model of this work could be helpful to gain more insight into the behaviour of coupled BECs. In particular a similar approach to realize a $\mathcal{PT}$-symmetric quantum system via the coupling of two condensate wave functions was studied in [82] and revealed complicated stability properties. This system should also be representable in our four-mode description such that analytic expressions should be obtainable.

In the second part of this work (section 4.1 to 4.2), we have shown how the Gross-Pitaevskii equation for dipolar Bose-Einstein condensates can be analytically continued with an ansatz of coupled Gaussians using bicomplex numbers. Especially the representation in the idempotent basis of the bicomplex numbers can be used to separate the bicomplex equations into twice the number of coupled complex equations. This allows for the reuse of an algorithm developed for the integration of the complex equations.

In section 4.3 we have demonstrated the properties of the exceptional points associated with the bifurcations. In particular, the critical points where two or three bifurcations coalesce were examined. We have also shown that there exists at least one parameter for which an encircling of the critical parameter value results in the permutation of all five states participating in the exceptional point and therefore this is indeed a fifth order exceptional point.

We have shown that a dipolar Bose-Einstein condensate in a $\mathcal{PT}$-symmetric trap has a much richer bifurcation scenario than a condensate without long-range interactions. Most of the properties examined in this work have revealed interesting mathematical relations in the bicomplex parameter space, which is experimentally inaccessible. However, the understanding of the bifurcation scenrio is important since bifurcations crucially influence the stabiliy of a condensate [79].

A Probability currents

In this appendix the probability currents of the different model systems from chapter 3 are shown for additional parameter ranges. The figures A.1 to A.4 show the currents for the matrix model from equation (3.25). The figures A.6 and A.7 show the probability current for the spatially extended model (3.7).

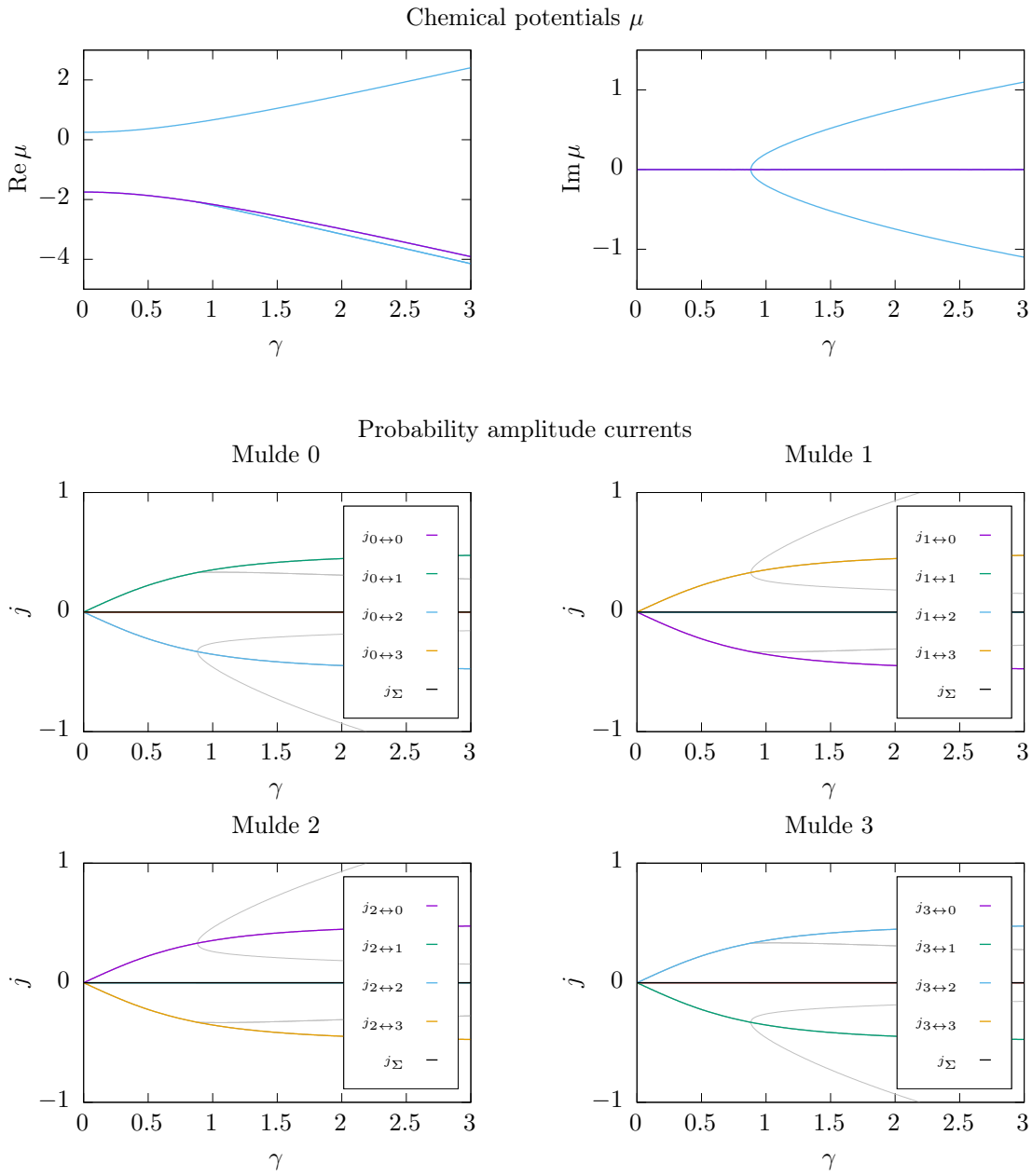

Figure A.1.: Same as figure 3.5 but for the state s_2 for $g = 1.5$.

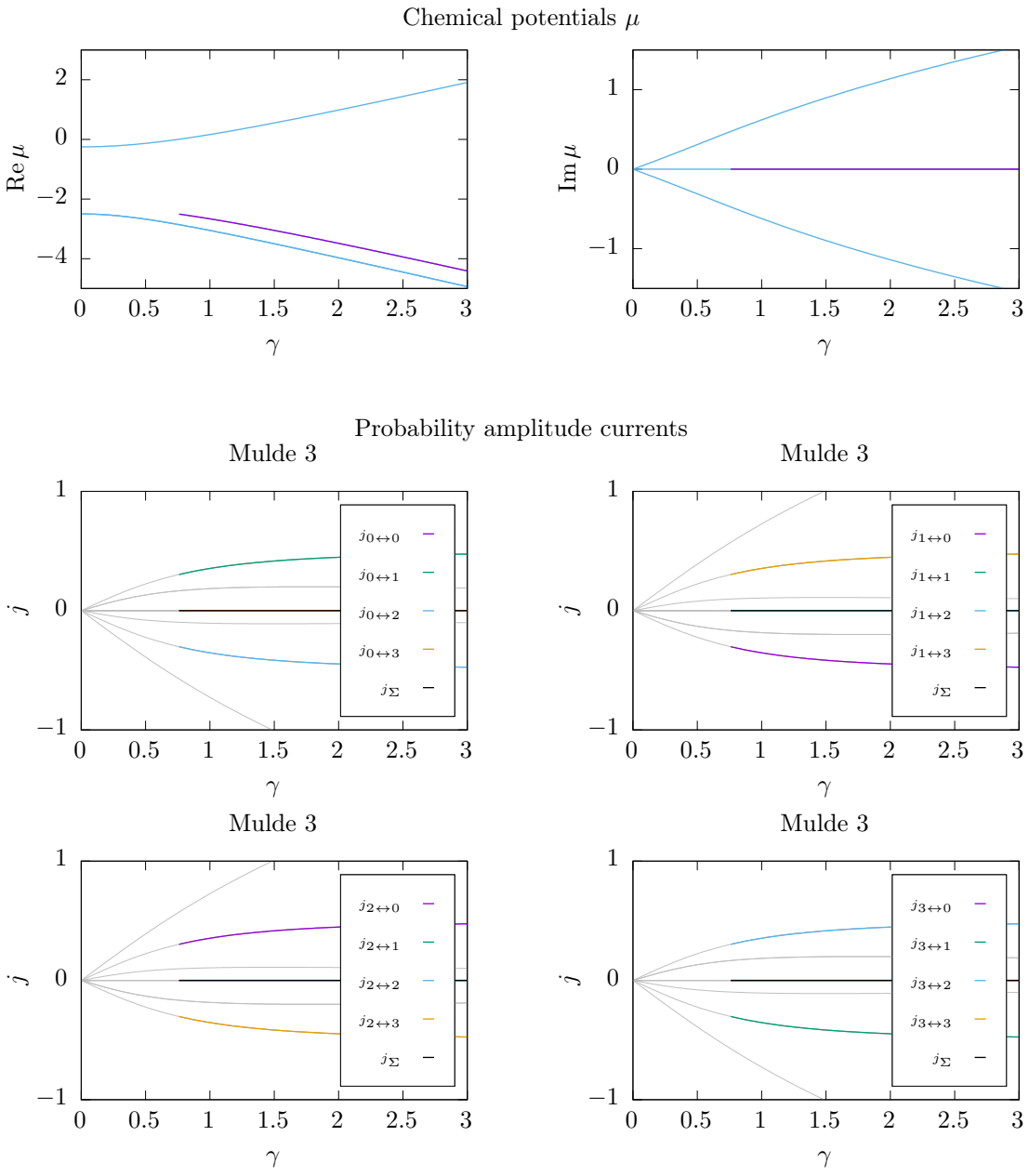

Figure A.2.: Same as figure 3.5 but for the state s_2 for $g = 2.5$.

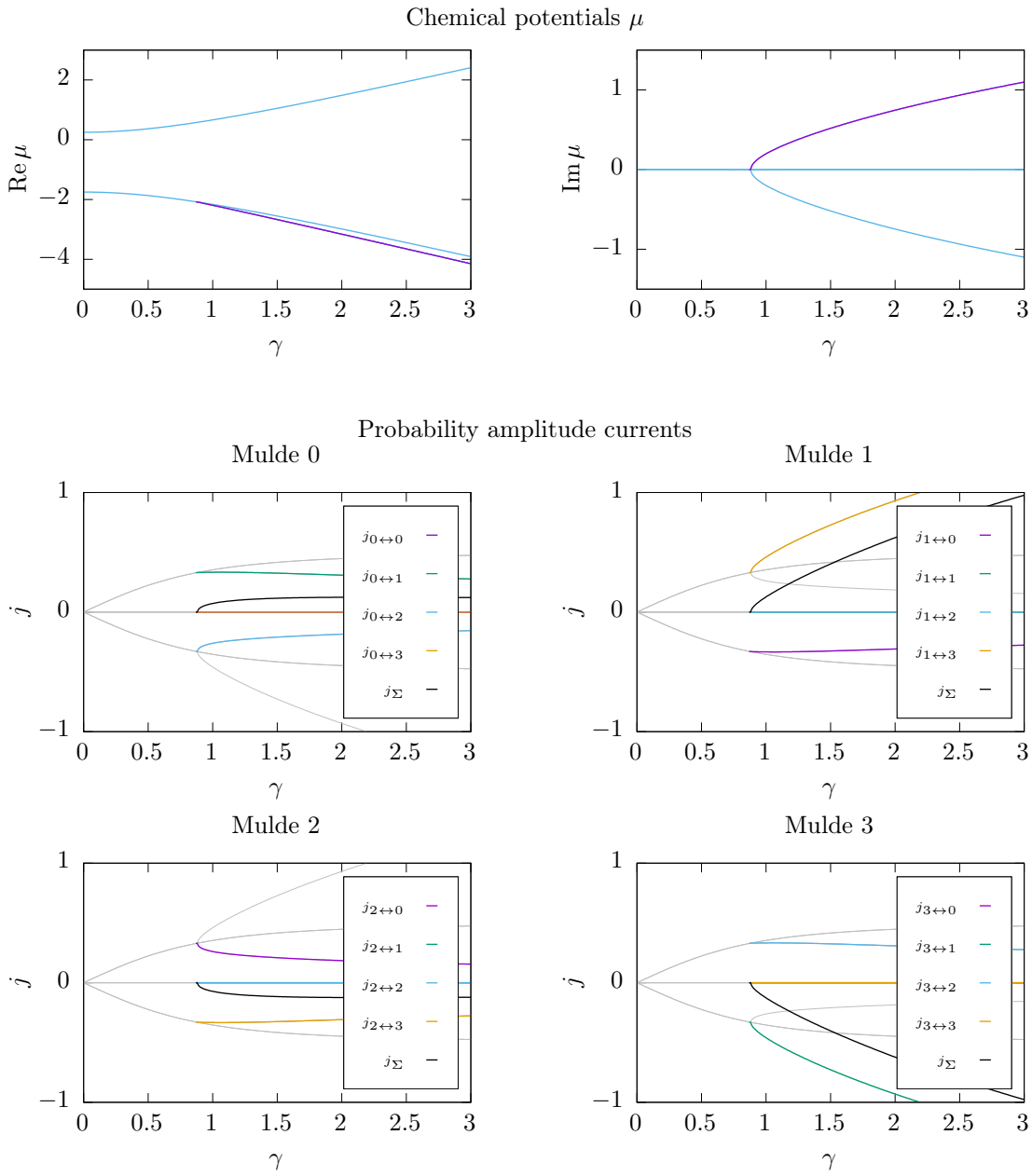

Figure A.3.: Same as figure 3.5 but for the $\mathcal{PT}$-broken state a_2 for $g = 1.5$.

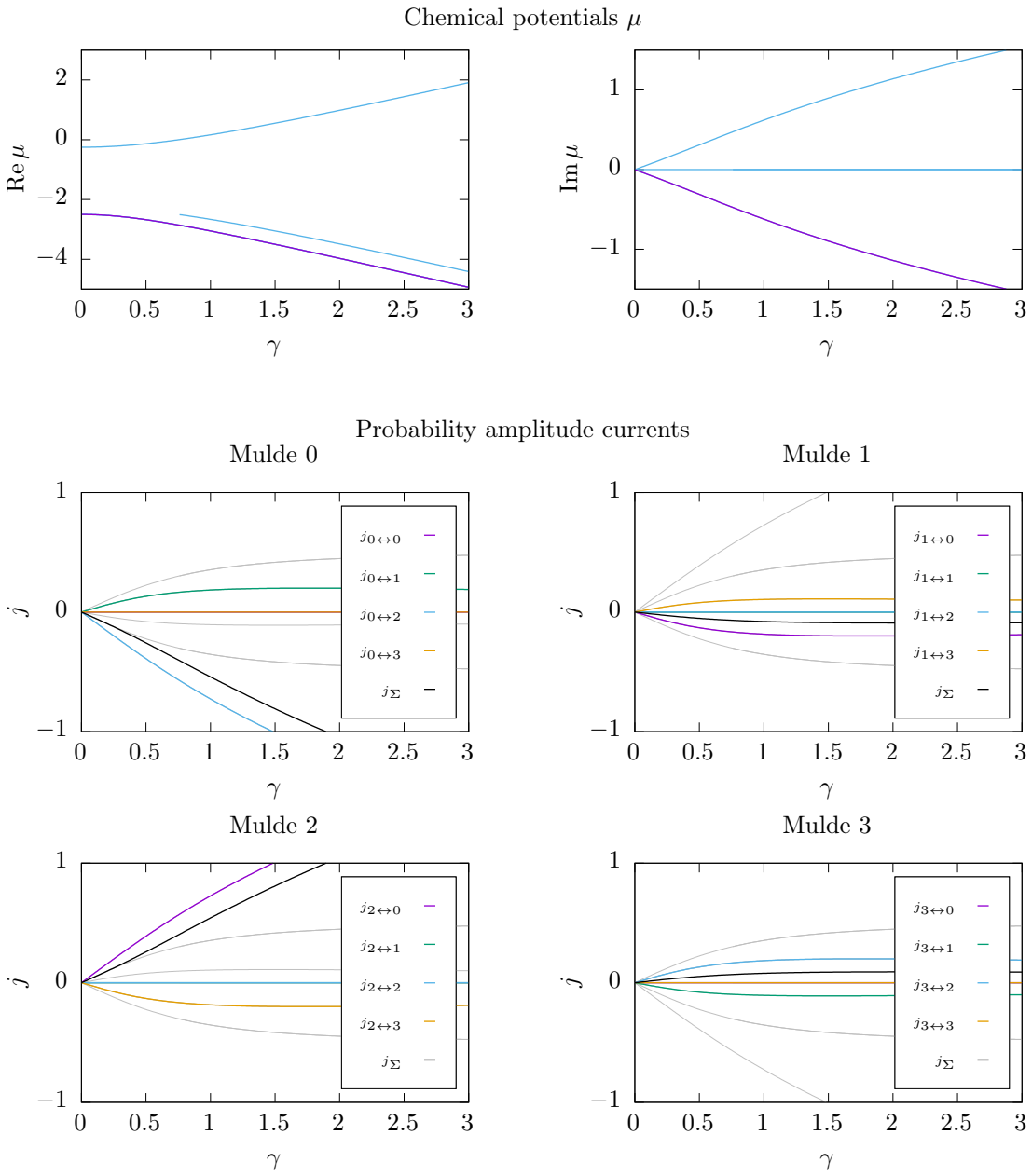

Figure A.4.: Same as figure 3.5 but for the $\mathcal{PT}$-broken state a_1 for $g = 2.5$.

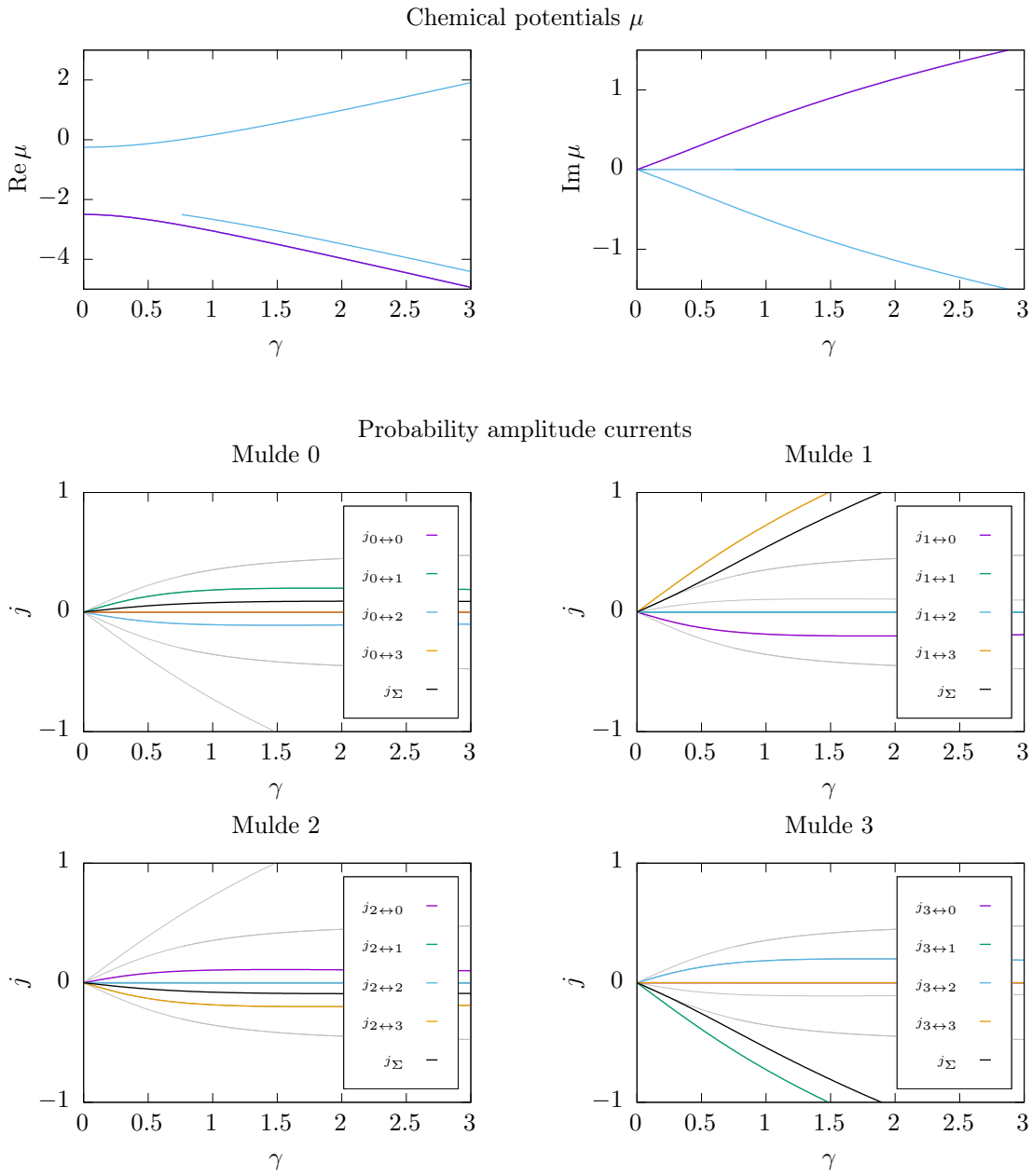

Figure A.5.: Same as figure 3.5 but for the $\mathcal{PT}$-broken state a_2 for $g = 2.5$.

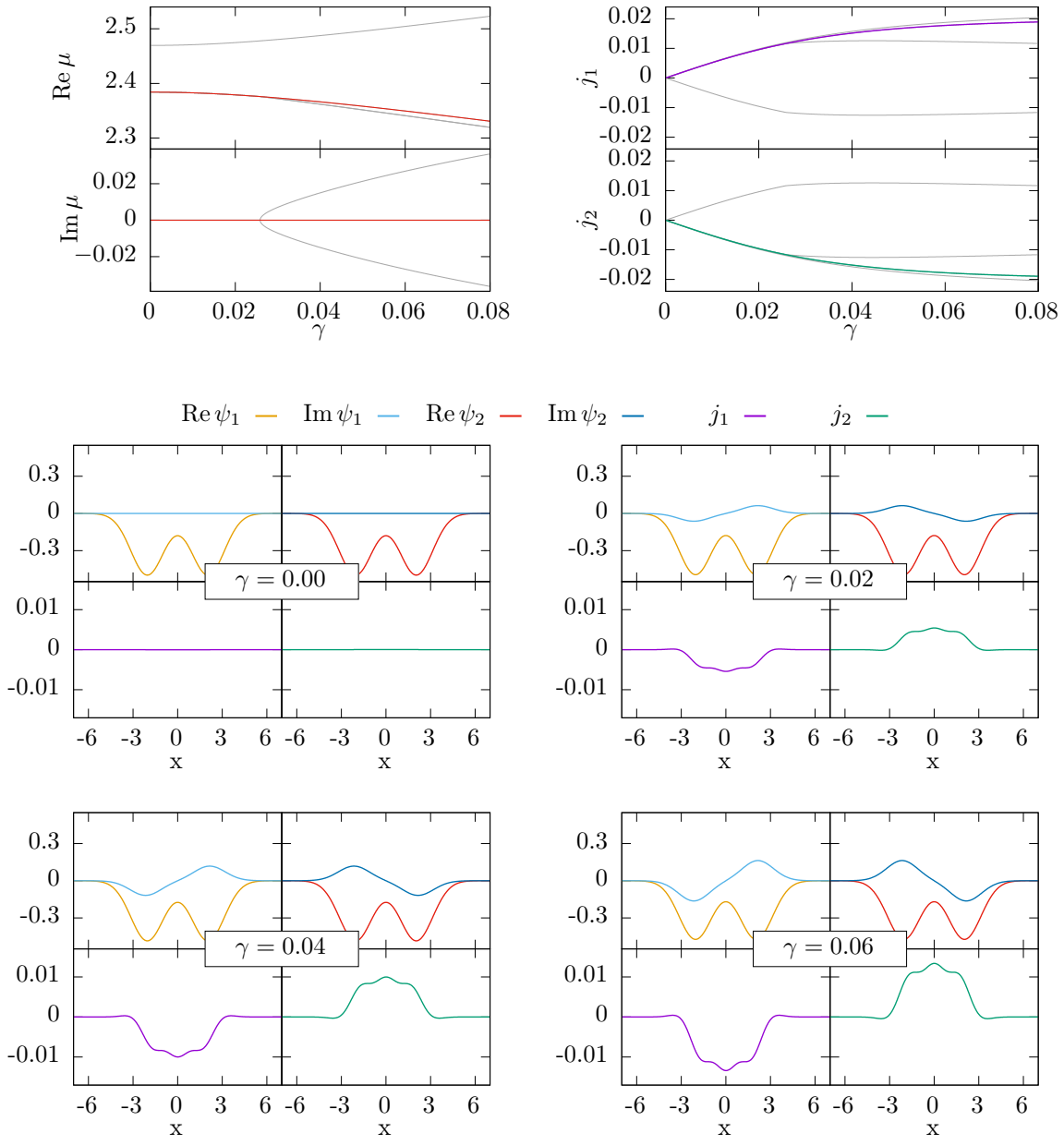

Figure A.6.: Probability current in the two modes for the stationary state s_2 in the spatially extended model (3.7).

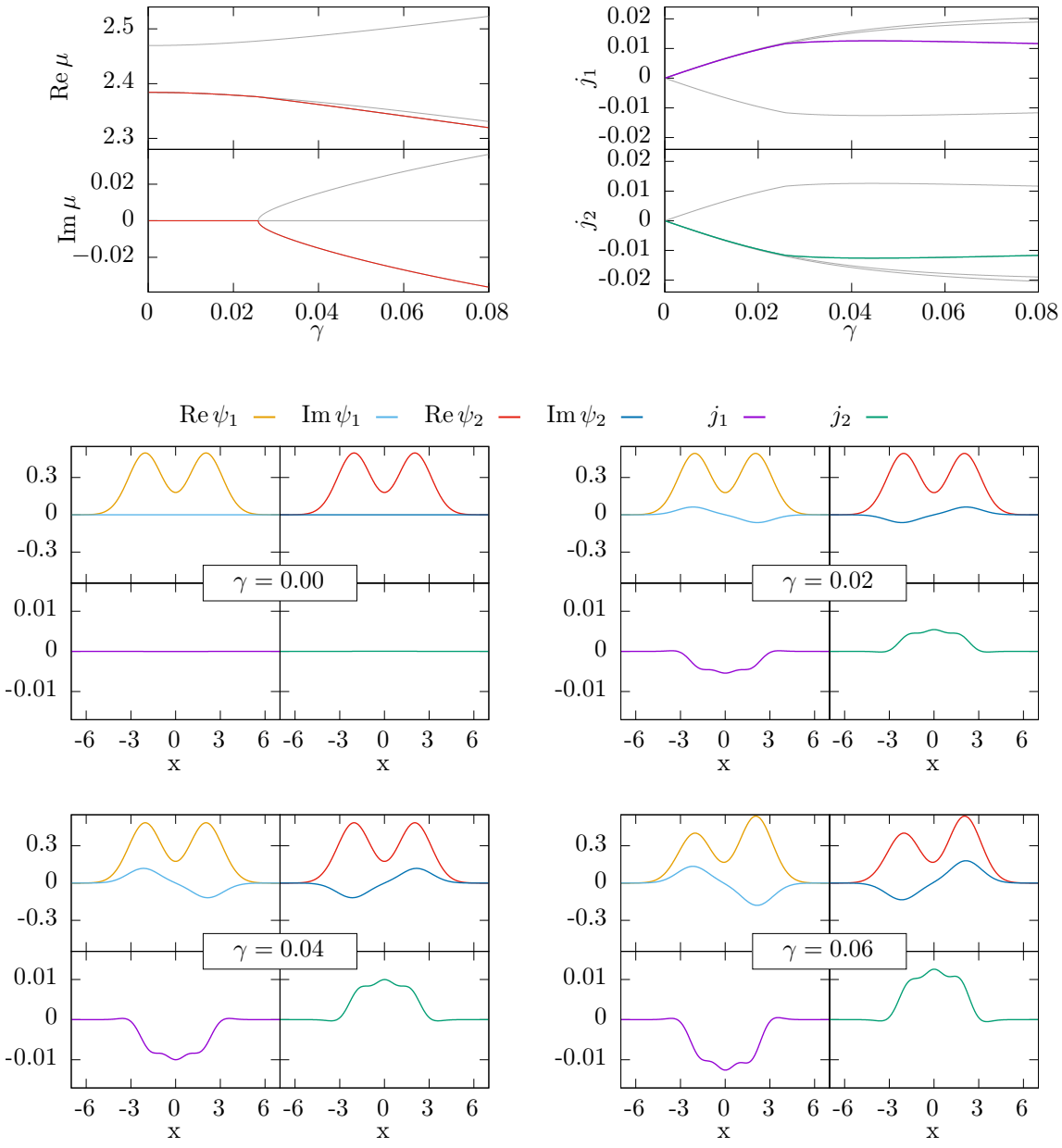

Figure A.7.: Probability current in the two modes for the $\mathcal{PT}$-broken solution a_2 in the spatially extended model (3.7).

Bibliography

[1] A. Einstein. Quantentheorie des einatomigen idealen Gases. *Sitzungsberichte der Preußischen Akademie der Wissenschaften* pp. 261–267 (1924).

[2] A. Einstein. Quantentheorie des einatomigen idealen Gases, II. Abhandlung. *Sitzungsberichte der preußischen Akademie der Wissenschaften* (1925).

[3] S. Bose. Plancks Gesetz und Lichtquantenhypothese. *Zeitschrift für Physik* 26, 178–181 (1924).

[4] M. H. Anderson, J. R. Ensher, M. R. Matthews, C. E. Wieman, and E. A. Cornell. Observation of Bose-Einstein Condensation in a Dilute Atomic Vapor. *Science* 269, 198 (1995).

[5] C. C. Bradley, C. A. Sackett, J. J. Tollett, and R. G. Hulet. Evidence of Bose-Einstein Condensation in an Atomic Gas with Attractive Interactions. *Phys. Rev. Lett.* 75, 1687 (1995).

[6] K. B. Davis, M. O. Mewes, M. R. Andrews, N. J. van Druten, D. S. Durfee, D. M. Kurn, and W. Ketterle. Bose-Einstein Condensation in a Gas of Sodium Atoms. *Phys. Rev. Lett.* 75, 3969 (1995).

[7] A. Griesmaier, J. Werner, S. Hensler, J. Stuhler, and T. Pfau. Bose-Einstein Condensation of Chromium. *Phys. Rev. Lett.* 94, 160401 (2005).

[8] L. Santos, G. V. Shlyapnikov, P. Zoller, and M. Lewenstein. Bose-Einstein Condensation in Trapped Dipolar Gases. *Phys. Rev. Lett.* 85, 1791–1794 (2000).

[9] Q. Beaufils, R. Chicireanu, T. Zanon, B. Laburthe-Tolra, E. Maréchal, L. Vernac, J.-C. Keller, and O. Gorceix. All-optical production of chromium Bose-Einstein condensates. *Phys. Rev. A* 77, 061601 (2008).

[10] M. Lu, N. Q. Burdick, S. H. Youn, and B. L. Lev. Strongly Dipolar Bose-Einstein Condensate of Dysprosium. *Phys. Rev. Lett.* 107, 190401 (2011).

[11] C. M. Bender, S. Boettcher, and P. N. Meisinger. $\mathcal{PT}$-symmetric quantum mechanics. *J. Math. Phys.* 40, 2201 (1999).

[12] H. F. Jones and Jr. E. S. Moreira. Quantum and classical statistical mechanics of a class of non-Hermitian Hamiltonians. *J. Phys. A* 43, 055307 (2010).

[13] V. Jakubský and M. Znojil. An explicitly solvable model of the spontaneous $\mathcal{PT}$-symmetry breaking. *Czech. J. Phys.* 55, 1113 (2005).

[14] H. Mehri-Dehnavi, A. Mostafazadeh, and A. Batal. Application of pseudo-Hermitian quantum mechanics to a complex scattering potential with point interactions. *J. Phys. A* 43, 145301 (2010).

[15] C. E. Ruter, K. G. Makris, R. El-Ganainy, D. N. Christodoulides, M. Segev, and D. Kip. Observation of parity-time symmetry in optics. *Nat. Phys.* 6, 192–195 (2010).

[16] I. V. Barashenkov, G. S. Jackson, and S. Flach. Blow-up regimes in the $\mathcal{PT}$-symmetric coupler and the actively coupled dimer. *Phys. Rev. A* 88, 053817 (2013).

[17] S. Deffner and A. Saxena. Jarzynski Equality in $\mathcal{PT}$-Symmetric Quantum Mechanics. *Phys. Rev. Lett.* 114, 150601 (2015).

[18] S. Albeverio, S. Fassari, and F. Rinaldi. The discrete spectrum of the spinless one-dimensional Salpeter Hamiltonian perturbed by δ-interactions. *J. Phys. A* 48, 185301 (2015).

[19] A. Mostafazadeh. Nonlinear Spectral Singularities for Confined Nonlinearities. *Phys. Rev. Lett.* 110, 260402 (2013).

[20] S. Bittner, B. Dietz, U. Günther, H. L. Harney, M. Miski-Oglu, A. Richter, and F. Schäfer. $\mathcal{PT}$ Symmetry and Spontaneous Symmetry Breaking in a Microwave Billiard. *Phys. Rev. Lett.* 108, 024101 (2012).

[21] J. Schindler, A. Li, M. C. Zheng, F. M. Ellis, and T. Kottos. Experimental study of active *LRC* circuits with $\mathcal{PT}$ symmetries. *Phys. Rev. A* 84, 040101 (2011).

[22] J. Schindler, Z. Lin, J. M. Lee, H. Ramezani, F. M. Ellis, and T. Kottos. $\mathcal{PT}$-symmetric electronics. *J. Phys. A* 45, 444029 (2012).

[23] A. Ruschhaupt, F. Delgado, and J. G. Muga. Physical realization of $\mathcal{PT}$ -symmetric potential scattering in a planar slab waveguide. *J. Phys. A* 38, L171 (2005).

[24] A. Guo, G. J. Salamo, D. Duchesne, R. Morandotti, M. Volatier-Ravat, V. Aimez, G. A. Siviloglou, and D. N. Christodoulides. Observation of $\mathcal{PT}$-Symmetry Breaking in Complex Optical Potentials. *Phys. Rev. Lett.* 103, 093902 (2009).

[25] H. Ramezani, T. Kottos, R. El-Ganainy, and D. N. Christodoulides. Unidirectional nonlinear $\mathcal{PT}$-symmetric optical structures. *Phys. Rev. A* 82, 043803 (2010).

[26] Z.H. Musslimani, Konstantinos G. Makris, R. El-Ganainy, and D. N. Christodoulides. Optical solitons in PT periodic potentials. *Phys. Rev. Lett.* 100, 30402 (2008).

[27] K. G. Makris, R. El-Ganainy, D. N. Christodoulides, and Z. H. Musslimani. $\mathcal{PT}$-Symmetric Periodic Optical Potentials. *Int. J. Theo. Phys.* 50, 1019 (2011).

[28] K. G. Makris, R. El-Ganainy, D. N. Christodoulides, and Z. H. Musslimani. Beam Dynamics in $\mathcal{PT}$ Symmetric Optical Lattices. *Phys. Rev. Lett.* 100, 103904 (2008).

[29] K. G. Makris, R. El-Ganainy, D. N. Christodoulides, and Z.H. Musslimani. $\mathcal{PT}$-symmetric optical lattices. *Phys. Rev. A* 81, 063807 (2010).

[30] Y. D. Chong, L. Ge, and A. D. Stone. $\mathcal{PT}$-Symmetry Breaking and Laser-Absorber Modes in Optical Scattering Systems. *Phys. Rev. Lett.* 106, 093902 (2011).

[31] Peng, B and Kaya, Ş. Ö. and Lei, F. and Minufu, F. and Gianfreda, M. and Long, G. L. and Fan, S. and Nori, F. and Bender, C. M. and Yang, L. Parity-time-symmetric whispering-gallery microcavities. *Nat. Phys.* 10, 394–398 (2014).

[32] D. Dast, D. Haag, H. Cartarius, and G. Wunner. Quantum master equation with balanced gain and loss. *Phys. Rev. A* 90, 052120 (2014).

[33] R. Gutöhrlein, J. Schnabel, I. Iskandarov, H. Cartarius, J. Main, and G. Wunner. Realizing $\mathcal{PT}$-symmetric BEC subsystems in closed Hermitian systems. *J. Phys. A* 48, 335302 (2015).

[34] T. Kato. *Perturbation theory for linear operators*. Springer, Berlin (1966).

[35] H. Cartarius, J. Main, and G. Wunner. Exceptional Points in Atomic Spectra. *Phys. Rev. Lett.* 99, 173003 (2007).

[36] W. D. Heiss. Chirality of wavefunctions for three coalescing levels. *Journal of Physics A: Mathematical and Theoretical* 41, 244010 (2008).

[37] E. M. Graefe, U. Günther, H. J. Korsch, and A. E. Niederle. A non-Hermitian $\mathcal{PT}$ symmetric Bose-Hubbard model: eigenvalue rings from unfolding higher-order exceptional points. *J. Phys. A* 41, 255206 (2008).

[38] G. Demange and E.-M. Graefe. Signatures of three coalescing eigenfunctions. *J. Phys. A: Math. Theor.* 45, 025303 (2012).

[39] W. D. Heiss. The physics of exceptional points. *Journal of Physics A: Mathematical and Theoretical* 45, 444016 (2012).

[40] W. D. Heiss, H. Cartarius, G. Wunner, and J. Main. Spectral singularities in $\mathcal{PT}$-symmetric Bose–Einstein condensates. *J. Phys. A* 46, 275307 (2013).

[41] S. Ronen, D. C. E. Bortolotti, and J. L. Bohn. Radial and Angular Rotons in Trapped Dipolar Gases. *Phys. Rev. Lett.* 98, 030406 (2007).

[42] R. Fortanier, D. Dast, D. Haag, H. Cartarius, J. Main, G. Wunner, and R. Gutöhrlein. Dipolar Bose-Einstein condensates in a $\mathcal{PT}$-symmetric double-well potential. *Phys. Rev. A* 89, 063608 (2014).

[43] R. Gutöhrlein, J. Main, H. Cartarius, and G. Wunner. Bifurcations and exceptional points in dipolar Bose-Einstein condensates. *J. Phys. A* 46, 305001 (2013).

[44] W. Nolting. *Grundkurs Theoretische Physik 5/2: Quantenmechanik - Methoden und Anwendungen*. Grundkurs Theoretische Physik. Springer-Verlag, 8th edition (2015).

[45] L. P. Pitaevskii and S. Stringari. *Bose-Einstein Condensation*. Oxford University Press (2003).

[46] M. Ueda. *Fundamentals and New Frontiers of Bose-Einstein Condensation*. World Scientific (2010).

[47] W. Nolting. *Grundkurs Theoretische Physik 6: Statistische Physik*. Grundkurs Theoretische Physik. Springer-Verlag, 7th edition (2014).

[48] Inouye, S. and Andrews, M. R. and Stenger, J. and Miesner, H.-J. and Stamper-Kurn, D. M. and Ketterle, W. Observation of Feshbach resonances in a Bose-Einstein condensate. *Nature* 392, 151–154 (1998).

[49] C. Chin, R. Grimm, P. Julienne, and E. Tiesinga. Feshbach resonances in ultracold gases. *Rev. Mod. Phys.* 82, 1225–1286 (2010).

[50] Patrick Köberle. *Ground-state structures and dynamics of dipolar Bose-Einstein condensates in single and multi-layered traps*. Ph.D. thesis, Universität Stuttgart (2011).

[51] A. D. McLachlan. A variational solution of the time-dependent Schrodinger equation. *Mol. Phys.* 8, 39–44 (1964).

[52] S. Rau, J. Main, and G. Wunner. Variational methods with coupled Gaussian functions for Bose-Einstein condensates with long-range interactions. I. General concept. *Phys. Rev. A* 82, 023610 (2010).

[53] S. Rau, J. Main, H. Cartarius, P. Köberle, and G. Wunner. Variational methods with coupled Gaussian functions for Bose-Einstein condensates with long-range interactions. II. Applications. *Phys. Rev. A* 82, 023611 (2010).

[54] Andrej Junginger. *Variationsansätze für mehrschichtige, dipolare Bose-Einstein-Kondensate*. Diplomarbeit, Universität Stuttgart (2010).

[55] R. M. Fortanier. *Variational approaches to dipolar Bose-Einstein condensates*. Ph.D. thesis, Universität Stuttgart (2014). http://dx.doi.org/10.18419/opus-5124.

[56] Robin Gutöhrlein. *Bifurkationen und Ausnahmepunkte in dipolaren Bose-Einstein-Kondensaten*. Diplomarbeit, Universität Stuttgart (2012).

[57] E. Freitag and R. Busam. *Funktionentheorie 1*. Springer-Verlag, fourth edition (2006).

[58] M. V. Berry. Quantal Phase Factors Accompanying Adiabatic Changes. *Proceedings of the Royal Society of London A: Mathematical, Physical and Engineering Sciences* 392, 45–57 (1984).

[59] J. C. Garrison and E. M. Wright. Complex geometrical phases for dissipative systems. *Physics Letters A* 128, 177 – 181 (1988).

[60] H. Cartarius. *Exceptional points in atomic spectra and Bose-Einstein condensates*. Ph.D. thesis, Universität Stuttgart (2008).

[61] C. M. Bender and S. Boettcher. Real spectra in non-Hermitian Hamiltonians having $\mathcal{PT}$ symmetry. *Phys. Rev. Lett.* 80, 5243–5246 (1998).

[62] D. Dast, D. Haag, H. Cartarius, J. Main, and G. Wunner. Eigenvalue structure of a Bose–Einstein condensate in a $\mathcal{PT}$ -symmetric double well. *J. Phys. A* 46, 375301 (2013).

[63] E.-M. Graefe. Stationary states of a $\mathcal{PT}$ symmetric two-mode Bose–Einstein condensate. *J. Phys. A* 45, 444015 (2012).

[64] N. Moiseyev. *Non-Hermitian Quantum Mechanics*. Cambridge University Press, Cambridge (2011).

[65] S. Klaiman, U. Günther, and N. Moiseyev. Visualization of Branch Points in $\mathcal{PT}$-Symmetric Waveguides. *Phys. Rev. Lett.* 101, 080402 (2008).

[66] A. Mostafazadeh. Delta-function potential with a complex coupling. *J. Phys. A* 39, 13495 (2006).

[67] H. F. Jones. Interface between Hermitian and non-Hermitian Hamiltonians in a model calculation. *Phys. Rev. D* 78, 065032 (2008).

[68] A. Mostafazadeh and H. Mehri-Dehnavi. Spectral singularities, biorthonormal systems and a two-parameter family of complex point interactions. *J. Phys. A* 42, 125303 (2009).

[69] T. Mayteevarunyoo, B. A. Malomed, and G. Dong. Spontaneous symmetry breaking in a nonlinear double-well structure. *Phys. Rev. A* 78, 053601 (2008).

[70] K. Rapedius and H. J. Korsch. Resonance solutions of the nonlinear Schrödinger equation in an open double-well potential. *J. Phys. B* 42, 044005 (2009).

[71] D. Witthaut, K. Rapedius, and H. J. Korsch. The nonlinear Schrödinger equation for the delta-comb potential: quasi-classical chaos and bifurcations of periodic stationary solutions. *Journal of nonlinear mathematical physics* 16, 207 (2008).

[72] S. Fassari and F. Rinaldi. On the Spectrum of the Schrödinger Hamiltonian of the One-Dimensional Harmonic Oscillator Perturbed by Two Identical Attractive Point Interactions. *Rep. Math. Phys.* 69, 353 (2012).

[73] E. Demiralp. Bound states of n-dimensional harmonic oscillator decorated with Dirac delta functions. *J. Phys. A* 38, 4783 (2005).

[74] H.F. Jones. The energy spectrum of complex periodic potentials of the Kronig-Penney type. *Phys. Lett. A* 262, 242 (1999).

[75] Z. Ahmed. Energy band structure due to a complex, periodic, $\mathcal{PT}$-invariant potential. *Phys. Lett. A* 286, 231 (2001).

[76] H. Uncu, D. Tarhan, E. Demiralp, and Ö. E. Müstecaplioglu. Bose-Einstein condensate in a harmonic trap with an eccentric dimple potential. *Las. Phys.* 18, 331 (2008).

[77] H. Cartarius and G. Wunner. Model of a $\mathcal{PT}$-symmetric Bose-Einstein condensate in a δ-function double-well potential. *Phys. Rev. A* 86, 013612 (2012).

[78] D. Dast, D. Haag, H. Cartarius, Günter Wunner, R. Eichler, and J. Main. A Bose-Einstein condensate in a $\mathcal{PT}$-symmetric double well. *Fortschritte der Physik* 61, 124–139 (2013).

[79] D. Haag, D. Dast, A. Löhle, H. Cartarius, J. Main, and G. Wunner. Nonlinear quantum dynamics in a $\mathcal{PT}$-symmetric double well. *Phys. Rev. A* 89, 023601 (2014).

[80] M. Kreibich, J. Main, H. Cartarius, and G. Wunner. Hermitian four-well potential as a realization of a $\mathcal{PT}$-symmetric system. *Phys. Rev. A* 87, 051601(R) (2013).

[81] M. Kreibich, J. Main, H. Cartarius, and G. Wunner. Realizing $\mathcal{PT}$-symmetric non-Hermiticity with ultracold atoms and Hermitian multiwell potentials. *Phys. Rev. A* 90, 033630 (2014).

[82] F. Single, H. Cartarius, G. Wunner, and J. Main. Coupling approach for the realization of a $\mathcal{PT}$-symmetric potential for a Bose-Einstein condensate in a double well. *Phys. Rev. A* 90, 042123 (2014).

[83] J. Schnabel. *Kopplung von Bose-Einstein-Kondensaten in einer Doppel-δ-Falle zur Realisierung eines $\mathcal{PT}$-symmetrischen Quantensystems*. Bachelorthesis, Universität Stuttgart (2014).

[84] A. Trombettoni and A. Smerzi. Discrete Solitons and Breathers with Dilute Bose-Einstein Condensates. *Phys. Rev. Lett.* 86, 2353–2356 (2001).

[85] A. Smerzi and A. Trombettoni. Nonlinear tight-binding approximation for Bose-Einstein condensates in a lattice. *Phys. Rev. A* 68, 023613 (2003).

[86] G. Theocharis, P. G. Kevrekidis, D. J. Frantzeskakis, and P. Schmelcher. Symmetry breaking in symmetric and asymmetric double-well potentials. *Phys. Rev. E* 74, 056608 (2006).

[87] Y. A. Kuznetsov. *Elements of Applied Bifurcation Theory*, volume 112 of *Applied Mathematical Sciences*. Springer-Verlag, third edition (2004).

[88] R. Gutöhrlein, H. Cartarius, J. Main, and G. Wunner. Bifurcations and exceptional points in a PT-symmetric dipolar Bose–Einstein condensate. *J. Phys. A* 49, 485301 (2016).

[89] M.E. Shapiro, D.C. Struppa, and A. Vajiac. Bicomplex Numbers and their Elementary Functions. *Cubo (Temuco)* 14, 61 – 80 (2012).

[90] H. Frasch. *Analytische Fortsetzung der Gross-Pitaevskii-Gleichung für PT-symmetrische Bose-Einstein-Kondensate*. Bachelorthesis, Universität Stuttgart (2014).

Zusammenfassung in deutscher Sprache

In dieser Arbeit wurden zwei Fragestellungen untersucht. Im ersten Teil wurde die Frage beantwortet, ob man ein $\mathcal{PT}$-symmetrisches System als Untersystem in ein größeres hermitesches System einbetten kann. Das eingebettete System wurde dabei mit mehreren verschiedenen Modellen untersucht, die sich in der räumlichen Auflösung der Systeme unterscheiden. Zudem wurden Unterschiede und Gemeinsamkeiten zum zweidimensionalen Matrixmodell aus [63] aufgezeigt. Im zweiten Teil dieser Arbeit wurde die Ordnung von Ausnahmepunkten in einem $\mathcal{PT}$-symmetrischen Bose-Einstein-Kondensat untersucht, welches auch dipolare Wechselwirkungen besitzt.

Bevor diese Fragen untersucht werden, wird in Kapitel 2 dieser Arbeit jedoch zuerst einmal eine Zusammenfassung der wichtigsten theoretischen Grundlagen, welche im Laufe der Arbeit noch benötigt werden, gegeben. Insbesondere wird die zur Meanfieldbeschreibung von Bose-Einstein-Kondensaten verwendete Gross-Pitaevskii-Gleichung (2.25) hergeleitet (siehe Abschnitt 2.1). Wir beginnen hierfür mit einer kurzen Rekapitulation der Eigenschaten der Vielteilchenquantenmechanik. Unter der Annahme, dass wir uns in einem Temperaturbereich befinden, in dem praktisch alle Teilchen im Grundzustand sind und Fluktuationen vernachlässigt werden können, erhalten wir aus der Vielteilchenschrödingergleichung die Gross-Pitaevskii-Gleichung.

Man kann die Gross-Pitaevskii-Gleichung numerisch exakt mit Gitterverfahren lösen, jedoch können diese, in Abhängigkeit von den verwendeten Potentialen und vorhandenen Wechselwirkungen, einen großen numerischen Aufwand erfordern. Daher zeigen wir in Abschnitt 2.1.5 wie das zeitabhängigen Variationsprinzip auf die Gross-Pitaevskii-Gleichung angewand werden kann. Das zeitabhängige Variationsprinzip erlaubt durch Wahl eines für das gegebene Potential geeigneten Ansatzes für die Wellenfunktion, der auf einigen wenigen Parametern beruht, eine effiziente näherungsweise Bestimmung von Lösungen für die Gross-Pitaevskii-Gleichung [52, 53].

Wir gehen im Theorieteil zudem auf die grundlegenden Eigenschaften von Bifurkationen und Ausnahmepunkten ein. Insbesondere wird darauf eingegangen, dass der in der Arbeit verwendete Nachweis von Ausnahmepunkten, welcher auf einer Umkreisung des kritischen Punktes im komplexen Parameterraums beruht, nur eine untere Schranke für die Ordnung des Punktes liefert.

Im letzten Abschnitt 2.3 dieses Theoriekaptiels wird die Bedeutung des $\mathcal{PT}$-Operators erläutert. Es handelt sich bei diesem Operator um eine Kombination aus dem Paritätsoperator $\mathcal{P}$ und dem Zeitumkehroperator $\mathcal{T}$. In diesem Abschnitt werden wichtige Eigenschaften des Operators vorgestellt. Es wird zudem definiert was $\mathcal{PT}$-Symmetrie für lineare als auch nichtlineare Systeme bedeutet.

Einbettung eines $\mathcal{PT}$-symmetrischen Teilsystems in ein Hermitesches Gesamtsystem

Für die experimentelle Realisierung eines $\mathcal{PT}$-symmetrischen Doppelmuldenpotentials ist die konkrete Beschreibung der Umgebung, aus welcher die Ein- und Auskopplung von Teilchen erfolgt, oft beschrieben durch ein komplexes Potential von zentraler Bedeutung. Bisherige Untersuchungen [81] verwendeten Vielmuldensysteme mit zeitlich variablen Potentialtiefen, um das Aus- und Einkoppeln von Teilchen zu realisieren. In dieser Arbeit wurde untersucht, ob es möglich ist, ein $\mathcal{PT}$-symmetrisches Teilsystem in ein Hermitsches System einzubetten, dessen Parameter zeitlich konstant sind. Dies geschieht durch die Kopplung von zwei Doppelmuldensystemen, die sich gegenseitig als Partikelreservoir dienen (vgl. Abbildung 3.3).

Es werden in der Arbeit Systeme verschiedener Detailgrade untersucht. Beginnend mit einem System, in welchem die zwei Doppelmuldensystemen eindimensional beschrieben werden und räumlich ausgedehnte Potentialmulden sowie Kopplungsgebiete besitzen, wird ein einfaches vierdimensionales Matrixmodell abgeleitet (siehe Gleichung (3.25)). Die Kopplungsparameter der beiden Systeme ersetzen die Stärke der Ein- und Auskopplung des offenen $\mathcal{PT}$-symmetrischen Doppelmuldenmodells.

Das vierdimensionale Matrixmodell besitzt drei relevante Kontrollparameter. Diese sind die Kopplung zwischen zwei Mulden v, die Kopplung zwischen den zwei Untersystemen γ und die Nichtlinearität g. Es wird nun die Phasenbeziehung zwischen den beiden Untersystemen festgehalten, um $\mathcal{PT}$-symmetrische Zustände zu erhalten. Es wurden analytische Lösungen für alle $\mathcal{PT}$-symmetrischen und $\mathcal{PT}$-gebrochenen Zustände gefunden. Für dieses Modell gibt es keine echten stationären $\mathcal{PT}$-gebrochenen Zustände mehr. Die chemischen Potentialwerte der stationären Lösungen des vierdimensionalen Matrixmodells aus Gleichung (3.58) unterscheiden sich in der Struktur auf den ersten Blick kaum von denen des zweidimensionalen

Matrixmodells [63] aus Gleichung (3.2). Nur ein unterschiedliches Vorzeichen unter der Wurzel führt dazu, dass die charakteristische Bifurkation zwischen den beiden Zuständen, die für größere Werte von γ im zweidimensionalen Modell auftritt, nicht länger existiert.

Es gibt Zustände, die für kurze Zeiten das Äquivalent der $\mathcal{PT}$-gebrochenen Zustände im zweidimensionalen Matrixmodell darstellen. Da diese Zustände jedoch die Norm der beiden Untersysteme zueinander verändern, handelt es sich hier nicht um echte stationäre Zustände. Das Bifurkationsverhalten dieser Zustände mit den stationären Zuständen hat jedoch wieder qualitativ starke Ähnlichkeit mit dem des zweidimensionalen Modells. Auch zeigen die stationären Zustände des Matrixmodells einen Ringstrom, d.h. in den Untersystemen gibt es einen Strom von der einen zur anderen Mulde.

In Abschnitt 3.2 wird nun das vierdimensionales Matrixmodell mit den detailierteren Modellen verglichen. Für diese können die Zustände nur noch numerisch berechnet werden. Die Ergebnisse zeigen eine sehr gute Übereinstimmung, solange die Voraussetzungen für die Näherungen, die für die Herleitung des Matrixmodells verwendet wurden, erfüllt sind, d.h. solange die einzelnen Mulden in den Untersystemen hinreichend voneinander getrennt sind.

Der Einfluss der Phasendifferenz zwischen den beiden Untersystemen wurde auch untersucht. Während die Kopplungsstärke γ zwischen den beiden Untersystemen die Rolle eines Bifurkationsparameters übernahm, nahm die Phasendifferenz ϕ_r die Rolle eines anderen ein, was zu einer zweiparametrigen Cuspbifurkation führte. Diese Bifurkation geht für $\phi_\mathrm{r} = 0$ in eine Heugabelbifurkation über. Auch konnten nur in diesem Fall $\mathcal{PT}$-symmetrische Zustände untersucht werden, was die Phasendifferenz zu einem kritischen Parameter für die $\mathcal{PT}$-symmetrischen Eigenschaften des Systems macht.

Das Matrixmodell kann noch weiter untersucht werden. Unter der Annahme, dass die beiden Mulden des Systems hinreichend isoliert sind, reduziert das Matrixmodell die Systembeschreibung auf eine kleine Zahl von Schlüsselparametern. Daher kann ein analytisch fortgesetztes Matrixmodel hilfreich sein, um weitere Einsichten in das Verhalten von gekoppelten Bose-Einstein-Kondensaten zu bekommen. Ein ähnlicher Ansatz zur Realisierung eines $\mathcal{PT}$-symmetrischen Quantensystems über die Kopplung von zwei Kondensatwellenfunktionen wurde in [82] untersucht und enthüllte komplexe Stabilitätseigenschaften. Dieses System sollte auch als Viermodenmodell repräsentierbar sein.

Ausnahmepunkte höherer Ordnung in dipolaren $\mathcal{PT}$-symmetrischen Bose-Einstein-Kondensaten

Der zweite Teil der Arbeit (siehe Kapitel 4) beginnt mit einer Einführung in die analytische Erweiterung von Funktionen. Insbesondere wird dargelegt, wie die schon komplexe, aber nicht analytische Gross-Pitaevskii-Gleichung erweitert werden kann. Hierfür spaltet man die Gleichung in ihren Real- und Imaginärteil auf. Nun können diese reellen Gleichungen analytisch fortgesetzt werden. Man stellt fest, dass eine Ersetzung des komplexen Zahlenraums mit dem bikomplexen unter Verwendung einer geeigneten komplexen Konjugation äquivalent ist. Die Verwendung von bikomplexen Zahlen bietet große Vorteile bei der numerischen Lösung der Gleichung, da diese eine idempotente Basis besitzen. Diese Basis wird von den beiden idempotenten Elementen $e^{\oplus}$ und $e^{\ominus}$ (siehe Gleichung (4.12)) gebildet. Diese erfüllen die Relation (4.13).

Mithilfe dieser Eigenschaften können die einzelnen Integralterme der Gross-Pitaevskii-Gleichung in zwei komplexe Komponenten zerlegt werden, für die existierende Algorithmen für komplexe Integrale implementiert werden können. Dies geschieht in Abschnitt 4.2. Vorsicht ist bei der Verwendung der Symmetrieeigenschaften verschiedener Integralterme geboten, die in [55] hergeleitet wurden. Diese müssen für die Verwendung mit bikomplexen Zahlen angepasst werden (siehe Gleichungen (4.58) bis (4.60)).

In Abschnitt 4.3 werden die numerischen Ergebnisse dargestellt und untersucht. Die Bifurkationsdiagramme sind nun vollständig, d.h. auch alle Zweige, welche nur in einer analytisch fortgesetzten Gleichung existieren, sind jetzt vorhanden. Die analytisch fortgesetzte Gross-Pitaevskii-Gleichung ermöglicht es zudem, die Ausnahmepunkte genauer zu untersuchen. Durch Umkreisen der Punkte im komplexen Parameterraum kann eine untere Schranke für die Ordnung der Punkte angegeben werden. Die Umkreisung im komplexen Streulängen- bzw. Kopplungsstärkenraum liefert noch kein eindeutiges Ergebnis. Es permutieren nicht alle an der Bifurkation beteiligten Parameter. Erst die Umkreisung mithilfe eines Symmetrieparameters, welcher die Symmetrie der beiden Potentialmulden bricht, schaft Klarheit. Nun vertauschen für die eine Bifurkation vier Parameter, d.h. es handelt sich hierbei um einen Ausnahmepunkt vierter Ordnung. Für die andere Bifurkation (siehe Abbildung 4.11) vertauschen sogar alle fünf Parameter. D.h. dieses System besitzt einen Ausnahmepunkt fünfter Ordnung.

Wir haben zudem gezeigt, dass das dipolare Bose-Einstein-Kondensate in einem $\mathcal{PT}$-symmetrischen Doppelmuldenpotential ein viel reichhaltigeres Bifurkationsszenario als das eines Kondensates ohne langreichweitiger Wechselwirkung zeigt. Viele Eigenschaften welche wir in dieser Arbeit untersucht haben, haben interessante ma-

thematische Eigenschaften im bikomplexen Parameterraum aufgezeigt, der experimentell jedoch nicht zugänglich ist. Jedoch ist ein möglichst vollständiges Verständnis der Bifurkationen wichtig, da sie einen großen Einfluss auf die Stabilität der Kondensate haben [79].

Robin Gutöhrlein

Lebenslauf

Geboren am 10. Juni 1986 in Stuttgart.

Schulausbildung

Sept. 1993 – Juli 1997	**Grundschule Hoheneck**.
Sept. 1997 – Juni 2006	**Goethe Gymnasium Ludwigsburg**.
27. Juni 2006	**Abschluss: Abitur**.

Studium

2006 – 2012	**Diplomstudiengang Physik**. Universität Stuttgart
2011 – 2012	**Diplomarbeit**, *Betreuer: Prof. Dr. Jörg Main, Mitberichter: Prof. Dr. Johannes Roth*, Thema: Bifurkationen und Ausnahmepunkte in dipolaren Bose-Einstein-Kondenstaten. 1. Institut für Theoretische Physik der Universität Stuttgart
10. Febr. 2012	**Abschluss: Diplom-Physiker (Dipl.-Phys.)**.

Berufliche und wissenschaftliche Tätigkeiten, Promotion

2013 – 2017	**Wissentschaftlicher Mitarbeiter mit Lehraufgaben**, *1. Institut für Theoretische Physik der Unitverisität Stuttgart*.
2013 – 2015	**Dozent**, *Duale Hochschule Baden-Württemberg*, Vorlesung: Technische Physik für Wirtschaftsingenieure.
2012 – 2017	**Promotion**, *Betreuer: Prof. Dr. Jörg Main, Mitberichter: Prof. Dr. Christian Holm*, Thema: PT-symmetric dipolar Bose-Einstein condensates: Embedding in a Hermitian system and higher-order exceptional points. 1. Institut für Theoretische Physik der Universität Stuttgart

Danksagung

Ich möchte mich auch bei allen Personen die mich bei der Entstehung dieser Dissertation unterstützt haben bedanken. Mein Dank gilt:

- Prof. Dr. Jörg Main, der durch seine Betreuung diese Arbeit erst möglich gemacht hat. Aber nicht nur seine fachliche Unterstützung, sondern auch die gemeinsamen Institutswanderurlaube haben die letzten Jahre zu einer besonderen Zeit gemacht.
- Prof. Dr. Günter Wunner danke ich für die freundliche Aufnahme am 1. Institut für Theoretische Physik.
- Prof. Dr. Christian Holm, für die Übernahme des Mitberichts.
- Priv.-Doz. Dr. Holger Catarius, der jederzeit für alle Fragen, egal ob wissenschaftlicher oder anderer Natur, da war und auf dessen Unterstützung man sich stets verlassen konnte. Ich bin mir auch sicher dass mir unsere gemeinsame Betreuung der ITP1-IT-Infrastruktur fehlen wird.
- Allen Kollegen des ITP1, die dieses Institut zu etwas ganz Besonderen gemacht haben, und dafür gesorgt haben, dass ich jeden Tag gerne zur Arbeit und ins Büro gekommen bin. Natürlich werden mir auch die vielen unvergesslichen Kaffeerundendiskussionen zu den unterschiedlichsten Themen immer in Erinnerung bleiben.
- Meinen Eltern, die mir mit ihrer Unterstützung sowohl das Physikstudium als auch diese Arbeit ermöglicht haben.

Ehrenwörtliche Erklärung

Ich erkläre, dass ich diese Dissertation, abgesehen von den ausdrücklich bezeichneten Hilfsmitteln, selbständig verfasst habe.

Stuttgart, den 28. Juli 2017 *Robin Gutöhrlein*